

RESPONSES OF MARINE CARBONATE SYSTEM TO WARMING AND SEA-ICE
RETREAT IN THE PACIFIC SECTOR OF THE ARCTIC OCEAN

by

BAOSHAN CHEN

(Under the Direction of Wei-Jun Cai)

ABSTRACT

The Arctic Ocean, particularly the Pacific sector of the Arctic Ocean, plays an important role in the global carbon cycle. To evaluate temporal and spatial variations and controlling mechanisms of this ocean's marine carbonate system in the responses to rapid sea ice retreat, two Chinese Arctic Research Expedition (CHINARE) cruises were conducted to measure dissolved inorganic carbon (DIC), total alkalinity (TAlk), and partial pressure of carbon dioxide ($p\text{CO}_2$) in summer 2008 and 2010. Through a direct high accuracy and precision comparison of field measurements of $p\text{CO}_2$ to $p\text{CO}_2$ values calculated from bottle measurements of DIC and TAlk and seven sets of dissociation constants, we concluded that calculated values agreed best with field measurements using the carbonic acid dissociation constants of *Mehrbach* ($1.5 \pm 5.7 \mu\text{atm}$) or the constants of *Lueker* ($2.3 \pm 5.4 \mu\text{atm}$) in a temperature range of -1.5 to 10.5 °C and a salinity range of 25.8 to 33.1.

Quasi-conservative surface TAlk distribution indicated that Rivers contributed the majority of freshwater on shelves while sea-ice meltwater dominated in the Canada Basin. Low TAlk river water and ice meltwater determined the majority of the

distribution pattern of the carbonate system. Biologically related $p\text{CO}_2$ and DIC were decreased by biological production on shelves and in the partially ice-covered basin areas, particularly around the margins of sea ice cover. Both mixing model approach and field observations revealed that atmospheric CO_2 invasion is the controlling mechanism which sustains high surface $p\text{CO}_2$ in an ice-free Canada Basin. Continuously increased surface $p\text{CO}_2$ due to air-sea gas exchange rapidly decreased the uptake capacity of CO_2 from the atmosphere. Additionally, carbon cycling in the water column has latitudinal features and responded to various stages of sea ice melt, showing CO_2 was fixed at the beginning of sea ice melt, then the carbon cycling was modified due to accumulation of freshwater in the surface with limited air-sea gas exchange, and finally, carbon uptake capacity was decreased due to limited nutrient supply and enhanced stratification and atmospheric CO_2 invasion.

INDEX WORDS: carbon dioxide, dissolved inorganic carbon, total alkalinity, $p\text{CO}_2$, CO_2 flux, air-sea exchange, dissociation constants, sea ice, biogeochemistry, Arctic Ocean, carbon cycling, nutrients, dissolved oxygen

RESPONSES OF MARINE CARBONATE SYSTEM TO WARMING AND SEA-ICE
RETREAT IN THE PACIFIC SECTOR OF THE ARCTIC OCEAN

by

BAOSHAN CHEN

B.S., Xiamen University, China, 2004

A Dissertation Submitted to the Graduate Faculty of The University of Georgia in Partial
Fulfillment of the Requirements for the Degree

DOCTOR OF PHILOSOPHY

ATHENS, GEORGIA

2015

© 2015

Baoshan Chen

All Rights Reserved

RESPONSES OF MARINE CARBONATE SYSTEM TO WARMING AND SEA-ICE
RETREAT IN THE PACIFIC SECTOR OF THE ARCTIC OCEAN

by

BAOSHAN CHEN

Major Professor:	Wei-Jun Cai
Committee:	James T. Hollibaugh
	Bill Miller
	Patricia L. Yager
	Brian Hopkinson

Electronic Version Approved:

Julie Coffield
Interim Dean of the Graduate School
The University of Georgia
May 2015

DEDICATION

To my lovely family

ACKNOWLEDGEMENTS

First of all, I want to thank my major advisor, Dr. Wei-Jun Cai, for giving me this opportunity to study the Arctic Ocean and his great help on my research. I want to thank all my committee members, Dr. James T. Hollibaugh, Dr. Bill Miller, Dr. Patricia L. Yager, and Dr. Brian Hopkinson, who have made valuable suggestions to this work.

I wish to thank the captains and crew of the icebreaker R/V Xuelong for their excellent work and assistance in completing this study. Many thanks to the Chinese National Arctic and Antarctic Data Center, Dr. Jianfang Chen, Dr. Liqi Chen, and Dr. Weidong Ji for collecting and sharing the nutrient, underway $p\text{CO}_2$, dissolved oxygen, chlorophyll a , and primary production data.

I am grateful to the great help from all lab members in the past years, especially Dr. Yongchen Wang and Ms. Guirong Han for their laboratory support. I would also like to thank and Xinping Hu, Wei-Jen Huang, Liang Xue, and Heng Sun for their great help on cruise preparation and sample analysis.

Special thanks to all the friends and colleagues in our department. Finally, I would like to thank my father, mother, and sister for their support in these years.

TABLE OF CONTENTS

	Page
ACKNOWLEDGEMENTS	v
LIST OF TABLES	vii
LIST OF FIGURES	viii
CHAPTER	
1 INTRODUCTION AND LITERATURE REVIEW	1
2 ASSESSMENT OF INTERNAL CONSISTENCY OF THE MARINE CARBONATE SYSTEM AND SAMPLING CONSIDERAIONS IN THE ARCTIC OCEAN BASED ON SUMMER 2010 DATA.....	13
3 THE CARBONATE SYSTEM IN SURFACE WATERS OF THE PACIFIC SECTOR OF THE ARCTIC OCEAN: RESPONSES TO SEA-ICE RETREAT AND FRESHENING	67
4 THE INFLUENCE OF RECENT SEA ICE RETREAT ON ACCELERATED CO ₂ UPTAKE AND CARBON CYCLING IN THE INTERIOR BASIN OF THE WESTERN ARCTIC OCEAN	121
5 SUMMARY	173

LIST OF TABLES

	Page
Table 2.1: Determinations of dissociation constants of carbonic acid in natural seawater (SW) and artificial seawater (ASW)	57
Table 2.2: Surface-water regional ranges of CTD temperature, CTD salinity, underway $p\text{CO}_2$, and stepwise pressure and temperature $p\text{CO}_2$ corrections	58
Table 2.3: Regional $p\text{CO}_2$ differences	59
Table 3.1: Water column primary productivity measured in CHINARE2008	111
Table 3.2: Initial conditions used for simulations of atmospheric CO_2 invasion	112
Table 4.1: End-member properties of sea ice meltwater, meteoric water, Pacific water, and Atlanta water	163
Table 4.2: A summary of the depths of PO_4 , DIC, and AOU maxima in the Arctic Ocean in 1994 and 2010.....	164

LIST OF FIGURES

	Page
Figure 2.1: Map of sampling stations and sea ice cover during the CHINARE2010 cruise (summer 2010)	60
Figure 2.2: Vertical profiles of salinity, TAlk, and DIC measured at two Arctic Ocean Section 1994 (AOS94) stations and a CHINARE2010 station.....	61
Figure 2.3: Latitudinal distributions of underway surface-water $p\text{CO}_2$, Sea surface salinity, and Sea surface temperature.....	62
Figure 2.4: A comparison of measured $p\text{CO}_2$ and $p\text{CO}_2$ calculated from measured DIC, measured TAlk and seven different sets of dissociation constants.....	63
Figure 2.5: $\Delta p\text{CO}_2$ (calculated – measured) as a function of temperature and salinity for calculations with various sets of dissociation constants	64
Figure 2.6: Differences in calculated surface $p\text{CO}_2$ values (other constant – <i>Mehrbach</i>) as a function of temperature for seawater, a mixture of seawater and river water, and a mixture of seawater and sea ice meltwater	65
Figure 2.7: TAlk and salinity of bottles samples in the Canada Basin	66
Figure 3.1: Discrete sampling stations of CHINARE2008, CHINARE2010, AOS94 cruises and underway cruise track of MR99 cruise	113
Figure 3.2: Distributions of surface sea ice cover, temperature, and salinity for CHINARE2008 and CHINARE2010	114

Figure 3.3: Distributions of sea surface TAlk, DIC, and $p\text{CO}_2$ for CHINARE2008 and CHINARE2010.....	115
Figure 3.4: Latitudinal distribution of sea surface $p\text{CO}_2$ for CHINARE2008, CHINARE2010, AOS94 and MR99 cruises.....	116
Figure 3.5: Relationship between TAlk, DIC, and salinity during CHINARE2008 and CHINARE2010.....	117
Figure 3.6: Model simulations of factors influencing surface water $p\text{CO}_2$ in the Arctic Ocean	118
Figure 3.7: Latitudinal distribution of normalized sea surface $p\text{CO}_2$ to -1.6°C for CHINARE2008, CHINARE2010, AOS94 and MR99 cruises.....	119
Figure 3.8: Model simulations of sea surface $p\text{CO}_2$ variation responding to atmospheric CO_2 invasion for CHINARE2008 and MR99 cruises.....	120
Figure 4.1: Discrete sampling stations of CHINARE2010 and AOS94.....	165
Figure 4.2: Sections of temperature, salinity, nitrate, phosphate, and silicate along a section from the Chukchi Sea shelf to the North Pole in AOS94.....	166
Figure 4.3: Sections of temperature, salinity, nitrate, phosphate, and silicate along a section from the Chukchi Sea shelf to the North Pole in CHINARE2010	167
Figure 4.4: Sections of DIC and TAlk in AOS94 and CHINARE2010	168
Figure 4.5: Depth profiles of DIC, phosphate (PO_4), and AOU in CHINARE2010 and AOS94.....	169
Figure 4.6: Depth profiles of aerobically-related ΔDIC (measured – predicted) and fraction of sea ice meltwater (SIM), Pacific water (PW), Atlantic water (AW), and meteoric water (MW) in AOS94 and CHINARE2010.....	170

Figure 4.7: Depth integrated aerobically-related Δ DIC (measured – predicted) in AOS94 and CHINARE2010171

Figure 4.8: A conceptual model illustrating the rapid sea ice retreat and the associated physical, biogeochemical and biological changes during summer through three stages of sea ice melt.....172

CHAPTER 1

INTRODUCTION AND LITERATURE REVIEW

The Arctic appears to be the most sensitive region of the world in the responses to rapid climate change based on paleoclimatic evidence, recent field observations, and model simulations (Solomon et al., 2007). However, the Arctic Ocean Basin's role in determining regional carbon balance has been ignored in the past, because it was covered by perennial sea ice which is considered to impede air-sea carbon dioxide (CO₂) exchange, it has low biological production due to short photosynthetic season (English, 1961; Gosselin et al., 1997; Kinney et al., 1971), and the Arctic Ocean only comprises 2.6% of the total area and less than 1% of the volume of the world's oceans. In the past two decades, more and more research interests were focused on this fast changing ecosystem which is subject to significant freshening under the influence of increasing river discharge and substantial melt of sea ice during summertime.

Under the influence of rapid climate change, the Arctic Ocean is sensitive to the contemporaneous environmental changes. These include (1) Significant warming (ACIA, 2005) and unprecedented high temperature Atlantic water inflow of into the Arctic Ocean at the early 21st century (Spielhagen et al., 2011). (2) A substantial acceleration of summer sea ice loss since the 1990s, particularly since 2007 (Comiso et al., 2008; Maslanik et al., 2007; Wang and Overland, 2009) during which ice cover reached a new minimum record in summer 2012 (<http://nsidc.org>). (3) A reduction of multi-year sea ice (Johannessen et al., 1999) and a decrease in sea ice thickness (Kwok and Rothrock, 2009;

Rothrock et al., 2008; Rothrock et al., 2003). (4) Early melt of sea ice (Markus et al., 2009) and an increased length of melt season (Rigor et al., 2002; Smith, 1998; Stabeno and Overland, 2001). (5) An increase in river discharge which has increased by 7% from 1936 to 1999 from the Arctic Ocean's six largest rivers (Peterson et al., 2002). (6) Ecosystem transitions (Arrigo et al., 2008; Arrigo and van Dijken, 2011; Grebmeier et al., 2006; Li et al., 2009; Pabi et al., 2008). The combination of part or all of the processes stated above would result in a highly dynamic state of the Arctic Ocean in the coming decades (Bates et al., 2011).

The unprecedented melt of sea ice in summer would result in a significantly freshened Arctic Ocean and thus alter the distribution of carbonate system. Although sea ice melt in the Arctic Ocean has increased steadily since the late 1970's, sea ice retreat into the deep basin in the Pacific sector of the Arctic Ocean has only occurred since 2007 with the multiyear sea ice area reduced by 40% (Nghiem et al., 2007). The Arctic Ocean was estimated to be ice-free by summer 2050 due to recently accelerated retreat of summer sea ice extent (Wang and Overland, 2009). So far, the freshwater content of the Arctic Ocean has been increased by as much as 8500 km³ in the past decade (McPhee et al., 2009; Rabe et al., 2011), which is equivalent to 19% of the total freshwater budget in the Arctic Ocean (Aagaard and Carmack, 1989). An accelerated freshening of the Arctic Ocean to an ice-free stage can significantly influence the distribution of the carbonate system according to distinct characteristics of seawater, river water, and sea ice meltwater. Freshening affected ecosystem processes (Li et al., 2009; Wassmann and Reigstad, 2011) could modulate the carbon uptake rate, causing further modifications to the carbonate

system. The combined effect of these processes increases the complexity of the carbonate system's response to freshening and this response has been poorly documented.

It was also suggested that the Arctic surface waters will sequester more CO₂ from the atmosphere in summer because of several reasons. (1) Undersaturated surface waters with respect to atmospheric CO₂ on most of the open shelves and in some open basin areas in summer (Bates, 2006; Bates et al., 2006; Cai et al., 2010; Mucci et al., 2010; Murata and Takizawa, 2003). (2) Increasing areas of open water due to sea ice melt. (3) Decreasing salinity in surface waters due to increasing river discharge (Peterson et al., 2002) and sea ice melt in which more CO₂ can be dissolved. In addition, (4) an increase in CO₂ invasion will likely impact ocean ecosystems via acidification (Steinacher et al., 2009; Yamamoto-Kawai et al., 2009). The resulting ocean acidification could in turn influence the Arctic Ocean marine carbonate system, the distribution of macronutrients, trace metals, and climate-relevant gases, and additionally negatively impact calcifying organisms (Amundsen et al., 2013). These complex feedbacks make the study of CO₂ system in the Arctic Ocean to be of interest to the scientific community.

However, there is a paucity of observations of carbon cycle in the deep Arctic Ocean basin due to the harsh Arctic climate. Therefore, how the carbonate system has responded to freshening, in particular over the deep basins, is still poorly known. For example, estimates of the net annual uptake of CO₂ had large uncertainties in this highly dynamic environment (Anderson et al., 1990; Anderson et al., 1998; Bates, 2006; Bates and Mathis, 2009; Kaltin and Anderson, 2005; Lundberg and Haugan, 1996). The evaluations of annual CO₂ uptake from the atmosphere differ by several times, from 24 Tg C yr⁻¹ (Anderson et al., 1998) based on an estimate of DIC mass balance to 66 Tg C yr⁻¹ (Bates,

2006) estimated from direct measurements of discrete DIC and TALK samples. A lack of representative data sets inhibits a verification if the increase in the estimated air-sea CO₂ flux comes from the result of climate change, or just reflects a combination of uncertainty coming from different methods, spatial and temporal variability, and very limited data coverage. In this case, more data need to be documented for a better estimate of CO₂ flux.

Moreover, there is a controversy about whether the Arctic Ocean will absorb more CO₂ from the atmosphere after sea ice retreat. It has been predicted that the Arctic Ocean will sequester much greater amounts of CO₂ from the atmosphere as a consequence of sea ice decline due to longer duration of open water and concomitant higher ocean primary production (Arrigo et al., 2008; Arrigo and van Dijken, 2011; Bates and Mathis, 2009). However this prediction was based on observations from either highly productive ocean margins or ice-covered basins prior to the recent major ice retreat (Anderson et al., 1998; Bates, 2006). On contrary, deepening of the chlorophyll maximum and nutricline was observed in the interior of the Canada Basin as a consequence of enhanced freshening (McLaughlin and Carmack, 2010). Therefore increased stratification might decrease nutrient supply from deep water, which in turn would affect carbon fixation. Whether the Arctic Ocean will take up a significant amount of CO₂ from the atmosphere is still being debated. These considerations indicate that the response of the carbonate system to the changing Arctic is influenced by various environmental factors, including contributions from various sources of freshwater, open water duration, stratification, nutrient availability, hydrography, and sea ice dynamics. Carbon cycling in the western Arctic Ocean is highly seasonal as a result of extreme changes in sea ice coverage and river

discharge, storm forcing and insolation. However, we still know little about the annual carbonate system dynamics based on limited data available.

To contribute our efforts to study the carbon cycling in the Arctic Ocean in the responses to freshening, we conducted two Chinese National Arctic Research Expedition (CHINARE) cruises in summer 2008 and 2010 in the Pacific sector of the Arctic Ocean (western Arctic Ocean). Our cruises surveyed the Bering Sea, Chukchi Sea, Canada Basin, and Makarov Basin. The details of the cruises will be described in the following chapters. The Pacific sector of the Arctic Ocean has its advantages to study sea ice retreat associated carbon cycling. It consists of a major passage (Bering Strait) which is important in controlling Arctic Ocean nutrient budgets and in maintaining the stratification of the Arctic Ocean, an important flow-through shelf (Chukchi Sea shelf) which occupies 12% of the total Arctic shelf areas and contributes 15% of the total pan-Arctic shelf primary production (Sakshaug, 2004), and deep Canada Basin which is featured by clockwise Beaufort Gyre in which freshwater is accumulated in the past decade. This dissertation consists of five chapters. Chapter one is Introduction. Chapter two to four are the main parts of this dissertation. Chapter five is the summary of this dissertation.

Chapter two will focus on the internal consistency check of the carbonate system. Due to the harsh Arctic climate, few studies of the Arctic Ocean carbon cycle have been conducted. In those early studies, limited carbonate system parameters were sampled. Unmeasured carbonate parameters should be calculated from the other carbonate parameters. This practice needs internal consistency among carbonate system parameters

to be evaluated, which has never been systematically done in the cold Arctic Ocean. We performed a high precision and accuracy comparison of field measurements of $p\text{CO}_2$ to calculated $p\text{CO}_2$ values from DIC and TAlk to evaluate which available sets of constants should be recommended.

Chapter three will discuss the surface distributions of DIC, TAlk and $p\text{CO}_2$, in particular how the distributions respond to sea ice melting. A three end-member mixing model will be used study the distributions of quasi-conservative TAlk and biologically influenced DIC and discuss their controlling mechanisms. Then we will focus on the distribution and controlling mechanisms of surface $p\text{CO}_2$. Another mixing model approach will be used to simulate the amount of $p\text{CO}_2$ changes in difference biogeochemical processes by assuming Pacific water upwells onto the Bering Sea shelf and then flows into the deep Canada Basin. Finally, we incorporate field observations into the mixing model to verify if the simulation agrees with field measurements.

Chapter four will study the carbon cycling in the water column. We will put our focus on historical changes between the Arctic Ocean Section 1994 cruise (AOS94) and CHINAR2010 cruise in the Chukchi Abyssal Plateau where carbon cycling was influenced by inflow of Pacific water and sea ice retreat. A significant difference between AOS94 and CHINAER2010 is that the Chukchi Abyssal Plateau was heavily ice-covered in 1994 while ice-free/partially ice-covered in 2010. In addition, we will also compare the differences in carbon cycling in the Makarov Basin where Pacific water has no influence in that area. A four-component conservative mixing model will be used to separate the contribution of various biogeochemical processes on carbon production/respiration. A

schematic conceptual model of carbon cycling at three different stages of sea ice melt in the interior basin will be created.

Finally, Chapter five will summarize the main findings in Chapters 2–4 in terms of carbon cycling in the responses to rapid summer sea ice retreat and freshwater accumulation in the Pacific sector of the Arctic Ocean over the past decade.

References

- Aagaard, K. and Carmack, E.C., 1989. The Role of Sea Ice and Other Fresh Water in the Arctic Circulation. *J. Geophys. Res.*, 94(C10): 14485-14498.
- ACIA, 2005. Arctic Climate Impact Assessment - Scientific Report. Cambridge University Press, Cambridge, UK, 1046 pp.
- Amundsen, H. et al., 2013. AMAP Assessment 2013: Arctic Ocean Acidification. Arctic Monitoring and Assessment Programme (AMAP).
- Anderson, L.G., Dyrssen, D. and Jones, E.P., 1990. An Assessment of the Transport of Atmospheric CO₂ into the Arctic Ocean. *J. Geophys. Res.*, 95(C2): 1703-1711.
- Anderson, L.G., Olsson, K. and Chierici, M., 1998. A carbon budget for the Arctic Ocean. *Global Biogeochem. Cycles*, 12(3): 455-465.
- Arrigo, K.R., van Dijken, G. and Pabi, S., 2008. Impact of a shrinking Arctic ice cover on marine primary production. *Geophys. Res. Lett.*, 35(19).
- Arrigo, K.R. and van Dijken, G.L., 2011. Secular trends in Arctic Ocean net primary production. *J. Geophys. Res.*, 116: C09011.
- Bates, N.R., 2006. Air-sea CO₂ fluxes and the continental shelf pump of carbon in the Chukchi Sea adjacent to the Arctic Ocean. *J. Geophys. Res.*, 111: C10013.
- Bates, N.R., Cai, W.J. and Mathis, J.T., 2011. The Ocean Carbon Cycle in the Western Arctic Ocean: Distributions and Air-Sea Fluxes of Carbon Dioxide. *Oceanography*, 24(3): 186-201.
- Bates, N.R. and Mathis, J.T., 2009. The Arctic Ocean marine carbon cycle: evaluation of air-sea CO₂ exchanges, ocean acidification impacts and potential feedbacks. *Biogeosciences*, 6(11): 2433-2459.

- Bates, N.R., Moran, S.B., Hansell, D.A. and Mathis, J.T., 2006. An increasing CO₂ sink in the Arctic Ocean due to sea-ice loss. *Geophys. Res. Lett.*, 33(23).
- Cai, W.J. et al., 2010. Decrease in the CO₂ Uptake Capacity in an Ice-Free Arctic Ocean Basin. *Science*, 329(5991): 556-559.
- Comiso, J.C., Parkinson, C.L., Gersten, R. and Stock, L., 2008. Accelerated decline in the Arctic Sea ice cover. *Geophys. Res. Lett.*, 35(1).
- English, T.S., 1961. Some biological oceanographic observations in the central North Polar Sea drift station Alpha, 1957-1958. Arctic Institute of North America.
- Gosselin, M., Levasseur, M., Wheeler, P.A., Horner, R.A. and Booth, B.C., 1997. New measurements of phytoplankton and ice algal production in the Arctic Ocean. *Deep-Sea Res. II*, 44(8): 1623-1644.
- Grebmeier, J.M. et al., 2006. A Major Ecosystem Shift in the Northern Bering Sea. *Science*, 311(5766): 1461-1464.
- Johannessen, O.M., Shalina, E.V. and Miles, M.W., 1999. Satellite evidence for an Arctic sea ice cover in transformation. *Science*, 286(5446): 1937-1939.
- Kaltin, S. and Anderson, L.G., 2005. Uptake of atmospheric carbon dioxide in Arctic shelf seas: evaluation of the relative importance of processes that influence *p*CO₂ in water transported over the Bering-Chukchi Sea shelf. *Mar. Chem.*, 94(1-4): 67-79.
- Kinney, P.J., Loder, T.C. and Groves, J., 1971. Particulate and dissolved organic matter in the Amerasian Basin of the Arctic Ocean. *Limnol. Oceanogr.*, 16(1): 132-137.
- Kwok, R. and Rothrock, D.A., 2009. Decline in Arctic sea ice thickness from submarine and ICESat records: 1958–2008. *Geophys. Res. Lett.*, 36(15): L15501.

- Li, W.K.W., McLaughlin, F.A., Lovejoy, C. and Carmack, E.C., 2009. Smallest Algae Thrive As the Arctic Ocean Freshens. *Science*, 326(5952): 539.
- Lundberg, L. and Haugan, P.M., 1996. A Nordic Seas–Arctic Ocean carbon budget from volume flows and inorganic carbon data. *Global Biogeochem. Cycles*, 10(3): 493-510.
- Markus, T., Stroeve, J.C. and Miller, J., 2009. Recent changes in Arctic sea ice melt onset, freezeup, and melt season length. *Journal of Geophysical Research-Oceans*, 114.
- Maslanik, J.A. et al., 2007. A younger, thinner Arctic ice cover: Increased potential for rapid, extensive sea-ice loss. *Geophys. Res. Lett.*, 34(24).
- McLaughlin, F.A. and Carmack, E.C., 2010. Deepening of the nutricline and chlorophyll maximum in the Canada Basin interior, 2003-2009. *Geophys. Res. Lett.*, 37(24): L24602.
- McPhee, M.G., Proshutinsky, A., Morison, J.H., Steele, M. and Alkire, M.B., 2009. Rapid change in freshwater content of the Arctic Ocean. *Geophys. Res. Lett.*, 36.
- Mucci, A., Lansard, B., Miller, L.A. and Papakyriakou, T.N., 2010. CO₂ fluxes across the air-sea interface in the southeastern Beaufort Sea: Ice-free period. *J. Geophys. Res.*, 115: C04003.
- Murata, A. and Takizawa, T., 2003. Summertime CO₂ sinks in shelf and slope waters of the western Arctic Ocean. *Cont. Shelf Res.*, 23(8): 753-776.
- Nghiem, S.V. et al., 2007. Rapid reduction of Arctic perennial sea ice. *Geophys. Res. Lett.*, 34(19).
- Pabi, S., van Dijken, G.L. and Arrigo, K.R., 2008. Primary production in the Arctic Ocean, 1998-2006. *J. Geophys. Res.*, 113: C08005.

- Peterson, B.J. et al., 2002. Increasing river discharge to the Arctic Ocean. *Science*, 298(5601): 2171-2173.
- Rabe, B. et al., 2011. An assessment of Arctic Ocean freshwater content changes from the 1990s to the 2006-2008 period. *Deep-Sea Research Part I-Oceanographic Research Papers*, 58(2): 173-185.
- Rigor, I.G., Wallace, J.M. and Colony, R.L., 2002. Response of sea ice to the Arctic oscillation. *J. Clim.*, 15(18): 2648-2663.
- Rothrock, D.A., Percival, D.B. and Wensnahan, M., 2008. The decline in arctic sea-ice thickness: Separating the spatial, annual, and interannual variability in a quarter century of submarine data. *J. Geophys. Res.*, 113(C5).
- Rothrock, D.A., Zhang, J. and Yu, Y., 2003. The arctic ice thickness anomaly of the 1990s: A consistent view from observations and models. *J. Geophys. Res.*, 108(C3).
- Sakshaug, E., 2004. Primary and secondary production in the Arctic Seas, The organic carbon cycle in the Arctic Ocean. Springer, pp. 57-81.
- Smith, D.M., 1998. Recent increase in the length of the melt season of perennial Arctic sea ice. *Geophys. Res. Lett.*, 25(5): 655-658.
- Solomon, S. et al., 2007. IPCC, 2007: Climate change 2007: The physical science basis. Contribution of Working Group I to the fourth assessment report of the Intergovernmental Panel on Climate Change.
- Spielhagen, R.F. et al., 2011. Enhanced Modern Heat Transfer to the Arctic by Warm Atlantic Water. *Science*, 331(6016): 450-453.

- Stabeno, P.J. and Overland, J.E., 2001. Bering Sea shifts toward an earlier spring transition. *Eos, Transactions American Geophysical Union*, 82(29): 317-321.
- Steinacher, M., Joos, F., Frolicher, T.L., Plattner, G.K. and Doney, S.C., 2009. Imminent ocean acidification in the Arctic projected with the NCAR global coupled carbon cycle-climate model. *Biogeosciences*, 6(4): 515-533.
- Wang, M.Y. and Overland, J.E., 2009. A sea ice free summer Arctic within 30 years? *Geophys. Res. Lett.*, 36.
- Wassmann, P. and Reigstad, M., 2011. Future Arctic Ocean Seasonal Ice Zones and Implications for Pelagic-Benthic Coupling. *Oceanography*, 24(3): 220-231.
- Yamamoto-Kawai, M., McLaughlin, F.A., Carmack, E.C., Nishino, S. and Shimada, K., 2009. Aragonite Undersaturation in the Arctic Ocean: Effects of Ocean Acidification and Sea Ice Melt. *Science*, 326(5956): 1098-1100.

CHAPTER 2

ASSESSMENT OF INTERNAL CONSISTENCY OF THE MARINE CARBONATE SYSTEM AND SAMPLING CONSIDERATIONS IN THE ARCTIC OCEAN BASED ON SUMMER 2010 DATA¹

¹ To be submitted to *Marine Chemistry*

Abstract

The Arctic Ocean has experienced tremendous change in recent years. To evaluate temporal and spatial variations of this ocean's marine carbonate system, a rigorous evaluation of the quality and internal consistency of field data and the applicability of existing thermodynamic constants is needed. This work represents such an effort. Using data collected during the Chinese Arctic Research Expedition (CHINARE) cruise of summer 2010, we compared underway measurements of the partial pressure of carbon dioxide ($p\text{CO}_2$) to $p\text{CO}_2$ values calculated from bottle measurements of dissolved inorganic carbon (DIC) and total alkalinity (TAlk) and seven sets of dissociation constants. Overall, excluding consideration of the areas of active sea ice melt, we found that underway measured $p\text{CO}_2$ agreed best with $p\text{CO}_2$ values calculated using the carbonic acid dissociation constants of *Mehrbach* (mean difference of $1.5 \mu\text{atm} \pm$ standard deviation of $5.7 \mu\text{atm}$) or the constants of *Lueker* ($2.3 \pm 5.4 \mu\text{atm}$). The data covered a temperature range of -1.5 to 10.5 °C and a salinity range of 25.8 to 33.1. In addition, the differences between the underway measurements of $p\text{CO}_2$ and calculated $p\text{CO}_2$ values were positively related to temperature and salinity, showing calculated values of $p\text{CO}_2$ higher than measured values in the high temperature Bering Sea, while lower in the cold Canada Basin. The low Arctic temperatures fall outside the range of conditions used for experimental determinations of these constants. It was estimated that calculated $p\text{CO}_2$ was underestimated by $\sim 5 \mu\text{atm}$ due to extrapolation to the Arctic lower temperatures. Moreover, large differences between measured and calculated $p\text{CO}_2$ values occurred in areas with partial ice cover. Potential explanations for these large differences

include stratification-related sampling artifacts and dissolution of ikaite (calcium carbonate) precipitates in samples. Dissolution of CaCO_3 is the potential mechanism resulting in large difference between measured and calculated $p\text{CO}_2$ values. Other potential explanations supported that an underestimation of calculated $p\text{CO}_2$ in cold waters should be associated with the temperature and salinity dependencies of the dissociation constants. The marine carbonate system in the Arctic Ocean is influenced by a combination of processes, and further assessment of their relative roles is needed.

1. Introduction

In recent decades, the Arctic Ocean is sensitive to the contemporaneous environmental changes, including significant warming (ACIA, 2005), a substantial acceleration of summer sea ice loss since the 1990s, particularly since 2007 (Comiso et al., 2008; Maslanik et al., 2007; Wang and Overland, 2009), and ecosystem transitions (Arrigo et al., 2008; Arrigo and van Dijken, 2011; Grebmeier et al., 2006; Li et al., 2009; Pabi et al., 2008), which result in a highly dynamic state of the Arctic Ocean in the coming decades (Bates et al., 2011). Under the rapid climate changes, the amount of atmospheric CO₂ invaded into the Arctic surface waters will be increased in summer due to: 1) undersaturated surface waters with respect to atmospheric CO₂ on most of the open shelves and in some open basin areas in summer (Bates, 2006; Bates et al., 2006; Cai et al., 2010b; Mucci et al., 2010; Murata and Takizawa, 2003), 2) increasing areas of open water due to sea ice melt; 3) decreasing salinity in surface waters due to increasing river discharge (Peterson et al., 2002) and sea ice melt. The resulting ocean acidification could influence the Arctic Ocean marine carbonate system, the distribution of macronutrients, trace metals, and climate-relevant gases, and additionally negatively impact calcifying organisms (Amundsen et al., 2013). These complex feedbacks make the study of CO₂ system in the Arctic Ocean to be of interest to the scientific community.

Due to the harsh Arctic climate, few studies of the Arctic Ocean carbon cycle have been conducted. In the early studies, dissolved inorganic carbon (DIC) and total alkalinity (TAlk) were generally, sometimes including pH, the only two carbonate parameters measured in discrete seawater samples for all the cruises (e.g., the International Arctic Ocean Expedition 91, Arctic Ocean Section 94, Polarstern Arctic 96 Expedition, Joint

Ocean Ice Study 97, Beringia 05, and the Western Arctic Shelf Basin Interactions Project). Recent programs have measured more carbonate system parameters and have conducted widespread underway surface measurements. These recent activities include the cruises of the biennial Chinese National Arctic Research Expedition (CHINARE) and several other programs (Fransson et al., 2009; Mathis et al., 2012; Murata and Takizawa, 2003; Robbins et al., 2013). For the historical change studies of the carbonate system in the Arctic Ocean, high precision/accuracy carbonate parameters are required for direct comparison between various cruises. Due to the sampling limitation, unmeasured carbonate parameters should be calculated from the other carbonate parameters. This practice needs internal consistency among carbonate system parameters to be evaluated, which has never been systematically done in the cold Arctic Ocean.

The marine carbonate system contains four measurable parameters: DIC, TAlk, pH, and $p\text{CO}_2$ (or the fugacity of CO_2 , $f\text{CO}_2$). These parameters are related by thermodynamic models, and any two parameters can be used to characterize other parameters. If more than two parameters are measured, then data quality and internal consistency of the data set can be evaluated. These calculations require ancillary measurements of sample temperature (T), salinity (S), pressure, phosphate, and silicate, as well as environmentally appropriate characterizations of the first and second apparent dissociation constants of carbonic acid, K_1 and K_2 (Dickson et al., 2007; Park, 1969). In the Arctic Ocean in particular, reliable dissociation constants for carbonic acid in cold marine waters would facilitate the calculation of historical parameters that were not directly measured.

The equilibria of the carbonate system in solution are shown in Eqs. (1) and (2). The definitions of K_1 and K_2 are given in Eqs. (3) and (4).



$$K_1 = [\text{H}^+][\text{HCO}_3^-] / [\text{CO}_2^*] \quad (3)$$

$$K_2 = [\text{H}^+][\text{CO}_3^{2-}] / [\text{HCO}_3^-] \quad (4)$$

Here CO_2^* represents the combined concentrations of H_2CO_3 and aqueous CO_2 . Brackets represent total concentrations of the enclosed chemical species.

Some determinations of K_1 and K_2 (Table 2.1) were made in natural seawater (Mehrbach et al., 1973; Millero et al., 2006; Mojica Prieto and Millero, 2002). Others used artificial seawater (Goyet and Poisson, 1989; Hansson, 1973; Roy et al., 1993). These various constants are not always directly comparable because different investigators also worked within different ranges of temperature (T) and salinity (S) and they may have used different pH concentration scales. In addition to the original measurements, refitting work has also been conducted through various combinations of original measurements (Dickson and Millero, 1987; Lueker et al., 2000). Other studies have worked with pooled data (Dickson and Millero, 1987; Millero, 1995; Millero, 2010). One point of commonality is that all of the determinations summarized in Table 2.1 cover the temperature range of 5 to 30°C and the salinity range of 20 to 40.

Despite these numerous works, disagreement still exist among the resulting sets of constants. As a result, the magnitude of differences between directly measured carbonate parameters and corresponding calculated values from other measured carbonate parameters depends in part on which set of constants is used for the calculations. Overall, internal consistency tests conducted in the laboratory (Lee et al., 1996; Lueker et al.,

2000; Millero et al., 2006; Mojica Prieto and Millero, 2002) and in the field (Lee et al., 2000; Lee et al., 1997; Millero et al., 2002; Wanninkhof et al., 1999) indicate that the constants made in natural seawater are more reliable than those made in artificial seawater. On the basis of these studies, the constants of Mehrbach et al. (1973) has therefore been generally recommended for carbon studies in the open ocean, owing to the more accurate value of pK_2 .

For work in the Arctic Ocean, a critical consideration is the range of temperatures and salinities encountered in the field. Even in summer, sea surface temperatures in ice-covered areas can be as low as -1.5°C . In addition, the Arctic Ocean is increasingly influenced by river runoff and sea ice meltwater. Between 1936 and 1999, discharge from the Arctic Ocean's six largest rivers increased 7% (Peterson et al., 2002). Under the influence of extensive sea ice melt, summertime surface salinity now decreases significantly in ice-free areas—e.g., down to 24 in the southern Canada Basin (Cai et al., 2010b). None of the carbonic acid dissociation constants (Table 2.1) has been determined at temperatures sufficiently low to encompass the entire range encountered in the Arctic Ocean.

The selection of which constants to use for Arctic Ocean studies may be based on recommendations from previous studies (e.g., the oft-recommended Mehrbach constants), or they may be taken from the lowest-temperature conditions examined during experimental determinations of the constants (e.g., the Roy et al. constants or the Goyet and Poisson constants). Some practices using different input combinations of carbonate parameters recommended same set of dissociation constants in internal consistency evaluations. For example, the constants of Roy et al. (1993) yielded the best internal

consistency for the DIC, pH, and TAlk data set of the Polarstern Arctic 1996 cruise (Jutterström and Anderson, 2005) and the $f\text{CO}_2$, pH, and TAlk data set of (Chierici and Fransson, 2009). In contrast, discordant results were observed between different cruises even if the same input combination was used. For an input of DIC, pH, and TAlk data set, the Mehrbach et al. (1973) constants as refit by Dickson and Millero (1987) gave the best result rather than the Roy et al. (1993) constants for the Beringia 2005 cruise (Jutterström and Anderson, 2010).

With different conclusions arising from analyses of different data sets, it is not clear which set of dissociation constants gives the best internal consistency for Arctic conditions. To date, different sets of constants are being used (Bates, 2006; Bates and Mathis, 2009; Chierici and Fransson, 2009; Jutterström and Anderson, 2005; Jutterström and Anderson, 2010; Mucci et al., 2010) partly due to the differences in calculated carbonate parameter values between various sets of constants are smaller in cold waters than in warmer waters. It raises a question of how accurate of carbonate parameters calculated at low temperatures and salinities is inherent in the calculations. For the internal consistency test between direct measurements of $p\text{CO}_2$ (or $f\text{CO}_2$) and corresponding calculated values in the Arctic, the standard deviation of $f\text{CO}_2$ differences was high (up to $\pm 16.3 \mu\text{atm}$) (Chierici and Fransson, 2009), which was about twice as large as a previous study (8 to $10 \mu\text{atm}$) conducted in temperate oceans (Wanninkhof et al., 1999). Thus, a rigorous evaluation is required to evaluate the effect of different constants on internal-consistency assessments over Arctic Ocean T and S ranges, as well as the accuracy of the calculated values. Determinations are also needed of how well the current sets of constants can be extrapolated to low T and S conditions.

In this paper, we use recent (summer CHINARE2010) high-precision field measurements of sea surface $p\text{CO}_2$, DIC, and TAlk in the Pacific sector of the Arctic Ocean to examine the internal consistency implications of seven diverse sets of carbonic acid dissociation constants. Specifically, we compare directly measured values of $p\text{CO}_2$ with values calculated using measurements of DIC and TAlk in conjunction with the different sets of constants. Our oceanic measurements cover a temperature range of -1.5 to 10.5°C , a salinity range of 25.8 to 33.1, and a $p\text{CO}_2$ range of 88 to $386 \mu\text{atm}$. Our overall aim is to determine the best set of dissociation constants for Arctic marine carbon cycle studies and to assess the accuracy of the resulting calculated values. We also discuss sampling procedures and ocean processes that could potentially contribute to observed differences between measured and calculated values of $p\text{CO}_2$ in Arctic waters.

2. Methods

Inorganic CO_2 system data were obtained during the Chinese Arctic Research Expedition of summer 2010 (CHINARE2010), from early July to late August. The cruise track covered the Pacific sector of the Arctic Ocean, including the Bering Sea basin, Bering Sea shelf, Chukchi Sea, and Canada Basin (Fig. 2.1). Water column samples of DIC, TAlk, temperature and salinity, and surface samples of phosphate and silicate were measured at 77 stations. Underway sea surface temperature (SST), sea surface salinity (SSS), and surface $p\text{CO}_2$ were also measured continuously along the cruise track. Water column DIC and TAlk were compared with historical Arctic Ocean Section 1994 (AOS94) cruise data which is available in the CARINA data product (<http://cdiac.ornl.gov/oceans/CARINA/>). Underway $p\text{CO}_2$ measurements collected on

station were compared with $p\text{CO}_2$ values calculated from surface-water bottle measurements of DIC and TAlk.

Remotely sensed sea ice coverage data were retrieved from the Advanced Microwave Scanning Radiometer – Earth Observing System (AMSR- E) sensor with a resolution of 12.5 x 12.5 km. These data were downloaded from NOAA’s ERDDAP data server (<http://coastwatch.pfeg.noaa.gov/erddap/griddap/index.html?page=1&itemsPerPage=1000>). The sea ice cover data were matched to the coordinate and sampling time of each station.

2.1. DIC and TAlk measurements: discrete sample collection and analysis

Discrete DIC and TAlk samples were collected from 12 L Niskin bottles mounted on a 24-bottle rosette equipped with a SeaBird CTD 911. Surface samples were collected at 3–5 m depth within the surface mixed layer. We transferred seawater from each Niskin bottle into one pre-cleaned 250 mL borosilicate glass bottles for both DIC and TAlk analysis. To allow for thermal expansion, 1 mL of seawater was removed using a plastic pipette. To halt biological activity, 100 μL of saturated mercuric chloride solution was added to each sample bottle. The bottles were then sealed using Apiezon[®] L greased ground-glass stoppers. Samples were stored at 4°C in the dark and were analysed after the cruise.

DIC and TAlk were measured using automated devices and the analytical techniques and procedures documented in Cai et al. (2010a) and Huang et al. (2012). TAlk was determined by potentiometric titration, using 0.1 M hydrochloric acid and an open-cell titration system. All TAlk samples were analysed in pre-thermostated (25°C) glass cells.

For each sample, 25 mL subsamples were sequentially titrated until we obtained two replicates with a precision within 0.1%. The average of the two values is reported. DIC was determined at room temperature using a non-dispersive infrared method. Each seawater sample was acidified using phosphoric acid. The evolved CO₂ gas was extracted and carried by pure N₂ gas to the infrared CO₂ detector (Li-Cor 6262) for quantification. The precision of both the TAlk and DIC measurements was $\pm 2 \mu\text{mol/kg}$. The accuracies of the TAlk and DIC measurements were determined by routine analysis of certified reference materials (CRM) provided by A. G. Dickson, Scripps Institution of Oceanography.

2.2. Inter-lab comparisons of DIC and TAlk analyses

Complementary to the CHINARE2010 cruise, the precision and accuracy of our DIC and TAlk methods were further quantitatively evaluated in a blind, anonymous inter-laboratory comparison sponsored by the NOAA Ocean Acidification program. For this exercise, two natural seawater samples (Batch #124 and Batch #125) were collected off the coast of California and prepared at the Scripps Institution of Oceanography by A. G. Dickson. These two samples, with substantially different $p\text{CO}_2$ values, were analyzed for salinity, DIC, and TAlk before distribution to participating test labs. We analyzed these samples several times over a period of 12 days.

For DIC, our Batch #124 average and standard deviation were $2016.1 \pm 1.02 \mu\text{mol/kg}$ ($n = 6$); the assigned value was $2015.72 \pm 0.74 \mu\text{mol/kg}$. For Batch #125, our DIC value was $2139.0 \pm 0.98 \mu\text{mol/kg}$ ($n = 4$); the assigned value was $2141.94 \pm 0.37 \mu\text{mol/kg}$. For TAlk, our Batch #124 average and standard deviation were $2215.9 \pm 0.71 \mu\text{mol/kg}$ ($n = 6$); the assigned value was $2215.08 \pm 0.49 \mu\text{mol/kg}$. For Batch #125, our TAlk value was

$2215.6 \pm 0.31 \mu\text{mol/kg}$ ($n = 8$); the assigned value was $2216.26 \pm 0.52 \mu\text{mol/kg}$. In summary, our measurements exhibited good reproducibility, showing considerably smaller variation than the overall uncertainties of our methods. In addition, our results agreed well with the assigned values, thus confirming the accuracy of our measurements.

2.3. Underway $p\text{CO}_2$ measurements

Underway sea surface temperature, salinity, and $p\text{CO}_2$ data were collected continuously along the cruise track (Fig. 2.1). Surface seawater was collected from an intake on the port side of the ship at about 4 m depth. This shallow intake depth was designed to capture representative surface biogeochemical signals. To minimize clogging by sea ice, the seawater was then routed through a sea chest containing overlapping stainless steel mesh filters of different pore sizes. To reduce the residence time of the sample seawater, this sea chest is as small as 3 m^3 in volume. Seawater was pumped from the sea chest at a flow rate of 6 m^3 per hour to the ship's labs for inline analysis of $p\text{CO}_2$. Additionally, seawater in the sea chest is updated faster by the force of wave, leading to fast response to surface water $p\text{CO}_2$ variation.

SST and SSS were measured by an SBE21 (Sea-Bird Electronics) thermosalinograph installed in the sea chest. Underway $p\text{CO}_2$ was measured by an automated system (General Oceanics, Inc.) continuously using a non-dispersive infrared detector Li-840 (LICOR, Inc.) at a sampling interval of 2 minutes. This autonomous system was calibrated every 3 hours using four compressed CO_2 gas standards obtained from NOAA's Earth System Research Laboratory (ESRL), Global Monitoring Division in Boulder, CO. These gas standards are directly traceable to the World Meteorological

Organization (WMO) scale. The precision of underway $p\text{CO}_2$ measurements of this system is $0.1 \mu\text{atm}$, and overall accuracy is estimated at $2 \mu\text{atm}$ as documented by Pierrot et al. (2009). We refer to the instrument-observed values of underway $p\text{CO}_2$ as $p\text{CO}_2(\text{obs})$.

2.4. Salinity difference between underway and CTD systems

The Arctic Ocean is distinctive due to the massive influences of river discharge and sea ice meltwater. According to circulation pattern, the northward flowing Pacific-origin waters are diluted by river water to form river modified seawater on the shelves, then by sea ice meltwater in the Canada Basin. In particular, water masses are more complex on the shelves than in the basin. The intake port for the underway system was located about 20 m from the CTD-rosette sampling site, which was on the ship's starboard side. Therefore, salinity differences were used to evaluate if these two systems sampled the same water mass. On this basis, we excluded some shelf stations located on the front of water masses, which showed significantly larger salinity difference between CTD and the underway system records than surrounding stations. Finally, 77 stations were selected for comparison as shown in Fig. 2.1.

The salinity differences ($\text{salinity}(\text{CTD}) - \text{salinity}(\text{Underway})$) showed that salinity measured by CTD were higher than the underway records over all stations. The mean difference and standard deviation were the smallest (0.019 ± 0.007) in the Bering Sea basin. These values were increasing northward in the Bering Sea shelf (0.060 ± 0.036), Chukchi Sea (0.097 ± 0.05), and Canada Basin (0.109 ± 0.043). Considering the Bering Sea basin was well mixed in the top 30 m layer, the mean salinity difference was treated as a systematic error between two systems. The higher salinity differences north of the

Bering Sea basin can be explained by weak horizontal gradients indicating slightly different mixing ratio between seawater and river water on the shelves, and between seawater and sea ice meltwater in the Canada Basin. Because the salinity differences were small enough, we will directly compare measured $p\text{CO}_2$ from the underway system and calculated $p\text{CO}_2$ from the CTD system. Then, we apply a small salinity correction (+0.019) to the underway salinities to further evaluate the influences of river water and sea ice meltwater on the accuracy of underway $p\text{CO}_2$ measurements.

2.5. Calculation of bottle $p\text{CO}_2$ values

The bottle measurements of DIC and TAlk (surface samples) were used to calculate bottle $p\text{CO}_2$ values, which we express here as $p\text{CO}_2(\text{DIC}, \text{TAlk})$. For these calculations, we used the Excel version of CO2SYS (Pierrot et al., 2006), downloaded from <http://cdiac.ornl.gov/ftp/co2sys/>. DIC and TAlk served as the two input inorganic carbon system parameters. Other inputs included the seawater temperature, salinity measured by the CTD, and a pressure of 1 atm. The dissociation constant of bisulfate was supplied as input from Dickson (1990), and the boron concentration was from Uppström (1974). Concentrations of total phosphate and silica were also provided as input. In the high nutrient-low chlorophyll (HNLC) Bering Sea basin, these weak acids are present in relatively high concentrations and can contribute significantly to alkalinity.

For the dissociation constants of carbonic acid (Table 2.1), seven different sets of equations were used and compared: the equations of Hansson (1973), as refit by Dickson and Millero (1987), hereafter referred to as “*Hansson*”; Mehrbach et al. (1973), as refit by Dickson and Millero (1987), “*Mehrbach*”; Goyet and Poisson (1989), “*G&P*”; Roy et al. (1993), “*Roy*”; Lueker et al. (2000), “*Lueker*”; Mojica Prieto and Millero (2002),

“*MP&M*”; and Millero (2010), “*Millero*”. For convenience, we included only those sets of dissociation constants determined or refitted from original experimental data (as opposed to those refit from pooled data). Constants refit from pooled data show great consistency with the original works. We did not separately include the constants of Millero et al. (2006) because they are essentially the same as those of Millero (2010).

2.6. Conversion of underway $p\text{CO}_2$ measurements to bottle conditions

To make the on-station instrument-observed values of underway $p\text{CO}_2$ directly comparable to their bottle-data counterparts ($p\text{CO}_2(\text{DIC}, \text{TAlk})$), we applied pressure and temperature corrections to $p\text{CO}_2(\text{obs})$. These corrected underway values of $p\text{CO}_2$ are labeled as $p\text{CO}_2(\text{UW})$.

Values of $p\text{CO}_2(\text{obs})$ are reported for pressures measured in the equilibrator of the underway system and for sea surface temperatures measured in the sea chest, but $p\text{CO}_2(\text{DIC}, \text{TAlk})$ is calculated at 1 atm. So we first corrected for this pressure difference by using Eq. (5) to convert $p\text{CO}_2(\text{obs})$ to the $p\text{CO}_2$ values that would have been observed at 1 atm (1013.25 hPa):

$$p\text{CO}_2(\text{obs}, 1 \text{ atm}) = p\text{CO}_2(\text{obs}) \times 1013.25 / P \quad (5)$$

where $p\text{CO}_2(\text{obs}, 1 \text{ atm})$ are pressure converted values. P is the barometric pressure measured in the equilibrator of the underway system in ship’s underway lab.

Small temperature differences were observed between the underway and CTD systems, so $p\text{CO}_2(\text{obs}, 1 \text{ atm})$ was then converted to the $p\text{CO}_2$ value that would have been observed at the in situ temperature of the DIC and TAlk bottle samples. For this correction, the empirical equation proposed by Takahashi et al. (1993) was applied:

$$pCO_2(\text{UW}) = pCO_2(\text{obs}, 1\text{atm}) \times \exp\left(0.0423 \times (t_{(\text{DIC}, \text{TAlk})} - t_{(\text{obs})})\right) \quad (6)$$

where $t_{(\text{DIC}, \text{TAlk})}$ is the temperature measured by the CTD, and $t_{(\text{obs})}$ is the sea surface temperature measured in the underway sea chest by the SBE21. This normalization equation, which yields ~4.23% change in pCO_2 per one-degree Celsius change in temperature due to the thermodynamic effect of cooling/warming on seawater. This empirical coefficient agrees well with thermodynamic calculations (Millero, 1995).

The stepwise corrections for the effects of pressure and temperature (δpCO_2) are minor (Table 2.2). For pressure, the mean correction was 0.7 μatm (± 1.5 μatm standard deviation). For temperature, the mean correction was -1.2 μatm (± 2.4 μatm standard deviation). A negative sign indicates that the corrected value was lower than the uncorrected value. In the northernmost Arctic Ocean, pressure considerations can be important. Here, the low atmospheric pressure resulted in a pressure correction of up to 4.7 μatm increase in pCO_2 . Correcting the underway pCO_2 measurements to CTD temperatures resulted in a decrease of up to 9.7 μatm in pCO_2 . This effect is more significant in cold Arctic waters than in the warmer waters of temperate oceans. In the following descriptions and discussion, we use only the fully corrected $pCO_2(\text{UW})$ measurements, hereafter referred to as “measured pCO_2 .”

3. Results

3.1. Comparison of CHINARE2010 and historical AOS94 DIC and TAlk profiles

Our cruise track revisited some areas sampled during the 1994 Arctic Ocean Section cruise (AOS94). It is a good opportunity to further evaluate our data quality or to assess if the historical carbonate data could be comparable. In the Arctic Ocean bottom layer,

where the residence time of seawater is as long as 300 years, comparison of our data with the historical data may yield some insight into data quality.

Fig. 2.2 shows vertical profiles of salinity, TAlk, and DIC measured at two AOS94 stations (stations 17 and 18) and a nearby CHINARE2010 station (SR18) in the Canada Basin (Fig. 2.1). In deep waters (depth >1000 m), all three parameters were nearly unchanged over the 16 years between the two cruises. At AOS94 Station18 (depth 1052 m), $S = 34.8941$, TAlk = 2303 $\mu\text{mol/kg}$, and DIC = 2161.3 $\mu\text{mol/kg}$. The corresponding CHINARE2010 values (Station SR18, depth = 999 m) are $S = 34.8677$, TAlk = 2306 $\mu\text{mol/kg}$, and DIC = 2163.1 $\mu\text{mol/kg}$. The TAlk and DIC differences are 3 $\mu\text{mol/kg}$ and 1.8 $\mu\text{mol/kg}$, respectively, with a small difference in salinity. If we scale the TAlk and DIC values of AOS94 and CHINARE2010 to the average salinity of 34.8809 (i.e., (TAlk or DIC) * $S_{\text{(average)}} / S_{\text{(observed)}}$), then TAlk and DIC differences between two cruises are only 4.7 $\mu\text{mol/kg}$ and 3.5 $\mu\text{mol/kg}$, respectively, showing relatively constant differences which might be caused by systematic errors of measurements or advanced analytical precision in recent decades. This comparison suggests that the TAlk and DIC data of these cruises are consistent. On one hand, it confirms the quality of our data, and on the other hand, it implies that these historical datasets are qualified for the study of long-term changes of the carbonate system as that did in Cai et al. (2010b).

3.2. Distributions of sea ice, SST, SSS, and surface $p\text{CO}_2$

In order to systematically evaluate how well the measurements of underway $p\text{CO}_2$ agrees with the calculated values, the study area is separated into the Bering Sea basin, Bering Sea shelf, Chukchi Sea, and Canada Basin to facilitate the description and discussion due to their distinct hydrographic and biogeochemical features. The large-

scale distribution of sea ice cover is shown in Fig. 2.1. South of the Canada Basin, no sea ice was observed (purple colored dots). Within the Canada Basin, ice cover increased abruptly from 35% up to 85% between two adjacent stations. We therefore divided the Canada Basin into two regions: one lightly (<35%) ice covered and the other densely (>35%) ice covered. At high latitudes, sea ice cover was consistently heavy (>85%). Two transects encountered regions of partial ice cover (blue and green colored dots). The eastern cruise track, located between 72°N and 75°N near the Beaufort Sea, had 0–45% ice cover when it was sampled in mid-July. The western track, located between 75°N and 80°N, close to the East Siberian Sea, was sampled in late August during a time of extensive sea ice melting. Ice cover here was 0–50%.

The latitudinal features of sea surface $p\text{CO}_2$, SST, and SSS are shown in Fig. 2.3 and summarized in Table 2.2. Over the entire study area, measured surface $p\text{CO}_2$ values ranged from 88 μatm (Chukchi Sea) to 385 μatm (Bering Sea), suggesting that most of the study area was a sink for atmospheric CO_2 ($\sim 385 \mu\text{atm}$) during the summer cruise (Fig. 2.3a). In the Bering Sea basin, surface $p\text{CO}_2$ ranged from 195 to 385 μatm , decreasing from the central basin to the shelf break. This pattern was due to enhanced biological production on the Bering Sea shelf. SST and SSS, in contrast, were nearly invariant (SST range = 7.21–8.48 °C, and SSS range = 31.65–33.14; Fig. 2.3b, c).

On the Bering Sea shelf and in the Chukchi Sea, highly variable surface $p\text{CO}_2$ values were observed. Standard deviation on the Bering shelf was 78.9 μatm ; in the Chukchi Sea, 53.2 μatm . The high Bering shelf variation is consistent with the complex hydrographic setting. The relatively fresh and warm waters of coastal Alaska (salinity 25.9, temperature 10.5 °C) typically exhibit high $p\text{CO}_2$ (367.5 μatm) due to the influence of

river runoff (Mathis et al., 2011; Striegl et al., 2007). In addition, we observed evidence on local upwelling on the northwestern Bering shelf, resulting in a notable temperature decrease, down to 0.5 °C. The Chukchi Sea is less subject to riverine input and upwelling. Here, most of the surface $p\text{CO}_2$ values fell within the range of 150–250 μatm , increasing slightly with increasing latitude. Due to the influence of melting sea ice, a northward trend of decreasing temperature (from 6 to 0 °C) and decreasing salinity (from 32 to 27) was observed.

The Canada Basin exhibited relatively constant $p\text{CO}_2$ (243–333 μatm), with $p\text{CO}_2$ decreasing northward from the slope to 85°N, then increasing poleward from there. The slightly higher $p\text{CO}_2$ of 313.6 (± 11.4) μatm in the lightly ice-covered southern Canada basin was associated with atmospheric CO_2 invasion into the open water (Cai et al., 2010). In the densely ice-covered more northerly region, salinity increased and temperatures stayed near the freezing temperature of about -1.5°C . The average surface $p\text{CO}_2$ of 289.2 with a standard deviation of ± 20.3 μatm indicated undersaturation with respect to atmospheric CO_2 .

3.3. Internal consistency: Comparison of measured $p\text{CO}_2$ and $p\text{CO}_2$ calculated using different dissociation constants

To examine the internal consistency of the carbonate system data according to different sets of carbonic acid dissociation constants (Table 2.1), we compared the corrected underway $p\text{CO}_2$ measurements ($p\text{CO}_2(\text{UW})$) to the $p\text{CO}_2$ values calculated from the bottle-sample measurements of DIC and TAlk ($p\text{CO}_2(\text{DIC}, \text{TAlk})$) in Fig. 2.4. Overall, the *Mehrbach* and *Lueker* constants yield the best agreement (i.e., best fit to the 1:1 line in Fig. 2.4). The *MP&M* and *Millero* constants also yield calculated values that

correspond well with measured values. For the *G&P* and *Roy* constants, fewer of the calculated values show reasonable agreement with measured values. The *Hansson* constants yield the highest calculated $p\text{CO}_2$ values and do not work well for this data set.

Some geographic distinctions are also evident. In waters south of the Canada Basin, calculated $p\text{CO}_2$ values are generally higher than measured values (Fig. 2.4, black circle, red triangle, and blue square). Within the Canada Basin, calculated values are generally lower. In the portion of the basin with light ice cover (black cross), calculated $p\text{CO}_2$ values are lower than measured values no matter which set of constants is used. In the areas with dense ice cover (green inverted triangle), calculated $p\text{CO}_2$ values are higher than measured values for the constants of *Millero* and *Hansson*. These same patterns can be seen in the regional means of the differences ($\Delta p\text{CO}_2 = \text{calculated} - \text{measured}$) shown in Table 2.3.

Temperature and salinity conditions encountered within the Bering Sea basin ($7.2^\circ\text{C} \leq T \leq 8.5^\circ\text{C}$ and $31.7 \leq S \leq 33.1$; Table 2) fell within the ranges covered by all of the sets of dissociation constants considered in this work (Table 2.1). This regional data set therefore provides an opportunity to directly compare the internal consistency implications of the various constants within their optimal ranges of application. In this analysis (Table 2.3), the constants of *Mehrbach* and *Lueker* again yield the smallest $\Delta p\text{CO}_2$ values: $2.2 \pm 4.6 \mu\text{atm}$ and $2.5 \pm 4.5 \mu\text{atm}$, respectively. *MP&M* and *Millero* also give reasonable agreement, with mean differences of $10 \mu\text{atm}$ and $7.6 \mu\text{atm}$, respectively. Mean differences are significantly larger for the other constants: up to $14.5 \mu\text{atm}$ for *G&P* and for *Roy* and up to $20.5 \mu\text{atm}$ for *Hansson*. These findings are consistent with earlier recommendations to use the constants of *Mehrbach* (Lee et al., 2000; Millero et

al., 2002; Wanninkhof et al., 1999) or *Lueker* (Dickson et al., 2007). The uncertainties of $\sim 5 \mu\text{atm}$ (standard deviation) in $\Delta p\text{CO}_2$ from *Mehrbach* and *Lueker* agree with the uncertainty of approximately 8–10 μatm reported for the field comparison conducted in the north Atlantic Ocean, Indian Ocean, and south Pacific Ocean by Wanninkhof et al. (1999).

On the shelf of the Bering Sea, most samples were also from waters within the recommended temperature and salinity ranges of application. Here the calculated and measured $p\text{CO}_2$ values also show good agreement, with a mean regional $\Delta p\text{CO}_2$ of $5.1 \pm 3.6 \mu\text{atm}$ for *Mehrbach* and $5.5 \pm 3.7 \mu\text{atm}$ for *Lueker*.

In areas north of the Bering Sea shelf, sea surface temperatures fell below the shared temperature range of 5 to 30°C, but all sample salinities still fell within the shared range of application ($S > 20$) (Table 2.2). Excluding the $p\text{CO}_2$ data collected from the lightly ice-covered portion of the Canada Basin and excluding consideration of $\Delta p\text{CO}_2$ values calculated using the *Hansson* constants, two general features in mean $\Delta p\text{CO}_2$ are evident (Table 2.3). First, continuously decreasing mean $\Delta p\text{CO}_2$ is observed with increasing latitude for every set of dissociation constants. Second, variation across the mean $\Delta p\text{CO}_2$ values calculated with different constants at first decreases with increasing latitude but then grows larger again in the northernmost Canada Basin.

Consider, for example, latitudinal changes for the *Mehrbach* and *Roy* case. Both of them have been commonly used for calculation of carbonate parameters in the Arctic Ocean. Mean $\Delta p\text{CO}_2$ values (Table 2.3) decrease poleward, from 2.2 μatm and 14.4 μatm in the Bering Sea basin to 0.7 μatm and 5.6 μatm in the Chukchi Sea, and further still to –3.3 μatm and –6.3 μatm in the colder and fresher northern Canada Basin.

These general latitudinal trends in mean $\Delta p\text{CO}_2$ are seen for several of the constants, with some exceptions (Table 2.3). The constants of *Hansson*, for example, yield similar mean $\Delta p\text{CO}_2$ values across all regions except for the lightly ice-covered Canada Basin area. The constants of *Millero* yield mean $\Delta p\text{CO}_2$ values that decline just $1.2 \mu\text{atm}$ between the Chukchi Sea and the southern Canada Basin—much smaller than the drop observed for the other constants. The *G&P* and *Roy* constants yield large latitudinal changes in mean $\Delta p\text{CO}_2$, suggesting that constants determined in artificial seawater are more sensitive to temperature and/or salinity changes than those determined in natural seawater. Looking at the variation among mean $\Delta p\text{CO}_2$ values calculated across all sets of constants (Table 2.3), we see high variability in the Bering Sea basin (standard deviation = $5.5 \mu\text{atm}$). Proceeding northward, mean $\Delta p\text{CO}_2$ values converge in the Chukchi Sea (standard deviation = $2.4 \mu\text{atm}$) but spread again in the densely ice-covered section of the Canada Basin (standard deviation = $3.9 \mu\text{atm}$).

Overall, most of the calculated and measured $p\text{CO}_2$ values show good consistency (i.e., small $\Delta p\text{CO}_2$), especially for the Chukchi Sea and the northern (densely ice-covered) Canada Basin. The southern Canada Basin (light ice cover) was distinctive in yielding calculated $p\text{CO}_2$ values markedly lower than the measured values (i.e., negative $\Delta p\text{CO}_2$).

3.4. Relationship of $\Delta p\text{CO}_2$ with temperature and salinity

Fig. 2.5 shows the relationship between $\Delta p\text{CO}_2$ (calculated – measured) data and surface temperature and salinity for all stations outside the loosely ice-covered southern Canada Basin. Least squares linear regression indicates that for all sets of constants, $\Delta p\text{CO}_2$ increases with increasing temperature and with increasing salinity (i.e., all slopes

are positive). Variations in magnitude of slope are observed among the different constants.

$\Delta p\text{CO}_2$ values calculated from the *Mehrbach* constants and the *Lueker* constants are the least sensitive to changes in temperature and salinity. Overall, their variations in $\Delta p\text{CO}_2$ over the whole study area (5.4 to 5.7 μatm ; Table 2.3) are comparable with the probable error in calculated $p\text{CO}_2$ due to measurement uncertainties (Millero, 1995).

The linear regressions (Fig. 2.5) can largely explain the temperature and salinity dependence of calculated $p\text{CO}_2$ values for all of the constants. Using the $\Delta p\text{CO}_2$ range (mean \pm 1sd) of *Mehrbach* as a reference, the other constants significantly overestimate calculated $p\text{CO}_2$ values when $T > 4^\circ\text{C}$ or $S > 31$. *MP&M* and *Millero* agree better with *Mehrbach* and *Lueker* than do *G&P* and *Roy*. In contrast, an underestimation can be observed, in particular for the *G&P* and *Roy* constants, at temperatures below -1°C and over the salinity range of 25–29. In addition, $\Delta p\text{CO}_2$ increases slowly over a wide range of low temperature and salinity while fast over a narrow range of high temperature and salinity for all of the constants. For the *G&P* and *Roy* case, $\Delta p\text{CO}_2$ increases 20 μatm over $-2^\circ\text{C} < T < 6^\circ\text{C}$ or $25 < S < 31$, while another 20 μatm increase over a narrow T or S range ($6^\circ\text{C} < T < 9^\circ\text{C}$ or $31 < S < 33$). The implication is that K_1 and K_2 are least sensitive to temperature and salinity at low temperatures and low salinities.

3.5. Accuracy of $p\text{CO}_2$ calculations under Arctic Ocean hydrographic settings

The $p\text{CO}_2$ values calculated from the different sets of constants show different levels of accuracy ($\Delta p\text{CO}_2$) among the different geographic regions. As shown above, the *Mehrbach* and *Lueker* constants give the best results in terms of internal consistency, i.e. differences between measured and calculated $p\text{CO}_2$ or between different sets of constants.

Only a small difference of 0.3 μatm in mean $\Delta p\text{CO}_2$ is observed between them in the Bering Sea basin (Table 2.3). On the Bering Sea shelf and in the Chukchi Sea, the mean difference is still $\leq 0.6 \mu\text{atm}$. Within the northern Canada Basin, the difference is larger but still small (2.1 μatm).

Within the region of dense ice cover, the mean $\Delta p\text{CO}_2$ value of *Lueker* (-1.2 μatm) agrees best with that of *MP&M* (-1.3 μatm), while that of *Mehrbach* is smaller (-3.3 μatm). Because the *MP&M* constants include the experimental data of *Mehrbach*, we note that the slight difference in mean $\Delta p\text{CO}_2$ between *Lueker* and *Mehrbach* in the colder waters could be related to differences in fitting methods or to errors associated with converting the original experimental data to different pH scales during refitting (Dickson and Millero, 1987; Lueker et al., 2000).

In the densely ice-covered Canada Basin, the calculated $p\text{CO}_2$ values of *Mehrbach* and *Lueker* are lower than the measured values; in the Bering Sea basin, the reverse is true. If we use the Bering Sea basin as a reference case because its temperature and salinity values fall within the intervals of experimental determination for all the constants (Table 2.1), the $\Delta p\text{CO}_2$ values may indicate a potential underestimate of calculated $p\text{CO}_2$ values when the constants are applied to calculations at lower temperatures.

In summary, mean $\Delta p\text{CO}_2$ for *Mehrbach* and *Lueker* and the differences in $\Delta p\text{CO}_2$ between them over the entire study areas are small. Although we have no further evidence to determine whether *Mehrbach* or *Lueker* is more accurate in cold waters, given previous recommendations for calculations in temperate oceans (Lee et al., 2000; Millero et al., 2002; Wanninkhof et al., 1999), we conclude that the *Mehrbach* and *Lueker* sets of constants can be recommended for use over the entire temperature range

exhibited by the world's oceans, including the cold polar oceans. Even at low temperatures, the use of these constants causes an uncertainty of only up to 5.5 μatm in accuracy.

4. Discussion

4.1. Simulation of calculated $p\text{CO}_2$ as a function of T in different water mixtures

The internal consistency calculations can be evaluated in different ways—for example, by examining the dependence of the dissociation constants on T and S (Lee et al., 1996; Millero et al., 2002); by examining differences in calculated $p\text{CO}_2$ values as a function of T (Millero, 1995); or by comparing calculated and measured $p\text{CO}_2$ values over a range of T (Wanninkhof et al., 1999). These comparisons were often conducted at $S = 35$. The field comparisons of $\Delta p\text{CO}_2$ were conducted with different combination of T and S (Wanninkhof et al., 1999). The Arctic Ocean is characterized by mixing of seawater, river water, and sea ice meltwater. It is required to further evaluate the T dependency of calculated values in different water mixtures.

Here we calculate $p\text{CO}_2$ using the various sets of constants in three different media over the temperature range $-2.0 \leq T \leq 10.5$ °C (-2.0 °C is the freezing point of $S = 36$): seawater, a seawater and river water mixture, and a seawater and sea ice meltwater mixture (Fig. 2.6). The chemical properties of the three end-members are taken from Cai et al. (2010b). The seawater end-member has the properties of $S = 33.218$, $\text{TAlk} = 2257.9$ $\mu\text{mol/kg}$, and $\text{DIC} = 2261.4$ $\mu\text{mol/kg}$, determined from the 200 m layer of the Bering Sea slope. The river end-member is described by $S = 0$, $\text{TAlk} = 1100$ $\mu\text{mol/kg}$, and $\text{DIC} = 1150$ $\mu\text{mol/kg}$. The sea ice meltwater has the characteristics of $S = 5$, $\text{TAlk} = 450$

$\mu\text{mol/kg}$, and $\text{DIC} = 400 \mu\text{mol/kg}$. We consider two extreme mixing scenarios, with seawater mixing with either river water or sea ice meltwater to $S = 20$. We take the *Mehrbach*-based $p\text{CO}_2$ values as our reference case. Fig. 2.6 shows the differences between $p\text{CO}_2$ values calculated from various constants (expressed as $\Delta p\text{CO}_2 = p\text{CO}_{2(\text{other constants})} - p\text{CO}_{2(\text{Mehrbach})}$) as a function of temperature.

In oceanic water (Fig. 2.6a), the differences between *Lueker* and *Mehrbach* and between *Millero* and *Mehrbach* are relatively small and constant ($\Delta p\text{CO}_2 < 10 \mu\text{atm}$ over the entire temperature range). Although *MP&M* and *Millero* both incorporate the experimental data of *Mehrbach*, the slopes of these lines are of different signs: $\Delta p\text{CO}_{2(\text{Millero})}$ decreases slightly with increasing temperature whereas $\Delta p\text{CO}_{2(\text{MP\&M})}$ increases. For $T > 4^\circ\text{C}$, $\Delta p\text{CO}_{2(\text{MP\&M})}$ is greater than $10 \mu\text{atm}$. Values of $\Delta p\text{CO}_{2(\text{G\&P})}$ and $\Delta p\text{CO}_{2(\text{Roy})}$ depend strongly on temperature. Within the temperature range of -2 to 4°C , $p\text{CO}_2$ differences are within $\pm 10 \mu\text{atm}$. The *Hansson* $p\text{CO}_2$ values are distinctive in their lack of agreement with the *Mehrbach* values at any temperature. The large differences in $\Delta p\text{CO}_2$ for *G&P*, *Roy*, and *Hansson* at higher temperatures might be associated with the K_2 values determined in artificial seawater without borate. Interactions of HCO_3^- and CO_3^{2-} with $\text{B}(\text{OH})_3$ or $\text{B}(\text{OH})_4^-$ depend strongly on temperature (Mojica Prieto and Millero, 2002).

For the two seawater/freshwater mixtures, different patterns of $\Delta p\text{CO}_2$ ($p\text{CO}_{2(\text{other constants})} - p\text{CO}_{2(\text{Mehrbach})}$) are observed (Fig. 2.6b, c) than for the seawater-only case (Fig 6a.). One significant difference is the greater sensitivity of $\Delta p\text{CO}_{2(\text{MP\&M})}$ to changes in temperature. In the low-salinity media, the slopes of the *MP&M* data are on parallel with

the *G&P* and *Roy* slopes. Another difference is *Millero* and *Hansson* show invariant with temperature changes. The implication is that salinity affects the temperature dependence of at least some of the $\Delta p\text{CO}_2$ calculations.

The *Millero* and *MP&M* constants were both determined in natural seawater and both incorporate the experimental data of *Mehrbach*. However, they exhibit different temperature dependencies. Comparing over all three media, the relatively constant $\Delta p\text{CO}_2$ for *Millero* indicates that *Millero* agrees better with *Mehrbach* than does *MP&M*. However, *Millero* (2010) points out that K_1 and K_2 of *Millero*, which have been fitted for estuarine waters, differ significantly from *Lueker*'s values below salinity 15. Thus, if we extrapolate the $p\text{CO}_2$ calculation to the extremely low salinity sea ice or river end-member, the results from *Millero* at $S = 0$ might represent the best accuracy of calculated $p\text{CO}_2$. Future high-precision field measurements are needed to help explain this issue.

Due to the lower dependence of this $\Delta p\text{CO}_2$ on temperature in low- S mixtures, the constants, excluding *Hansson*, can be considered comparable with *Mehrbach* (i.e., within $\pm 10 \mu\text{atm}$) over the temperature ranges of -2 to $6 \text{ }^\circ\text{C}$ in the seawater/river mixture and -2 to $10 \text{ }^\circ\text{C}$ in the seawater/sea-ice mixture. The smaller range of $\Delta p\text{CO}_2$ variation across all in these two low-salinity mixtures can be explained by the decreased sensitivity of K_2 to borate, which results from the decreased interaction of CO_3^{2-} and boric acid at the lower concentrations of CO_3^{2-} in low- S waters. In addition, the smaller range of $\Delta p\text{CO}_2$ variation in seawater and meltwater mixture is also associated with low- $p\text{CO}_2$ value of sea ice meltwater, even if the differences in K_1 and K_2 might still be significantly high among different sets of constants.

A large uncertainty, which we cannot address with this data set, is the accuracy of $p\text{CO}_2$ calculations in riverine waters, where $p\text{CO}_2$ can be over 500 μatm . Under high- $p\text{CO}_2$ conditions ($>500 \mu\text{atm}$), calculations based on DIC and TALK measurements yield large deviations between calculated and measured values. This phenomenon has been seen in field data (Lee et al., 2000; Millero et al., 2002) and in laboratory data (Lueker et al., 2000). The causes of the large discrepancies are unknown. Other pairs of carbonate parameters besides DIC and TALK might be better for evaluating the internal consistency of data for river-carbon studies.

4.2. Processes potentially affecting $\Delta p\text{CO}_2$

Here we identify a few processes that could contribute to the observed differences in salinity and between calculated and measured $p\text{CO}_2$ values. In most instances, $\Delta p\text{CO}_2$ was small. However, in the Canada Basin area with ice cover $<35\%$, calculated $p\text{CO}_2$ values were up to 50 μatm lower than measured $p\text{CO}_2$.

As noted in the Methods section, the underway system (source of the measured $p\text{CO}_2$ values) and the CTD rosette (source of the calculated $p\text{CO}_2$ values) were separated by ~ 20 m and may have sampled waters of different character or may be subject to different sampling artifacts (e.g., warming of the seawater as it passes through the underway system). We corrected for some processes (i.e., P and T corrections; Table 2.2), but others may be important as well.

One important consideration is the strong density stratification exhibited by some Arctic Ocean waters in summer. In the CHINARE2010 data, all CTD-measured salinity values were higher than those measured by the underway system. These differences indicate that the underway system, might introduce fresh water lens in the thin surface

layer, i.e. sea ice meltwater or river water, due to the up and down movement of wave, whereas the CTD system, sampling at depths of 3–5 m did not. Additionally, the differences might be introduced only due to the gradient of water masses, such as large horizontal gradient on shelves, or the amount of sea ice melting was different between both sampling locations. All of these scenarios can be simulated by the mixing model among seawater, river water, and sea ice meltwater. Moreover, more atmospheric CO₂ could be dissolved if the salinity of surface seawater was decreased by river water or sea ice meltwater. Other than these scenarios, we also evaluate two more sampling artifacts, including dissolution of CaCO₃ in bottle samples and incomplete flushing of Niskin bottles.

4.2.1. River-water inputs and mixing

The influence of river water on the underway *p*CO₂ measurements is evaluated using data from the Bering Sea shelf and the Chukchi Sea. First, we calculated the percent volume of added river water required to account for the salinity difference observed between the underway and CTD systems:

$$Salinity_{(CTD)} \times (1 - river\%) + Salinity_{(river)} \times river\% = Salinity_{(underway)} \quad (7)$$

where *river%* indicates the volume percentage of river water in the mixture. Second, the DIC and TAlk values of the water sampled by the underway system were predicted from the volume percentages (Eq 7) as well as the DIC and TAlk values of surface seawater (CTD bottle sample) and river water (values given Section 4.1) (Eqs 8, 9):

$$DIC_{(CTD)} \times (1 - river\%) + DIC_{(river)} \times river\% = DIC_{(underway)} \quad (8)$$

$$TAlk_{(CTD)} \times (1 - river\%) + TAlk_{(river)} \times river\% = TAlk_{(underway)} \quad (9)$$

Finally, these $DIC_{(underway)}$ and $TAlk_{(underway)}$ values, along with the *Mehrbach* constants, were used to calculate $pCO_{2(underway)}$. These values were compared to the *Mehrbach* $pCO_{2(DIC, TAlk)}$ values previously calculated for the bottle samples (section 3.3). The difference between these two pCO_2 values reflects the influence of river water on the underway pCO_2 measurements.

This evaluation (Eq 7) shows that the volume of river water contributing to the waters sampled by the underway system in these river-influenced shelf areas is <0.7%. The resulting $pCO_{2(underway)}$ values are lower than the corresponding $pCO_{2(DIC, TAlk)}$ values by only $0.1 \pm 0.1 \mu\text{atm}$. This difference is much smaller than our ΔpCO_2 values. For the Bering Sea shelf, bottle pCO_2 values were greater than measured values by $5.1 \pm 3.6 \mu\text{atm}$. In the Chukchi Sea, bottle pCO_2 values were higher than the measured values by $0.7 \pm 4.6 \mu\text{atm}$. Thus, the influence of river water on waters sampled by the underway system is negligible.

4.2.2. In situ sea ice meltwater inputs and mixing

Although Arctic Ocean surface water is strongly mixed by wind forcing and sea ice movement, a thin layer of sea ice meltwater may still cap surface-ocean areas with fast sea ice melting in summer. The influence of in situ sea ice meltwater on underway pCO_2 measurements in the Canada Basin can be evaluated in the same manner as the influence of river water on the Bering and Chukchi Sea shelves (i.e., via Eqs. 7–9 but with the riverine end-member replaced by the sea ice meltwater end-member of section 4.1). The addition of sea ice meltwater to seawater would be expected to decrease surface-water pCO_2 values.

From Eq. 7, the estimated average contribution of sea ice meltwater in the Canada Basin is <0.9% by volume. The resulting $p\text{CO}_2(\text{underway})$ values are lower than the corresponding bottle $p\text{CO}_2(\text{DIC, TAlk})$ values by $1.6 \pm 0.9 \mu\text{atm}$. Differences were approximately the same in the lightly and densely ice-covered areas ($1.5 \pm 1.0 \mu\text{atm}$ and $1.6 \pm 0.8 \mu\text{atm}$, respectively). These values are smaller than the corresponding regional $\Delta p\text{CO}_2$ values ($-23 \pm 15.5 \mu\text{atm}$ in the lightly ice-covered region, and $-3.3 \pm 6.8 \mu\text{atm}$ in the region of heavy ice cover; Table 2.3). In addition, removing the influence of sea-ice melt from the measured $p\text{CO}_2$ would result in an even larger $\Delta p\text{CO}_2$ difference. We conclude that the underestimates of calculated $p\text{CO}_2$ values (i.e., the negative $\Delta p\text{CO}_2$ values) were caused not by sampling of more fresh water in the underway system but rather the temperature and salinity dependencies of K_1 and K_2 . Moreover, our current data cover only a limited salinity range, and we cannot predict whether our findings might be applicable to extremely low salinities (e.g., fresh river water or sea-ice melt water).

4.2.3. Atmospheric CO₂ invasion into sea ice meltwater in the Canada Basin

Because surface $p\text{CO}_2$ in the Arctic Ocean is undersaturated with respect to atmospheric CO₂ and because in situ sea ice meltwater can dissolve more CO₂ due to its low salinity, atmospheric CO₂ may readily invade this thin surface layer. During the CHINARE2010 cruise, surface meltwaters would have been only partially equilibrated with atmospheric CO₂ because months are required to reach equilibrium. CO₂ invasion increases meltwater DIC but does not change TAlk.

Here we evaluate the maximum influence of atmospheric CO₂ invasion by assuming an equilibrium between atmospheric CO₂ (385 μatm) and surface meltwater. The calculation is the same as in section 4.2.2 except that we let the surface meltwater

equilibrate with air. The amount of CO₂ invasion is calculated from the solubility of CO₂ in seawater and the $p\text{CO}_2$ difference between meltwater and the atmosphere. The volume of meltwater affected by CO₂ invasion is estimated from salinity difference of underway and CTD systems, as shown above. In this hypothetical example, the underway system measures the mixture of seawater and atmospheric CO₂ equilibrated surface meltwater. The resulting $p\text{CO}_{2(\text{underway})}$ of this mixture would be $0.4 \pm 0.2 \mu\text{atm}$ lower than the corresponding bottle $p\text{CO}_{2(\text{DIC, TAlk})}$ for the Canada Basin. Combining this result with the higher bottle $p\text{CO}_2$ of $1.6 \pm 0.9 \mu\text{atm}$ in the meltwater scenario of section 4.2.2, we find that atmospheric CO₂ invasion would increase underway $p\text{CO}_2$ by $1.2 \mu\text{atm}$ at most. In surface meltwater that is only partially equilibrated with the atmosphere, this influence would be even smaller. Therefore, this process can be neglected in field internal-consistency checks.

4.2.4. CaCO₃ dissolution in sample bottles

Crystals of ikaite (a polymorph of calcium carbonate, CaCO₃) may be present in waters associated with fast-melting ice. Ikaite has been documented in the Arctic Ocean through direct observation (Dieckmann et al., 2010) and, indirectly, through its high TAlk/DIC chemical signature in sea ice brine (Rysgaard et al., 2007). Ikaite crystals are stable at temperatures below 4°C and are unstable at room temperature (Rysgaard et al., 2012). It is therefore possible that CaCO₃ is present in waters collected in low ice cover ocean areas (e.g., southern Canada Basin), with subsequent dissolution during storage or analysis. Dissolution of CaCO₃ in seawater increases TAlk and DIC in a 2:1 ratio and can decrease $p\text{CO}_2$ in bottle samples. An estimate of $15 \mu\text{mol/kg}$ CaCO₃ dissolved in a water sample would be sufficient to explain the high $\Delta p\text{CO}_2$ observed in the lightly ice-covered

southern Canada Basin. This estimate amount of CaCO_3 dissolution in bottle samples is comparable to 160–240 $\mu\text{mol/kg}$ of ikaite estimated from melted sea ice (Rysgaard et al., 2012) and to 640–960 $\mu\text{mol/kg}$ observed in the summer ice in the Fram Strait (Rysgaard et al., 2013). Supporting evidence for CaCO_3 dissolution would include samples with (a) calculated $p\text{CO}_2$ much lower than measured $p\text{CO}_2$ and (b) anomalously high TAlk compared to samples with similar salinities.

Within the Canada Basin, we find that TAlk is linearly related to salinity in the densely ice-covered Canada Basin (Fig. 2.7a). The 95% confidence interval of the mean for these TAlk data represents that we can 95% certain a portion of TAlk data in the lightly ice-covered southern Canada Basin follow this linear relationship. It is noted that some TAlk data in the light sea ice cover areas are anomalously high compared to other data with similar salinities. We further use a threshold of 15 μatm , a sum of the accuracy of $p\text{CO}_2$ data in cold waters ($\sim 5 \mu\text{atm}$ from *Mehrbach*, section 3.5) and an uncertainty for the calculation of $p\text{CO}_2(\text{DIC, TAlk})$ for polar waters (10 μatm) (Wanninkhof et al., 1999), to separate large-magnitude $\Delta p\text{CO}_2$ data (Fig. 2.7b). This threshold is consistent with the uncertainty of $\Delta p\text{CO}_2(\text{calculated-measured})$ calculations ($-0.7 \pm 16.3 \mu\text{atm}$) as documented in an earlier field test of internal consistency (Chierici and Fransson, 2009). Almost all samples with absolute $\Delta p\text{CO}_2 > 15 \mu\text{atm}$ exhibit higher TAlk values at similar salinities. This pattern supports the hypothesis that dissolution of CaCO_3 in areas of recent ice melt, such as the southern Canada Basin, may influence the $p\text{CO}_2$ of bottle samples. Moreover, it also implies that only a portion of stations might be affected by CaCO_3 dissolution. In contrast, in the heavily ice-covered northern Canada Basin, the linear relationship between bottle TAlk and salinity suggests that no or indiscernible amount CaCO_3

dissolution in the heavily ice-covered Canada Basin. This possibility deserves further research.

4.2.5. Incomplete flushing of Niskin bottles

Lightly ice-covered Canada Basin experiencing fast summer sea ice melt, a strong vertical density gradient develops. As a result, the base of the surface mixed layer can be as shallow as 10 m (compared with 30 m in the more northerly region of dense ice cover). Such strong vertical gradients may lead to sampling artifacts. When the CTD sampling rosette is deployed from the ship, it descends through the water column with all Niskin bottles open. Upon ascent, bottles are selectively closed at certain depths to collect water samples. During sampling near/in a strongly stratified halocline, some residue of deeper waters may be incorporated into the shallower samples if the bottles are not thoroughly flushed during ascent. In the case of the southern Canada basin, some high-salinity subsurface water may be retained on the bottle inner wall, and therefore mixed with the overlying lower-salinity seawater of the surface layer that is ostensibly sampled. It means that higher $p\text{CO}_2$ value subsurface water than the surface water will increase the $p\text{CO}_2$ value of the seawater sampled in the Niskin bottle. Therefore, primary production might be importantly associated this case because it consumes DIC and decreases $p\text{CO}_2$ and thus influences the vertical distribution of $p\text{CO}_2$ in the euphotic zone.

A comparison of bottle salinities versus CTD salinities might be one way to identify and estimate the influence of incomplete flushing. Bottle salinities were not measured for our 2010 cruise, so we instead examined surface salinity differences between bottle data and CTD records which were also collected in the Chukchi Sea and Canada Basin from the Shelf Basin Interactions Project (SBI) cruise of summer 2002 (Bates, 2006). Data is

downloaded from: <http://cdiac.ornl.gov/ftp/oceans/CARINA/Healy/HLY-02-03/>. Stations #27 to #35 were located in waters ranging from 250 m to 3000 m depth, with ice cover between 10% and 55%. Five of these nine stations had surface-water bottle salinities higher than the corresponding CTD record. The mean difference was 0.03; the maximum difference was 0.08. These differences confirm that in a strongly stratified surface ocean, high-salinity subsurface waters may be brought to the surface in a Niskin bottle. The influence of subsurface water contributions finally results in higher bottle S , DIC, and TAlk.

We use these mean and maximum salinity differences to estimate the influence of subsurface water on calculations of bottle $p\text{CO}_2$. We characterize the subsurface water by averaging data from the 20 m layer over our lightly ice-covered stations: $S = 28.2$, TAlk = 2092.6 $\mu\text{mol/kg}$, and DIC = 1976.0 $\mu\text{mol/kg}$. Salinity differences are used to estimate the contribution of subsurface waters by volume. Then we mix this amount of subsurface water with surface water to predict S , DIC, and TAlk values to calculate a predicted bottle $p\text{CO}_2$. This calculation shows that an average of 4.9% and 1.8% subsurface water (by volume) can account for surface salinity increases of 0.08 and 0.03, respectively. Correspondingly, predicted bottle $p\text{CO}_2$ would be smaller than bottle $p\text{CO}_2$ by 0.8 ± 0.9 μatm for 0.08 unit salinity increase, and by 0.3 ± 0.3 μatm for 0.03 unit salinity increase. In addition, those five stations in the SBI2002 summer cruise showed similar results, showing predicted $p\text{CO}_2$ smaller than bottle $p\text{CO}_2$ by 3.8 ± 0.6 μatm for 0.08 unit salinity increase, and by 1.5 ± 0.2 μatm for 0.03 unit salinity increase. These values are negligibly small compared with the field discrepancies of up to 50 μatm .

5. Conclusions

We used recent high-precision Arctic Ocean field measurements of DIC, TAlk, and $p\text{CO}_2$, along with seven sets of carbonic acid dissociation constants, to evaluate the internal consistency of the CHINARE2010 carbonate system data set and to identify best-fit sets of dissociation constants. Our observations show that the constants of *Mehrbach* and *Lueker* yield the best internal consistency over the temperature range of -1.5 to 10.5 °C and the salinity range of 25.8 to 33.1. Considering our findings plus the recommendations of prior work in lower-latitude oceans, we recommend the use of these two sets of constants for studies of the global oceanic carbonate system.

In addition, across seven sets of dissociation constants, $\Delta p\text{CO}_2$ (calculated–measured) values depend on both temperature and salinity because $p\text{CO}_2$ calculation is a function of temperature and salinity. We observed that $\Delta p\text{CO}_2$ decreased with increasing latitude and concluded that this pattern is associated with the temperature and salinity dependencies of K_1 and K_2 .

We also estimate the accuracy of $p\text{CO}_2$ values calculated from measurements of DIC and TAlk and the *Mehrbach* and *Lueker* constants. For our Pacific-sector stations outside the Canada Basin area of active sea-ice melt and light ice cover, mean $\Delta p\text{CO}_2$ (calculated – measured) values were 1.5 ± 5.7 μatm for *Mehrbach* and 2.3 ± 5.4 μatm for *Lueker*. This good agreement indicates highly accurate $p\text{CO}_2$ calculations, even though K_1 and K_2 for these calculations were extrapolated to temperatures lower than those used to experimentally determine the constants. In the Bering Sea basin, where T and S fell within the recommended ranges of application for the dissociation constants, calculated

values of $p\text{CO}_2$ from *Mehrbach* and *Lueker* were higher than measured values (mean $\Delta p\text{CO}_2 = 2.4 \mu\text{atm}$). In the colder, ice-covered Canada Basin, the opposite was true: calculated $p\text{CO}_2$ values were lower than the observations (mean $\Delta p\text{CO}_2 = -2.2 \mu\text{atm}$). It indicates that the $p\text{CO}_2$ might be underestimated due to extrapolation to lower temperatures, with the uncertainty to be $\sim 5 \mu\text{atm}$ in accuracy. Largest differences in $\Delta p\text{CO}_2$ were observed in the southern Canada Basin, a region of active summer ice melt (<35% ice cover; $\Delta p\text{CO}_2 = -22 \mu\text{atm}$).

We also assessed the significance of several processes that might contribute to $\Delta p\text{CO}_2$ values. The influence of river water on shelf surface waters, in situ sea ice meltwater on Canada Basin waters, atmospheric CO_2 invasion into the surface layer of sea ice meltwater, and insufficient flushing of Nixsin bottle were all judged to be negligible. Dissolution of CaCO_3 (ikaite) in our sample bottles might, however, be sufficient to explain even the large $\Delta p\text{CO}_2$ values characteristic of the southern Canada Basin. More solid evidence is needed to verify the potential importance of this process. In summary, the marine carbonate system in the Arctic Ocean is influenced by a combination of processes, and further assessment of their relative roles is needed.

References

- ACIA, 2005. Arctic Climate Impact Assessment - Scientific Report. Cambridge University Press, Cambridge, UK, 1046 pp.
- Amundsen, H. et al., 2013. AMAP Assessment 2013: Arctic Ocean Acidification. Arctic Monitoring and Assessment Programme (AMAP).
- Arrigo, K.R., van Dijken, G. and Pabi, S., 2008. Impact of a shrinking Arctic ice cover on marine primary production. *Geophys. Res. Lett.*, 35(19).
- Arrigo, K.R. and van Dijken, G.L., 2011. Secular trends in Arctic Ocean net primary production. *J. Geophys. Res.*, 116: C09011.
- Bates, N.R., 2006. Air-sea CO₂ fluxes and the continental shelf pump of carbon in the Chukchi Sea adjacent to the Arctic Ocean. *J. Geophys. Res.*, 111: C10013.
- Bates, N.R., Cai, W.J. and Mathis, J.T., 2011. The Ocean Carbon Cycle in the Western Arctic Ocean: Distributions and Air-Sea Fluxes of Carbon Dioxide. *Oceanography*, 24(3): 186-201.
- Bates, N.R. and Mathis, J.T., 2009. The Arctic Ocean marine carbon cycle: evaluation of air-sea CO₂ exchanges, ocean acidification impacts and potential feedbacks. *Biogeosciences*, 6(11): 2433-2459.
- Bates, N.R., Moran, S.B., Hansell, D.A. and Mathis, J.T., 2006. An increasing CO₂ sink in the Arctic Ocean due to sea-ice loss. *Geophys. Res. Lett.*, 33(23).

- Cai, W.-J. et al., 2010a. Alkalinity distribution in the western North Atlantic Ocean margins. *J. Geophys. Res.*, 115: C08014.
- Cai, W.J. et al., 2010b. Decrease in the CO₂ Uptake Capacity in an Ice-Free Arctic Ocean Basin. *Sci*, 329(5991): 556-559.
- Chierici, M. and Fransson, A., 2009. Calcium carbonate saturation in the surface water of the Arctic Ocean: undersaturation in freshwater influenced shelves. *Biogeosciences*, 6(11): 2421-2431.
- Comiso, J.C., Parkinson, C.L., Gersten, R. and Stock, L., 2008. Accelerated decline in the Arctic Sea ice cover. *Geophys. Res. Lett.*, 35(1).
- Dickson, A.G., 1990. Standard Potential of the Reaction -
 $\text{AgCl(s)} + 1/2\text{H}_2(\text{g}) = \text{Ag(s)} + \text{HCl(aq)}$, and the Standard Acidity Constant of the Ion HSO_4^- in Synthetic Sea Water from 273.15 to 318.15 K. *J. Chem. Thermodyn.*, 22(2): 113-127.
- Dickson, A.G. and Millero, F.J., 1987. A Comparison of the Equilibrium-Constants for the Dissociation of Carbonic-Acid in Seawater Media. *Deep-Sea Res. I*, 34(10): 1733-1743.
- Dickson, A.G., Sabine, C.L. and Christian, J.R. (Editors), 2007. Guide to best practices for ocean CO₂ measurements. *PIES Special Publication*, 191 pp.
- Dieckmann, G.S. et al., 2010. Brief Communication: Ikaite (CaCO₃·6H₂O) discovered in Arctic sea ice. *Cryosphere*, 4(2): 227-230.

- Fransson, A., Chierici, M. and Nojiri, Y., 2009. New insights into the spatial variability of the surface water carbon dioxide in varying sea ice conditions in the Arctic Ocean. *Cont. Shelf Res.*, 29(10): 1317-1328.
- Goyet, C. and Poisson, A., 1989. New Determination of Carbonic-Acid Dissociation-Constants in Seawater as a Function of Temperature and Salinity. *Deep-Sea Res. A*, 36(11): 1635-1654.
- Grebmeier, J.M. et al., 2006. A Major Ecosystem Shift in the Northern Bering Sea. *Sci*, 311(5766): 1461-1464.
- Hansson, I., 1973. A new set of acidity constants for carbonic acid and boric acid in sea water. *Deep-Sea Res. Oceanogr. Abstr.*, 20(5): 461-478.
- Huang, W.J., Wang, Y.C. and Cai, W.J., 2012. Assessment of sample storage techniques for total alkalinity and dissolved inorganic carbon in seawater. *Limnol. Oceanogr. Methods*, 10: 711-717.
- Jutterström, S. and Anderson, L.G., 2005. The saturation of calcite and aragonite in the Arctic Ocean. *Mar. Chem.*, 94(1-4): 101-110.
- Jutterström, S. and Anderson, L.G., 2010. Uptake of CO₂ by the Arctic Ocean in a changing climate. *Mar. Chem.*, 122(1-4): 96-104.
- Lee, K., Millero, F.J., Byrne, R.H., Feely, R.A. and Wanninkhof, R., 2000. The recommended dissociation constants for carbonic acid in seawater. *Geophys. Res. Lett.*, 27(2): 229-232.

- Lee, K., Millero, F.J. and Campbell, D.M., 1996. The reliability of the thermodynamic constants for the dissociation of carbonic acid in seawater. *Mar. Chem.*, 55(3-4): 233-245.
- Lee, K., Millero, F.J. and Wanninkhof, R., 1997. The carbon dioxide system in the Atlantic Ocean. *J. Geophys. Res.*, 102(C7): 15693-15707.
- Li, W.K.W., McLaughlin, F.A., Lovejoy, C. and Carmack, E.C., 2009. Smallest Algae Thrive As the Arctic Ocean Freshens. *Sci*, 326(5952): 539.
- Lueker, T.J., Dickson, A.G. and Keeling, C.D., 2000. Ocean $p\text{CO}_2$ calculated from dissolved inorganic carbon, alkalinity, and equations for K_1 and K_2 : validation based on laboratory measurements of CO_2 in gas and seawater at equilibrium. *Mar. Chem.*, 70(1-3): 105-119.
- Maslanik, J.A. et al., 2007. A younger, thinner Arctic ice cover: Increased potential for rapid, extensive sea-ice loss. *Geophys. Res. Lett.*, 34(24).
- Mathis, J.T., Cross, J.N. and Bates, N.R., 2011. Coupling primary production and terrestrial runoff to ocean acidification and carbonate mineral suppression in the eastern Bering Sea. *J. Geophys. Res.*, 116: C02030.
- Mathis, J.T. et al., 2012. Storm-induced upwelling of high $p\text{CO}_2$ waters onto the continental shelf of the western Arctic Ocean and implications for carbonate mineral saturation states. *Geophys. Res. Lett.*, 39.

- Mehrbach, C., Culberso, Ch, Hawley, J.E. and Pytkowic, Rm, 1973. Measurement of the Apparent Dissociation-Constants of Carbonic-Acid in Seawater at Atmospheric-Pressure. *Limnol. Oceanogr.*, 18(6): 897-907.
- Millero, F.J., 1995. Thermodynamics of the Carbon Dioxide System in the Oceans. *Geochim. Cosmochim. Acta*, 59(4): 661-677.
- Millero, F.J., 2010. Carbonate constants for estuarine waters. *Marine and Freshwater Research*, 61(2): 139-142.
- Millero, F.J., Graham, T.B., Huang, F., Bustos-Serrano, H. and Pierrot, D., 2006. Dissociation constants of carbonic acid in seawater as a function of salinity and temperature. *Mar. Chem.*, 100(1-2): 80-94.
- Millero, F.J. et al., 2002. Dissociation constants for carbonic acid determined from field measurements. *Deep-Sea Res. I*, 49(10): 1705-1723.
- Mojica Prieto, F.J. and Millero, F.J., 2002. The values of $pK_1 + pK_2$ for the dissociation of carbonic acid in seawater. *Geochim. Cosmochim. Acta*, 66(14): 2529-2540.
- Mucci, A., Lansard, B., Miller, L.A. and Papakyriakou, T.N., 2010. CO₂ fluxes across the air-sea interface in the southeastern Beaufort Sea: Ice-free period. *J. Geophys. Res.*, 115: C04003.
- Murata, A. and Takizawa, T., 2003. Summertime CO₂ sinks in shelf and slope waters of the western Arctic Ocean. *Cont. Shelf Res.*, 23(8): 753-776.

- Pabi, S., van Dijken, G.L. and Arrigo, K.R., 2008. Primary production in the Arctic Ocean, 1998-2006. *J. Geophys. Res.*, 113: C08005.
- Park, P.K., 1969. Oceanic CO₂ System - an Evaluation of 10 Methods of Investigation. *Limnol. Oceanogr.*, 14(2): 179-186.
- Peterson, B.J. et al., 2002. Increasing river discharge to the Arctic Ocean. *Sci*, 298(5601): 2171-2173.
- Pierrot, D., Lewis, E. and Wallace, D., 2006. MS Excel program developed for CO₂ system calculations. ORNL/CDIAC-105a. Carbon Dioxide Information Analysis Center, Oak Ridge National Laboratory, US Department of Energy, Oak Ridge, Tennessee.
- Pierrot, D. et al., 2009. Recommendations for autonomous underway *p*CO₂ measuring systems and data-reduction routines. *Deep-Sea Res. II*, 56(8–10): 512-522.
- Robbins, L.L. et al., 2013. Baseline Monitoring of the Western Arctic Ocean Estimates 20% of Canadian Basin Surface Waters Are Undersaturated with Respect to Aragonite. *PLOS ONE*, 8(9): e73796.
- Roy, R.N. et al., 1993. The dissociation constants of carbonic acid in seawater at salinities 5 to 45 and Temperatures 0 to 45°C. *Mar. Chem.*, 44(2-4): 249-267.
- Rysgaard, S. et al., 2012. Ikaite crystals in melting sea ice - implications for *p*CO₂ and pH levels in Arctic surface waters. *Cryosphere*, 6(4): 901-908.

- Rysgaard, S., Glud, R.N., Sejr, M.K., Bendtsen, J. and Christensen, P.B., 2007. Inorganic carbon transport during sea ice growth and decay: A carbon pump in polar seas. *J. Geophys. Res.*, 112: C03016.
- Rysgaard, S. et al., 2013. Ikaite crystal distribution in winter sea ice and implications for CO₂ system dynamics. *Cryosphere*, 7(2): 707-718.
- Schlitzer, R., 2014. Ocean data view, <http://odv.awi.de>, 2014.
- Striegl, R.G., Dornblaser, M.M., Aiken, G.R., Wickland, K.P. and Raymond, P.A., 2007. Carbon export and cycling by the Yukon, Tanana, and Porcupine rivers, Alaska, 2001–2005. *Water Resour. Res.*, 43(2).
- Takahashi, T., Olafsson, J., Goddard, J.G., Chipman, D.W. and Sutherland, S.C., 1993. Seasonal variation of CO₂ and nutrients in the high-latitude surface oceans: A comparative study. *Global Biogeochem. Cycles*, 7(4): 843–878.
- Uppström, L.R., 1974. The boron/chlorinity ratio of deep-sea water from the Pacific Ocean. *Deep-Sea Res. Oceanogr. Abstr.*, 21(2): 161-162.
- Wang, M.Y. and Overland, J.E., 2009. A sea ice free summer Arctic within 30 years? *Geophys. Res. Lett.*, 36.
- Wanninkhof, R., Lewis, E., Feely, R.A. and Millero, F.J., 1999. The optimal carbonate dissociation constants for determining surface water *p*CO₂ from alkalinity and total inorganic carbon. *Mar. Chem.*, 65(3-4): 291-301.

Table 2.1

Determinations of dissociation constants of carbonic acid in natural seawater (SW) and artificial seawater (ASW)

Reference	Media	Temperature Range (°C)	Salinity range	Type
Hansson (1973)	ASW	5 to 30	20 to 40	Original work
Mehrbach et al. (1973)	SW	2 to 35	19 to 43	Original work
Mehrbach et al. (1973) refit by Dickson and Millero (1987)	SW	2 to 35	19 to 43	Refit
Hansson (1973) refit by Dickson and Millero (1987)	ASW	5 to 30	20 to 40	Refit
Mehrbach et al. (1973) and Hansson (1973) by Dickson and Millero (1987)	ASW/SW	2 to 35	20 to 40	Refit
Goyet and Poisson (1989)	ASW	-1 to 40	10 to 50	Original work
Roy et al. (1993)	ASW	0 to 45	5 to 45	Original work
Goyet and Poisson (1989) and Roy et al. (1993) refit by Millero (1995)	ASW	0 to 45	0 to 45	Refit
Lueker et al. (2000)	SW	2 to 35	19 to 43	Refit
Mojica-Prieto and Millero (2002)	SW	0 to 45	5 to 42	Original work
Millero et al. (2006)	SW	0 to 50	1 to 50	Original work
Millero (2010)	SW	0 to 50	1 to 50	Refit

Table 2.2

Surface-water regional ranges (and means \pm standard deviations) of CTD temperature, CTD salinity, underway $p\text{CO}_2$, and stepwise pressure and temperature $p\text{CO}_2$ corrections

Region	CTD Temperature ($^{\circ}\text{C}$)	CTD Salinity	$p\text{CO}_2(\text{UW})^{\text{a}}$ (μatm)	$\delta p\text{CO}_2(P)^{\text{b}}$ (μatm)	$\delta p\text{CO}_2(t)^{\text{c}}$ (μatm)
All stations	-1.5 to 10.5 (3.4 ± 3.8)	25.8 to 33.1 (30.1 ± 2.3)	88.2 to 385.1 (258.6 ± 69)	-2.2 to 4.7 (0.7 ± 1.5)	-9.7 to 3.7 (-1.2 ± 2.4)
Bering Sea basin	7.2 to 8.5 (7.7 ± 0.5)	31.6 to 33.1 (32.8 ± 0.4)	194.9 to 385.1 (295.1 ± 80.4)	-1.9 to -0.5 (-1.1 ± 0.5)	-4.4 to -0.7 (-2.1 ± 1.3)
Bering Sea shelf	0.5 to 10.5 (6.3 ± 2.4)	25.9 to 32.9 (31.2 ± 1.4)	137.8 to 367.5 (230.7 ± 78.9)	-1.3 to 1.2 (-0.1 ± 0.7)	-8.2 to 1.7 (-1.7 ± 2.3)
Chukchi Sea	-0.5 to 6.7 (4.0 ± 1.9)	27.2 to 32.3 (30.7 ± 1.5)	88.2 to 324.4 (214.8 ± 53.2)	0.1 to 3.8 (0.8 ± 1)	-9.7 to 3.7 (-0.6 ± 3.1)
Canada Basin stations with <35% ice cover	-1.2 to 0.4 (-0.6 ± 0.6)	25.8 to 27.2 (26.5 ± 0.4)	294.5 to 333.4 (313.6 ± 11.4)	0.6 to 2.8 (1.6 ± 0.7)	-6.1 to 2.5 (-1.3 ± 2.6)
Canada Basin stations with >35% ice cover	-1.5 to -0.8 (-1.4 ± 0.2)	25.8 to 30.6 (28.9 ± 1.6)	243 to 322.2 (289.9 ± 20.9)	-2.2 to 4.7 (2 ± 2.1)	-6.1 to 1.4 (-0.5 ± 1.8)

- Underway $p\text{CO}_2$ after application of pressure and temperature corrections (to match bottle data).
- Correction applied to convert instrument-observed underway $p\text{CO}_2$, $p\text{CO}_2(\text{obs})$ to 1 atm pressure.
- Correction applied to convert pressure-corrected underway $p\text{CO}_2$, $p\text{CO}_2(\text{obs}, 1 \text{ atm})$ to CTD temperature of corresponding bottle sample.

Table 2.3

Regional $p\text{CO}_2$ differences (means \pm standard deviations) in units of μatm : $\Delta p\text{CO}_2 =$
calculated – measured

Data set ^a	Bering Sea basin	Bering Sea shelf	Chukchi Sea	Canada Basin (lightly ice- covered)	Canada Basin (densely ice- covered)	All, except (Basin area with light ice-cover)
<i>Mehrbach</i>	2.2 \pm 4.6	5.1 \pm 3.6	0.7 \pm 4.6	-23 \pm 15.5	-3.3 \pm 6.8	1.5 \pm 5.7
<i>Lueker</i>	2.5 \pm 4.5	5.5 \pm 3.7	1.3 \pm 4.5	-21 \pm 15.6	-1.2 \pm 6.9	2.3 \pm 5.4
<i>MP&M</i>	10 \pm 4	11.3 \pm 4	5.6 \pm 5.1	-22.2 \pm 15.5	-1.3 \pm 7.3	6.6 \pm 7
<i>Millero</i>	7.6 \pm 4.1	9.8 \pm 4	5.5 \pm 4.4	-15.7 \pm 15.7	4.3 \pm 7	6.9 \pm 5.3
<i>G&P</i>	14.5 \pm 3.9	13.3 \pm 5.4	5.8 \pm 5.8	-25 \pm 15.3	-6 \pm 6.9	7 \pm 9.5
<i>Roy</i>	14.4 \pm 3.9	13.2 \pm 5.4	5.6 \pm 5.8	-25 \pm 15.3	-6.3 \pm 6.9	6.9 \pm 9.6
<i>Hansson</i>	20.5 \pm 4.4	19.9 \pm 5.8	15 \pm 4.9	-4.7 \pm 15.9	16.2 \pm 7.4	17.7 \pm 6.1

- a. The labels “*Mehrbach*”, “*Lueker*”, “*MP&M*”, “*Millero*”, “*G&P*”, “*Roy*”, and *Hansson* refer to as Mehrbach et al. (1973) as refit by Dickson and Millero (1987), Lueker et al. (2000), Mojica-Prieto and Millero (2002), Millero (2010), Goyet and Poisson (1989), Roy et al. (1993), and Hansson (1973) as refit by Dickson and Millero (1987), separately.

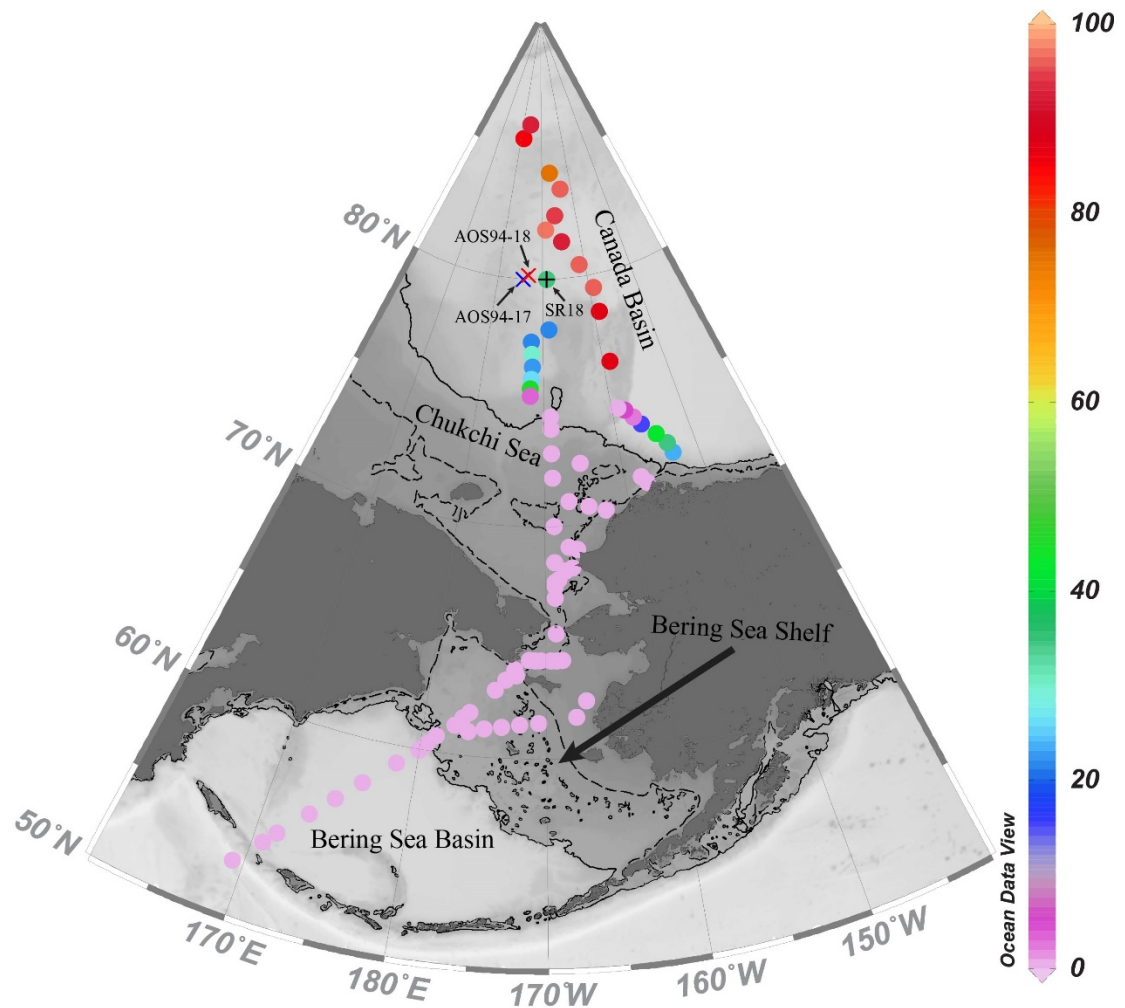


Figure 2.1. Map of sampling stations and sea ice cover during the CHINARE2010 cruise (summer 2010). The black lines indicate the 40 m isobath (dashed line) and the 200 m isobath (solid line). The colored dots indicates sea ice cover at each station. The colored cross symbols indicate AOS94 stations 17 (blue) and 18 (red). The black plus symbol indicates CHINARE2010 station SR18. This figure is plotted using Ocean Data View (Schlitzer, 2014).

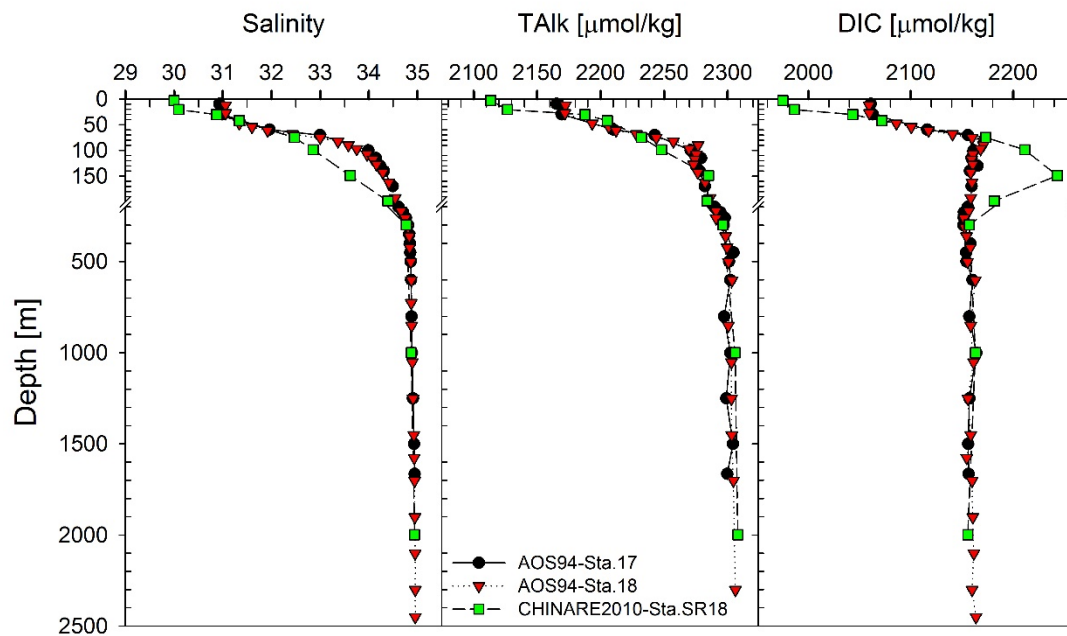


Figure 2.2. Vertical profiles of salinity, TAlk, and DIC measured at two Arctic Ocean Section 1994 (AOS94) stations and a CHINARE2010 station. Station locations: AOS94 Station 17 = 174.31°W , 79.99°N ; AOS94 Station 18 = 173.25°W , 80.15°N ; CHINARE2010 Station SR18 = 169.10°W , 79.99°N .

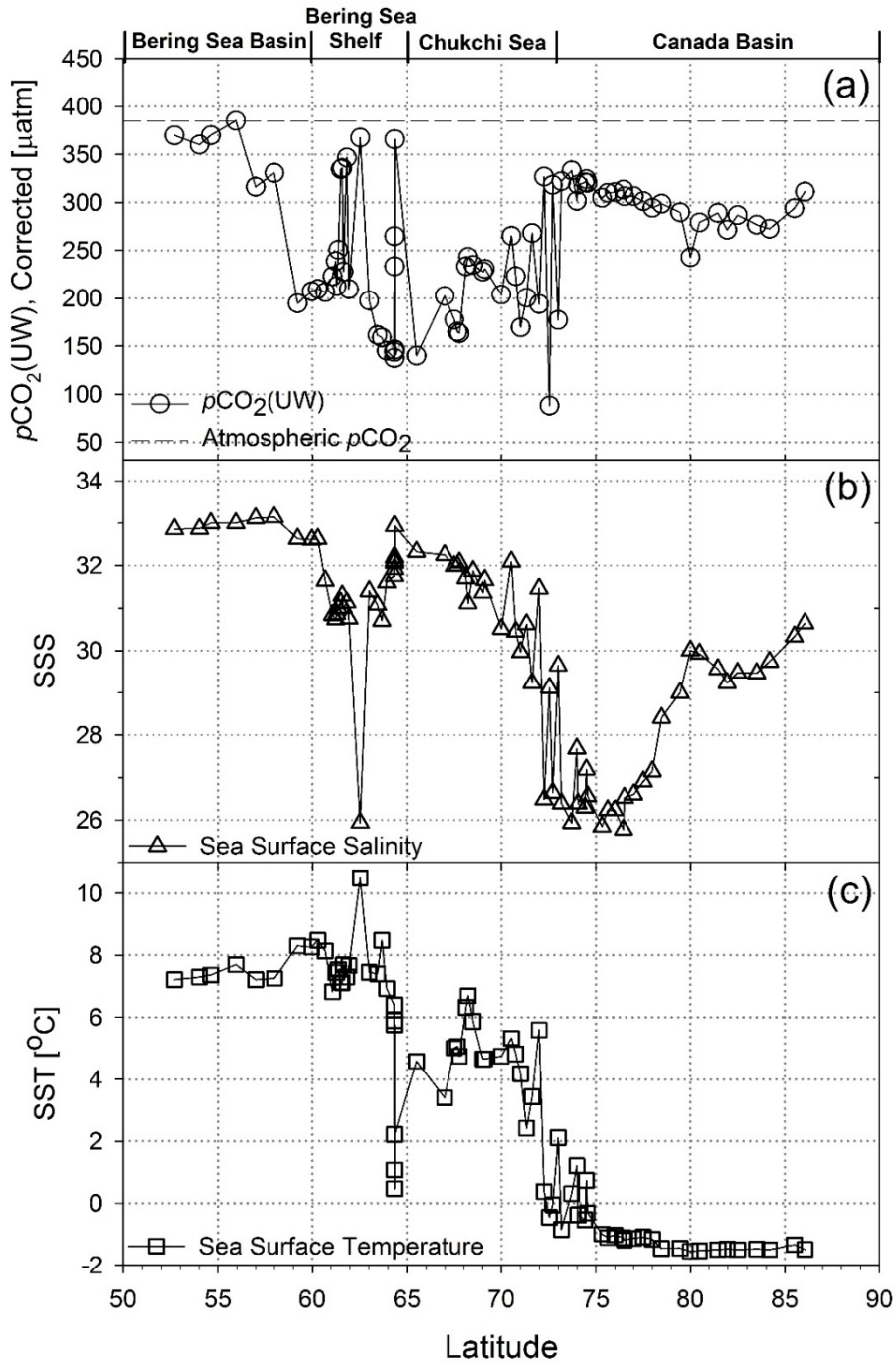


Figure 2.3. Latitudinal distributions of underway surface-water (a) $p\text{CO}_2(\text{UW})$, (b) Sea surface salinity, and (c) Sea surface temperature. The open circles indicate $p\text{CO}_2(\text{UW})$ (i.e., underway $p\text{CO}_2$ corrected to CTD temperatures and 1 atm pressure).

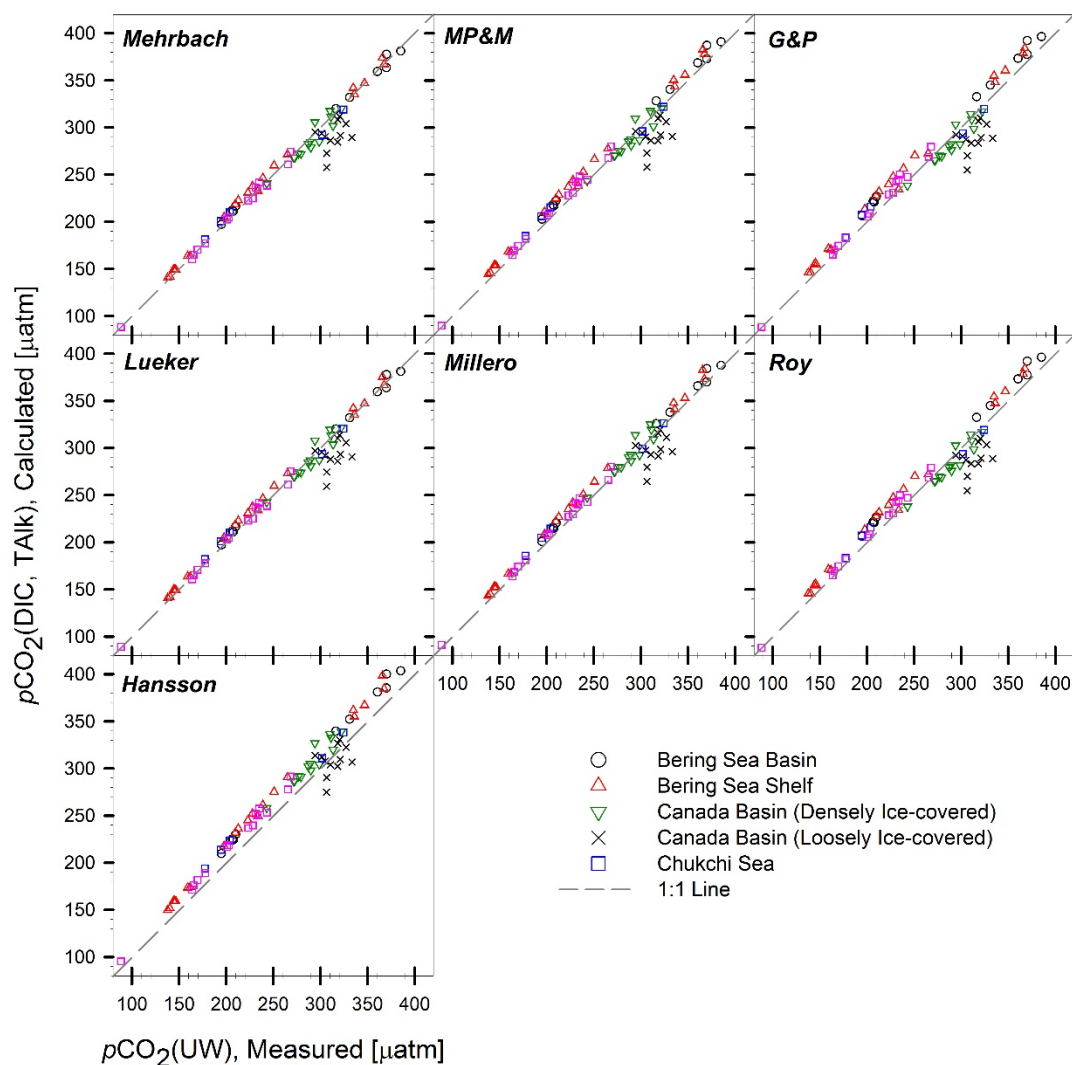


Figure 2.4. A comparison of measured $p\text{CO}_2$ and $p\text{CO}_2$ calculated from measured DIC, measured TAlk and seven different sets of dissociation constants. *Mehrbach* = Mehrbach *et al.* (1973) as refit by Dickson and Millero (1987). *Lueker* = Lueker *et al.* (2000), *Hansson* = Hansson (1973) as refit by Dickson and Millero (1987). *G&P* = Goyet and Poisson (1989). *Roy* = Roy *et al.* (1993). *MP&M* = Mojica-Prieto and Millero (2002). *Millero* = Millero (2010).

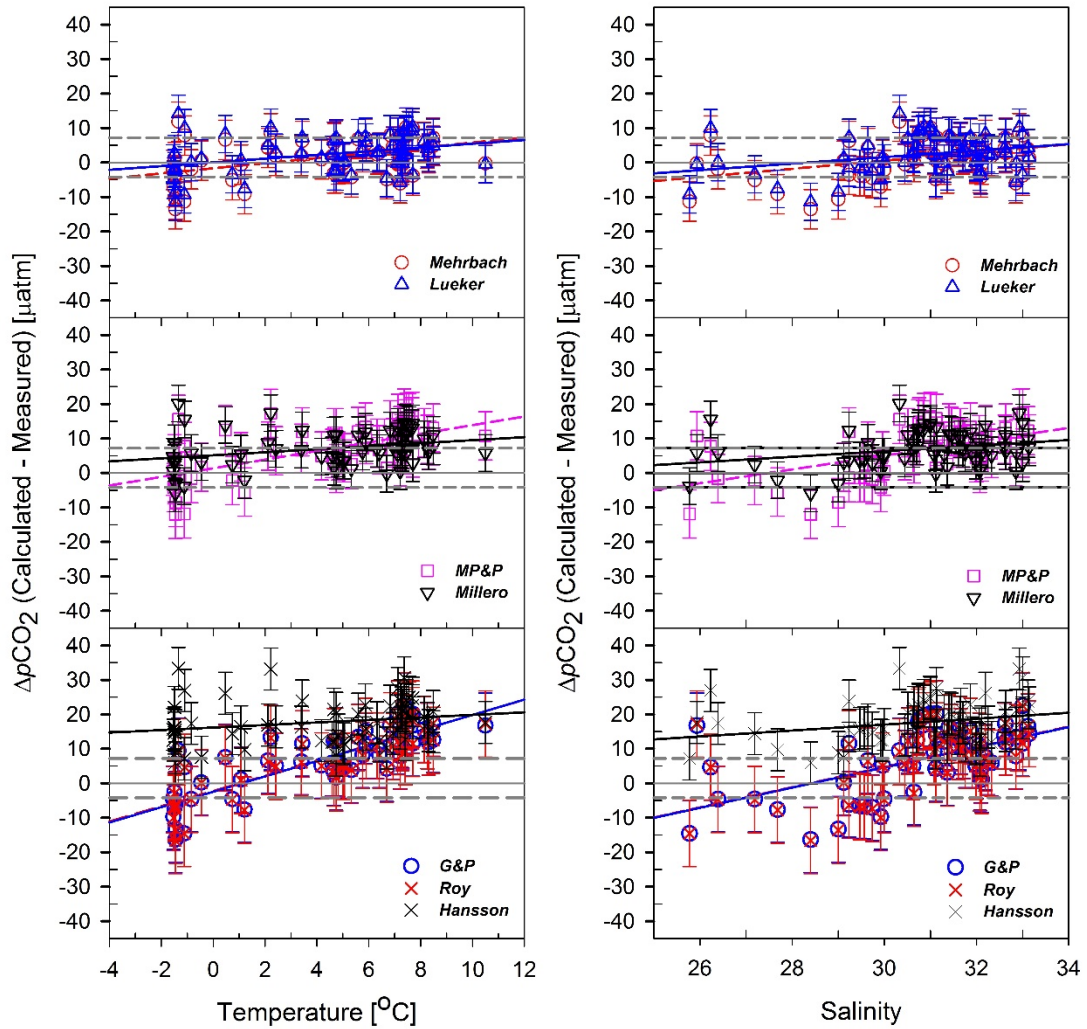


Figure 2.5. $\Delta p\text{CO}_2$ (calculated – measured) as a function of temperature (left panels) and salinity (right panels) for calculations with various sets of dissociation constants. Data from the southern Canada Basin are not included. Error bars indicate the standard deviation of the pooled $\Delta p\text{CO}_2$ data for the various constants. The gray dashed lines indicate the range of mean $\pm 1\sigma$ for $\Delta p\text{CO}_2$ of *Mehrbach*. The solid grey line indicates where $\Delta p\text{CO}_2 = 0 \mu\text{atm}$.

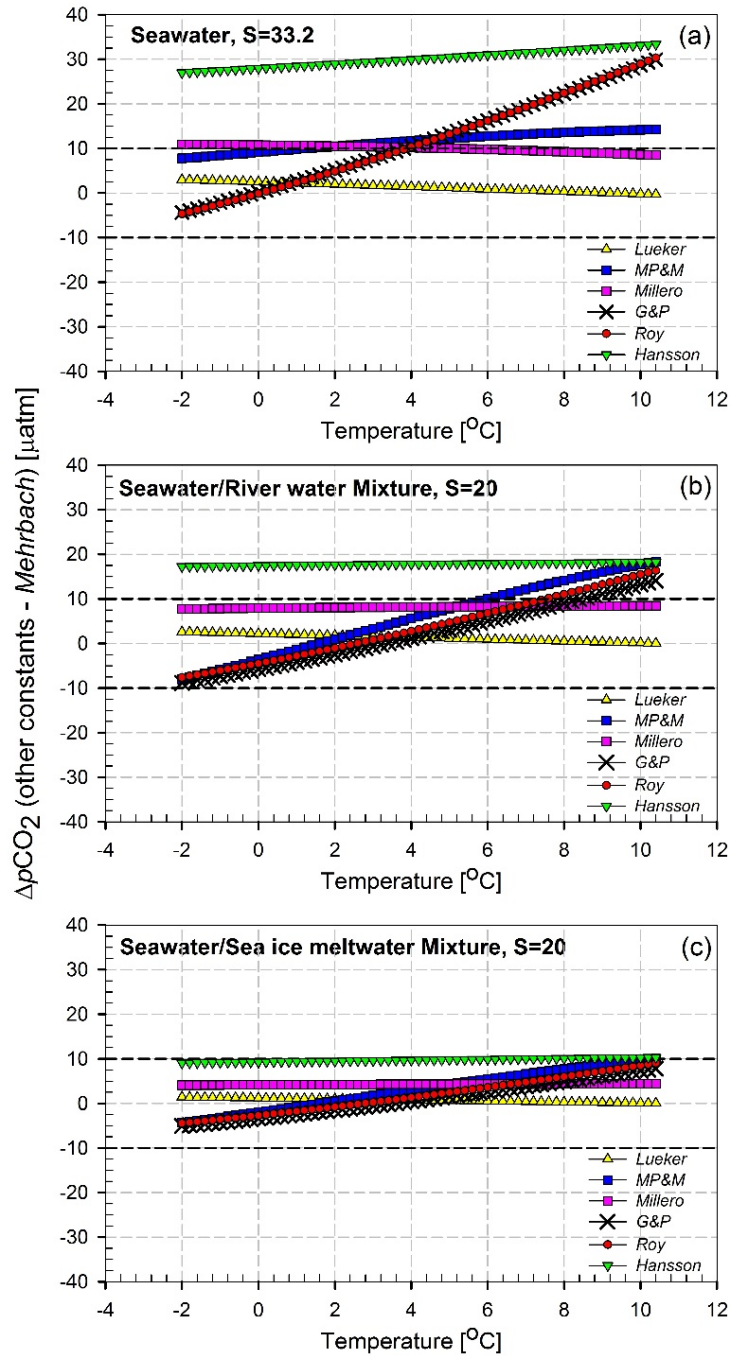


Figure 2.6. Differences in calculated surface $p\text{CO}_2$ values (other constant – Mehrbach) as a function of temperature for (a) seawater, (b) a mixture of seawater and river water, and (c) a mixture of seawater and sea ice meltwater. The black dashed lines indicate the uncertainty of $p\text{CO}_2(\text{DIC}, \text{TALK})$ for polar waters (Wanninkhof et al., 1999).

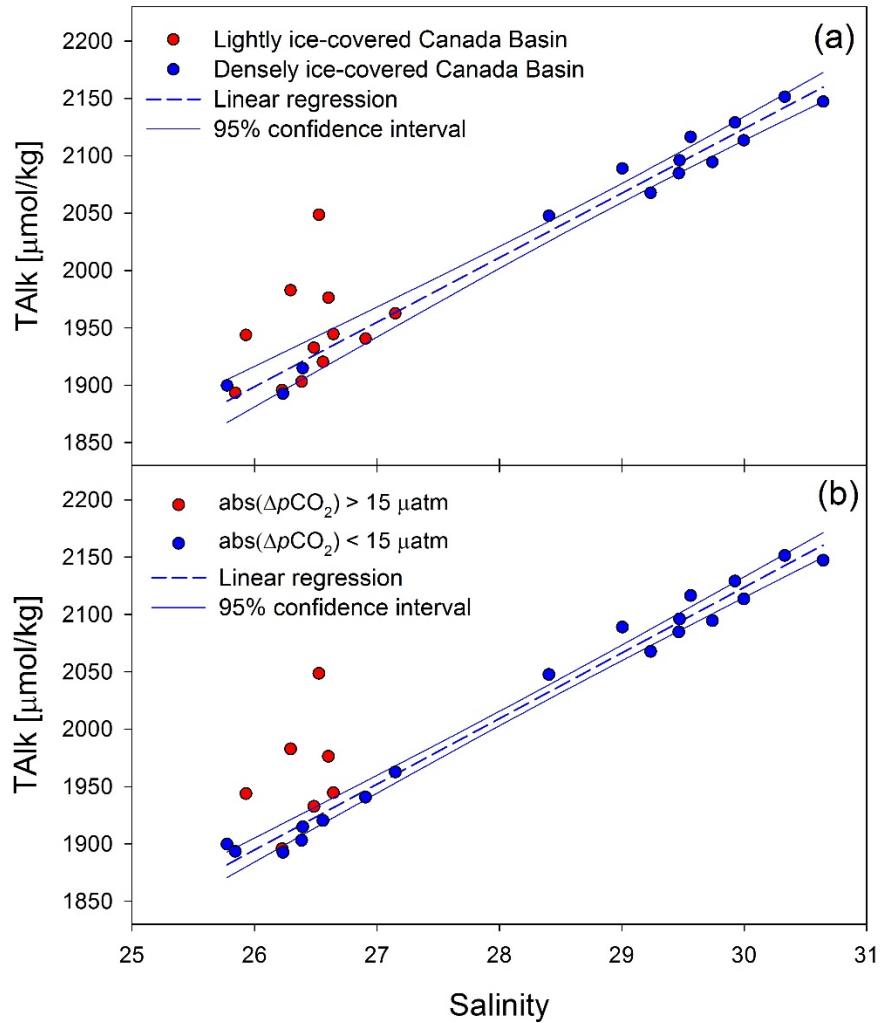


Figure 2.7. TALK and salinity of bottle samples in the Canada Basin. The blue short dashed lines indicate linear regression results of (a) TALK in the densely ice-covered Canada Basin and (b) $\text{abs}(\Delta p\text{CO}_2) < 15 \mu\text{atm}$ in the Canada Basin, where “ $\text{abs}(\Delta p\text{CO}_2)$ ” indicates absolute values of $\Delta p\text{CO}_{2(\text{calculated-measured})}$. The blue solid line indicates a 95% confidence interval for a regression.

CHAPTER 3
THE CARBONATE SYSTEM IN SURFACE WATERS OF THE PACIFIC SECTOR
OF THE ARCTIC OCEAN: RESPONSES TO SEA-ICE RETREAT AND
FRESHENING²

² To be submitted to *Journal of Geophysical Research*

Abstract

The Arctic Ocean has experienced unprecedented summer sea ice retreat under rapid global warming, particularly, since the summer of 2007. Increasing contributions from river discharge and sea-ice meltwater have significantly freshened the Arctic Ocean. To understand how the marine carbonate system has responded to the substantial freshening, we measured sea surface total dissolved inorganic carbon (DIC), total alkalinity (TAlk), and partial pressure of carbon dioxide ($p\text{CO}_2$), from the Bering Strait to the North Pole, during the Chinese Arctic Research Expedition (CHINARE) cruises of summer 2008 and 2010. Rivers contributed the majority of freshwater on shelves while sea-ice meltwater dominated in the Canada Basin. In addition, $p\text{CO}_2$ and DIC were decreased by biological production on shelves and in the partially ice-covered basin areas, particularly around the margins of sea ice cover. In contrast, biological consumption of DIC is negligible and balanced by CO_2 uptake from the atmosphere in the ice-free Canada Basin. Accordingly, the distribution of surface $p\text{CO}_2$ showed four distinct latitudinal zones (south-to-north): (1) very low (100 to 275 μatm) on shelves dominated by biological uptake, (2) relatively high (275 to 367 μatm) in the ice-free southern Canada Basin dominated by low production and rapid air-sea CO_2 exchange, (3) relatively low values (240 to 270 μatm) in the lightly ice-covered basin dominated by biological uptake and low gas flux, and (4) moderate (270 to 311 μatm) and relatively stable between 1994–present in the heavily ice-covered basin areas. Model simulation showed that rapidly increased surface $p\text{CO}_2$ could slow the speed of atmospheric CO_2 invasion, resulting in a rate of CO_2 uptake from the atmosphere about 85% lower than previous studies. Under the conditions of fast

freshening, the CO₂ uptake capacity in the ice-free areas of the Arctic Ocean basins would quickly weaken.

1. Introduction

The Arctic Ocean is subject to significant freshening under the influence of increasing river discharge and substantial melt of sea ice during summertime. Discharge from the Arctic Ocean's six largest rivers increased 7% from 1936 to 1999 (Peterson et al., 2002). The unprecedented melt of Arctic sea ice during summer, particularly since 2007, has also contributed large amounts of freshwater to the Arctic Ocean (Comiso et al., 2008; Maslanik et al., 2007; Perovich, 2011; Stroeve et al., 2012). Sea ice melt in the Arctic Ocean has increased steadily since the late 1970's, proceeding faster between 2007 and 2009 than any model prediction (Arrigo et al., 2008; Comiso et al., 2008; Wang and Overland, 2009). The Arctic Ocean thus will be further freshened due to the accelerated retreat of summer sea ice extent and it is predicted to be ice-free by summer 2050 (Wang and Overland, 2009). It was estimated that the freshwater content of the Arctic Ocean has increased by as much as 8500 km³ in the past decade (McPhee et al., 2009; Rabe et al., 2011), which is equivalent to 19% of the total freshwater budget in the Arctic Ocean (Aagaard and Carmack, 1989). The freshening of the Arctic Ocean can significantly influence the distribution of the carbonate system because of the distinct characteristics of seawater, river water, and sea ice meltwater. Changes in ecosystem processes caused by freshening (Li et al., 2009; Wassmann and Reigstad, 2011) could modulate the carbon uptake rate, causing further modifications to the carbonate system. In addition, loss of sea ice cover also influences the carbonate system through air-sea carbon dioxide (CO₂) gas exchange and will likely impact ocean ecosystems via acidification (Steinacher et al., 2009; Yamamoto-Kawai et al., 2009). The combined effect of these processes increases

the complexity of the carbonate system's response to freshening and this response has been poorly documented.

There is a paucity of observations of the Arctic Ocean basin carbon cycle due to the harsh Arctic climate. Therefore, how the carbonate system has responded to freshening, in particular over the deep basins, is still poorly known. As such, estimates of the net annual uptake of CO₂ are highly uncertain in this highly dynamic environment (Anderson et al., 1990; Anderson et al., 1998; Bates, 2006; Bates and Mathis, 2009; Kaltin and Anderson, 2005; Lundberg and Haugan, 1996). It has been predicted that the Arctic Ocean will sequester much greater amounts of CO₂ from the atmosphere as a consequence of sea ice decline due to longer duration of open water and concomitant higher ocean primary production (Arrigo et al., 2008; Arrigo and van Dijken, 2011; Bates and Mathis, 2009). However, this prediction was based on observations from either highly productive ocean margins or ice-covered basins prior to the recent major ice retreat (Anderson et al., 1998; Bates, 2006). Deepening of the chlorophyll maximum and nutricline was observed in the interior of the Canada Basin as a consequence of enhanced freshening (McLaughlin and Carmack, 2010). Increased stratification could potentially decrease nutrient supply from deep water, which in turn would affect carbon fixation. Whether the Arctic Ocean will take up a significant amount of CO₂ from the atmosphere is still being debated. These considerations indicate that the response of the carbonate system to the changing Arctic is influenced by various environmental factors, including contributions from various sources of freshwater, open water duration, stratification, nutrient availability, hydrography, and sea ice dynamics.

Since 2007, summer minimum sea ice cover has retreated from the shelf to the deep Canada Basin, which facilitated the study of the responses of the carbonate system to sea ice melting in the basin areas. In this study, we report surveys of the carbonate system over the Pacific sector of the Arctic Ocean during summer 2008 and 2010. Our cruise thoroughly sampled a large area of the Arctic Ocean from the Bering Strait to the North Pole, including the ice-free shelves and the ice-free southern Canada Basin, and lightly and heavily ice-covered basin areas. The surface distributions of carbonate parameters are presented and the mechanisms controlling regional distributions are discussed. Finally, we evaluate the role of an ice-free Arctic Ocean as a CO₂ source/sink with respect to atmospheric CO₂ and estimate the air-sea flux of CO₂.

2. Material and Methods

2.1. Cruise description

The Chinese Arctic Research Expeditions of summer 2008 (CHINARE2008) and summer 2010 (CHINARE2010) were conducted one and three years, respectively, after the substantial decline of summer sea ice in 2007. Both of these cruises were conducted from early July to late August. The start time of CHINARE2008 was about one week later than CHINARE2010. The cruise track covered the Pacific sector of the Arctic Ocean (Fig. 3.1). Both of these cruises started to survey the Arctic Ocean northward from the eastern track along the Chukchi Sea, Barrow Canyon, and Beaufort Sea, into Canada Basin, Alpha Ridge, and further Makarov Basin. On the returning southward western cruise track, we sampled the Mendeleev Ridge, Chukchi Plateau, and the western side of the Chukchi Sea. The 1994 Arctic Ocean Section cruise (AOS94) (data via: <http://cdiac.ornl.gov/ftp/oceans/CARINA/L.S.St.Laurent/18SN199407/>) is included for

comparison. The AOS94 cruise surveyed the East Siberian Sea side of the Canada Basin. Some of the sampling stations of AOS94 overlapped the western cruise tracks of CHINARE2008 and CHINARE2010. MR99 cruise is also included which was performed on board R/V *Mirai* in summer 1999 (Murata and Takizawa, 2003) covering areas of eastern Chukchi Sea and the Beaufort Sea.

2.2. Hydrographic setting

The Pacific Arctic sector receives freshwater from the northward flowing Pacific water through the Bering Strait, river runoff, and sea ice meltwater. Annually, the northward inflow of Pacific Water brings ~ 0.8 Sv ($1 \text{ Sv} = 10^6 \text{ m}^3/\text{s}$) seawater through the 80 km wide and 50 m deep Bering Strait (Fig. 3.1) (Coachman and Aagaard, 1988; Woodgate et al., 2005a; Woodgate et al., 2005b). This Pacific water provides about one-third ($\sim 1670 \text{ km}^3/\text{yr}$) of the annual total freshwater input into the Arctic Ocean (Aagaard and Carmack, 1989; Serreze et al., 2006). According to studies conducted on the general circulation in the Arctic Ocean (Coachman et al., 1975; Pickart et al., 2010; Weingartner et al., 2005), there are three distinct branches of Pacific water crossing the Bering Strait and flowing into the Arctic through some Chukchi shelf canyons, including 1) Anadyr water that flows through the western strait and exits through Hope and Herald canyons; 2) Bering shelf water that flows through central strait and exits through central channel; and 3) Alaska Coastal Water that flows through the eastern strait and exits through Barrow Canyon. The merged product of Anadyr water and Bering shelf water is called Bering Sea water (Coachman et al., 1975) which has a resulting summer salinity (S) of $32 < S < 33$ and temperature (T) of $0 \text{ }^\circ\text{C} < T < 2 \text{ }^\circ\text{C}$. The Alaska Coastal Water is fresher ($31 < S < 32$) and relatively warmer ($1 \text{ }^\circ\text{C} < T < 6 \text{ }^\circ\text{C}$). Moreover, the large rivers Kolyma,

Mackenzie, and Yukon discharge freshwater into their adjacent Pacific Arctic sector. The annual average discharges of Kolyma, Mackenzie, and Yukon rivers are 114 km³/yr, 322 km³/yr, and 214 km³/yr, respectively (Cooper et al., 2008). Yukon River water is incorporated into the Alaska Coastal Water. In addition to the two freshwater sources described above, sea ice meltwater and precipitation are two other freshwater sources into the Canada Basin.

2.3. DIC and TAlk sampling and measurements

Discrete dissolved inorganic carbon (DIC) and total alkalinity (TAlk) samples were collected in the surface mixed layer using a SeaBird CTD 911 system and a 24-bottle rosette equipped with 12 L Niskin bottles. We transferred seawater from each Niskin bottle into clean 250 mL borosilicate glass bottles that were used for both DIC and TAlk analysis. 1 mL of seawater was removed from the bottle to allow for thermal expansion during storage, and 100 μ L of saturated mercuric chloride solution was injected to halt biological activity. The bottles were then sealed using Apiezon[®] L greased ground-glass stoppers. Samples were stored at 4°C in the dark before analysis.

DIC and TAlk were measured using automated analyzers (Apollo SciTech, USA) and the analytical techniques and procedures are documented in Cai et al. (2010) and Huang et al. (2012). TAlk was determined by potentiometric titration, using 0.1 M hydrochloric acid and an open-cell titration system. All TAlk samples were analyzed in thermostated (25°C) glass cells. Each TAlk sample was titrated several times ($n = 2$ to 4) until we obtained two replicates with a precision within 0.1%. The average of the two values within 0.1% are reported. DIC was determined at room temperature. Each seawater sample (0.5 mL) was acidified using phosphoric acid. The evolved CO₂ gas was

quantified by an infrared CO₂ detector (Li-Cor 6262). DIC was also measured several times (n = 3 to 4). The precision of both the TAlk and DIC measurements was better than 0.1% ($\pm 2 \mu\text{mol/kg}$). The accuracies of the TAlk and DIC measurements were determined by routine analysis of certified reference materials provided by A. G. Dickson, Scripps Institution of Oceanography.

2.4. Underway $p\text{CO}_2$ measurements

Underway measurements of the partial pressure of carbon dioxide ($p\text{CO}_2$) were collected continuously along the cruise track (Fig. 3.1). Sea surface temperature and salinity were measured by an SBE21 (Sea-Bird Electronics) thermosalinograph. Underway $p\text{CO}_2$ was measured by an automated system (General Oceanics, Inc.) continuously using a non-dispersive infrared detector Li-840 (LICOR, Inc.) at a sampling interval of 2 minutes. This autonomous system was calibrated every 3 hours using four compressed CO₂ gas standards obtained from NOAA's Earth System Research Laboratory (ESRL). These gas standards are directly traceable to the World Meteorological Organization (WMO) scale. Here we report sea surface $p\text{CO}_2$ values that have been normalized to measured sea surface temperatures. The resolution of underway $p\text{CO}_2$ measurements with this system is 0.1 μatm , and overall accuracy was estimated at 2 μatm for seawater $p\text{CO}_2$ measurements as documented by Pierrot et al. (2009).

2.5. Selection of DIC, TAlk and salinity values for various end members

To simulate mixing scenarios between seawater, river water, and sea ice meltwater, the characteristic values of DIC, TAlk, and salinity for these end-members were chosen and summarized. Average values in 200 m slope waters at the northern edge of the Bering Sea (59.0 to 60.4°N) from the CHINARE2008 cruise are used as the seawater end-

member. In contrast, CHINARE2010 sparsely sampled this area and did not directly sample the 200 m layer, therefore we use CHINARE2008 data. However, a simple comparison of DIC and TAlk values around 200 m layer at stations close to the Bering Sea shelf was performed between CHINARE2008 and CHINARE2010 by scaling TAlk and DIC to salinity 35 (i.e., (DIC or TAlk) \times 35/*S*). This comparison shows no difference between the two. The seawater end-member has properties of $S = 33.218 \pm 0.046$, TAlk = 2257.9 ± 14.2 $\mu\text{mol/kg}$, and DIC = 2161.4 ± 5.1 $\mu\text{mol/kg}$ and $p\text{CO}_2$ of ~ 470 μatm at 2 °C. The TAlk = 1100 $\mu\text{mol/kg}$ of the river water end-member was taken from the PARTNERS project (Cooper et al., 2008). We set river DIC = 1150 $\mu\text{mol/kg}$, using the TAlk/DIC ratio of 0.956 for river waters (Guo et al., 2008). These TAlk and DIC values generate a river water $p\text{CO}_2$ of roughly 1000 μatm at a summer river temperature of 10 °C. Ice meltwater *S*, TAlk and DIC values were set at 5, 450 $\mu\text{mol/kg}$, and 400 $\mu\text{mol/kg}$, respectively, according to Rysgaard et al. (2007). As such, meltwater has a very low $p\text{CO}_2$ of roughly 20 μatm at a temperature of 5 °C in the ice-free Canada Basin.

2.6. Calculation of $p\text{CO}_2$ and air-sea CO_2 flux

For comparison of $p\text{CO}_2$ values between cruises, $p\text{CO}_2$ values for the AOS94 cruise were calculated from DIC and TAlk measurements because direct measurements were not available. Changes in $p\text{CO}_2$ in the surface mixed layer with time were also calculated from DIC and TAlk and used to simulate the dynamic process of CO_2 invasion from the atmosphere into ocean surface waters. . For these calculations, we used the Matlab version of CO2SYS (Pierrot et al., 2006) (downloaded from <http://cdiac.ornl.gov/ftp/co2sys/>) and the first and second apparent carbonic acid dissociation constants K_1 and K_2 of Mehrbach et al. (1973) as refit by Dickson and

Millero (1987). We used the dissociation constants of Millero et al. (2006) to calculate $p\text{CO}_2$ from DIC and TALK in the simulation of mixing processes among seawater, river water, and sea ice meltwater, because these constants were fit to cover low salinity freshwater.

The air-sea CO_2 exchange is calculated using equation (1):

$$F = k \times K_0 \times (p\text{CO}_{2(\text{water})} - p\text{CO}_{2(\text{air})}) \quad (1)$$

Where k is the gas transfer velocity of CO_2 gas and, K_0 is the solubility of CO_2 at specific temperature and salinity (Weiss, 1974). We used the coefficients given in Wanninkhof (1992) to calculate k . An average wind speed of 7 m/s was observed in the MR99–K05 cruise aboard R/V *Mirai* in summer 1999 (Murata and Takizawa, 2003), and this was used to estimate air-sea CO_2 gas exchange in the model simulation for a simple comparison between different cruises. $p\text{CO}_{2(\text{water})}$ is the $p\text{CO}_2$ value in surface waters. $p\text{CO}_{2(\text{air})}$ is an average of atmospheric $p\text{CO}_2$ values during the cruise. This average atmospheric $p\text{CO}_2$ value is from measurements made by NOAA at Point Barrow, AK (ftp://aftp.cmdl.noaa.gov/data/trace_gases/co2/flask/surface/co2_brw_surface-flask_1_ccgg_event.txt). Field measurements of atmospheric $p\text{CO}_2$ (~375 μatm) in CHINARE2008 is comparable with these records.

2.7. Sea ice cover and water column stratification

Sea ice cover for each station was retrieved from the Advanced Microwave Scanning Radiometer – Earth Observing System (AMSR- E) sensor with a resolution of 12.5 x 12.5 km. These data were downloaded from NOAA’s ERDDAP data server (data access: <http://coastwatch.pfeg.noaa.gov/erddap/griddap/index.html?page=1&itemsPerPage=1000>)

). Sea ice cover data were matched to the geographic coordinates and sampling time of each station. Water column stratification was evaluated as the depth of surface mixed layer, which was defined using the threshold method. The surface mixed layer is the depth at which potential density is 0.05 kg/m^3 greater than the surface potential density (Brainerd and Gregg, 1995).

3. Results

3.1. Sea ice cover

Distributions of sea ice cover for CHINARE2008 and CHINARE2010 are shown in Fig. 3.2a and Fig. 3.2d, respectively. Sea ice cover in CHINARE2008 was much less than CHINARE2010 in areas south of 80°N , in part reflecting the interannual variation in sea ice cover. It is also related to a difference of about one week for sampling on CHINARE2008. Hereinafter, sea ice cover $< 15\%$ is defined as ice-free condition, sea ice cover in a range of $15\text{--}85\%$ is defined as partially ice-covered condition, and sea ice cover $> 85\%$ is defined as heavily ice-covered condition. For CHINARE2008, there was no sea ice south of 76°N , including the Chukchi Sea shelf and southern Canada Basin. A sea ice cover transition zone located between 77°N and 85°N was partially ice-covered. The loss of permanent sea ice up to 85°N suggests a significant retreat of sea ice in summer 2008. A much larger area was covered by sea ice during CHINARE2010 compared with CHINARE2008. The Chukchi Sea shelf was ice-free on the 2010 cruise, but we encountered sea ice at the shelf break. The Arctic Ocean was heavily ice-covered at 76°N on the eastern cruise track. On our return from the northernmost point (88.4°N) with more sea ice melted in late August, the Arctic Ocean was still heavily covered by

sea ice at around 81°N. Sea ice cover data indicate that CHINARE2010 cruise encountered less sea ice melt than CHINARE2008.

3.2. Sea surface temperature and salinity

Sea surface temperature and salinity are plotted for CHINARE2008 in Fig. 3.2b and 3.2c, and for CHINARE2010 in Fig. 3.2e and 3.2f. The temperature distribution on both cruises reveals two zones of high surface temperature corresponding to no sea ice cover. One was on the shelf which is continuously influenced by warmer Pacific Water, and the second was in the ice-free Canada Basin, which was quickly heated by solar radiation following sea ice retreat. The warmest waters encountered on the shelf were along the coastline of Alaska, which was dominated by the warmer high temperature Alaska Coastal Current. Although temperature was high in an ice-free Canada Basin, temperature dropped quickly to near freezing temperatures in the partially and heavily ice-covered high latitude Canada Basin waters. Using topography and sea ice boundaries as references, we summarize the temperature ranges in 2008 for shelf ($-1.0\text{ °C} < T < 6.9\text{ °C}$), slope ($-0.2\text{ °C} < T < 1.6\text{ °C}$), ice-free southern Canada Basin ($-0.7\text{ °C} < T < 4.9\text{ °C}$), and ice-covered northern Canada Basin ($-1.6\text{ °C} < T < -1.0\text{ °C}$). The corresponding values for CHINARE2010 are shelf ($-1.3\text{ °C} < T < 7.8\text{ °C}$), slope ($-0.7\text{ °C} < T < 4.1\text{ °C}$), ice-free southern Canada Basin ($-1.0\text{ °C} < T < 0.3\text{ °C}$), and ice-covered Canada Basin ($-1.6\text{ °C} < T < 0\text{ °C}$). There was no difference in temperature ranges in shelf, slope and ice-covered basin waters. However, the temperatures in ice-free basin areas can be raised up to 5 °C, particularly in 2008, as high as in shelf waters.

Salinity distribution is more complex than temperature distribution due to a locally input of high temperature and low salinity coastal water. For example, Alaska Coastal water received freshwater around Point Hope, Alaska and showed a surface salinity minimum on CHINARE2008 (Fig. 3.2c). We summarize the regional salinity features: In 2008 for shelf ($27.4 < S < 32.4$), slope ($25.1 < S < 26.9$), ice-free southern Canada Basin ($24.1 < S < 26.8$), and ice-covered northern Canada basin ($26.7 < S < 30.3$). The corresponding values for CHINARE2010 are shelf ($27.7 < S < 32.3$), slope ($26.8 < S < 31.4$), ice-free southern Canada Basin ($25.8 < S < 26.6$), and ice-covered northern Canada basin ($25.8 < S < 30.6$). This summary indicates that no significant difference in salinity was observed in shelf and basin waters between 2008 and 2010. However, slope was dominated by shelf water when the basin is still heavily covered by sea ice, while it was strongly influenced by sea ice meltwater when ice in the basin was melted.

3.3. Sea surface DIC, TAlk, and $p\text{CO}_2$

Sea surface TAlk, DIC, and $p\text{CO}_2$ are plotted in Fig. 3.3a-3.3c for CHINARE2008, and in Fig. 3.3e-3.3f for CHINARE2010. The distributions of TAlk are similar to salinity on both cruises. TAlk values were high on the shelf except inshore of Alaska, which received freshwater input as shown in 2008. The lowest TAlk values observed in the ice-free Canada Basin were associated with the lowest salinity. TAlk values were higher in the ice-covered basin than in the ice-free basin. In contrast, DIC values covary with the changes in salinity in basin areas, while they are decoupled from salinity in most of the shelf waters that show a significant DIC drawdown. For example, both of the lowest TAlk value ($1762.1 \mu\text{mol/kg}$) and DIC value ($1689.4 \mu\text{mol/kg}$) were observed in the ice-

free Canada Basin in 2008. However, in 2010, the lowest TAlk value (1892.5 $\mu\text{mol/kg}$) was observed in the partially ice-covered southern Canada Basin, while the lowest DIC value (1675.1 $\mu\text{mol/kg}$) was observed on the central shelf. This decoupling suggests that both biological production and sea ice meltwater influence DIC distribution patterns.

The distribution of surface $p\text{CO}_2$ is more complex than DIC and TAlk. Sea surface $p\text{CO}_2$ values were below the atmospheric $p\text{CO}_2$ level ($\sim 375 \mu\text{atm}$) in the entire study area for both CHINARE2008 and 2010. Four distinct zones are clearly identifiable: (1) In shelf waters, very low $p\text{CO}_2$ values (100 to 275 μatm) were observed in both years. (2) In the southeastern Canada Basin (72.2°N–78°N and east of 160°W), high $p\text{CO}_2$ values (275 to 367 μatm) were observed in an ice-free condition in 2008 while in a partially ice-covered condition in 2010. Such high $p\text{CO}_2$ values have never been observed before in an ice-free condition in the Arctic basin. The salinity of CHINARE2008 was about 2 units lower than CHINARE2010, the surface temperature was 2 °C higher, and $p\text{CO}_2$ was 27 μatm higher. In contrast, no significant differences were observed between CHINARE2008 and 2010 in the southwestern Canada Basin (west of 160°W). (3) In the Canada Basin farther north (78°N–81°N), $p\text{CO}_2$ values (240 to 270 μatm) were lower than in surrounding waters. This region coincides with rapid sea ice retreat and a sea ice cover of 50–85%. (4) In the northern Canada Basin (north of 81°N), $p\text{CO}_2$ values (270 to 311 μatm) were relatively stable. Moreover, $p\text{CO}_2$ values increased rapidly across the shelf break into the interior basin. The broader continental shelf of the East Siberian Sea exhibits a high $p\text{CO}_2$ at 74°N which was only observed at 72°N on the Beaufort Sea side.

3.4. Comparison of surface $p\text{CO}_2$ between cruises

To further study how surface carbonate system responds to rapid sea ice melt from an ice-covered basin to an ice-free basin, we incorporate the $p\text{CO}_2$ data, a direct tool for air-sea CO_2 exchange study through open water, of Arctic Ocean Section 1994 cruise (AOS94) and MR99 cruise (MR99) (See Fig. 3.1) into our CHINARE data. AOS94 cruise was conducted from July to August in 1994 and surveyed the perennial ice-covered Arctic Ocean, while the MR99 cruise was conducted in September 1999 and observed more recent Arctic surface $p\text{CO}_2$ distribution. The AOS94 and MR99 cruises overlapped the western and eastern portions of our study area, respectively.

Measured surface $p\text{CO}_2$ of CHINARE and MR99 cruises and calculated $p\text{CO}_2$ of AOS94 cruise are plotted against latitude (Fig. 3.4). The shelf break is located at $\sim 72^\circ\text{N}$ on the Beaufort Sea side (including MR99, CHINARE2008 and 2010 eastern cruise tracks) and at $\sim 74^\circ\text{N}$ on the East Siberian Sea side (including AOS94, CHINARE2008 and 2010 western cruise tracks).

The shelf area was ice free for the MR99 cruise and partially ice-covered in AOS94 cruise. $p\text{CO}_2$ values were 200 to 350 μatm in MR99 and 150 to 250 μatm in AOS94. Considering the average atmospheric $p\text{CO}_2$ value of ~ 345 μatm in 1994 and ~ 365 μatm in 1999, the shelf area in summer was a sink for atmospheric CO_2 in the past decades, similarly observed in 2008 and 2010 cruises. An increase in surface $p\text{CO}_2$ values was observed over the past decade in the southern Canada Basin (72.2°N – 78°N), with highest values (275–367 μatm) measured during CHINARE 2008 & 2010 compared to the MR99 and AOS94 cruises (260–300 μatm and < 260 μatm , respectively). In the northern

Canada Basin ($> 78^{\circ}\text{N}$), surface $p\text{CO}_2$ values increased from 78°N to 81°N (297–333 μatm) and were lower and stable (287–306 μatm) north of 81°N in AOS94. In contrast, $p\text{CO}_2$ values decreased from 78°N to 81°N in CHINARE2010, but $p\text{CO}_2$ values were close to AOS94 in the higher latitudes ($> 81^{\circ}\text{N}$). Ekwurzel et al. (2001) confirmed that 78°N to 81°N region was strongly influenced by Eurasian shelf waters in AOS94. Although we cannot identify if our study area was influenced by high $p\text{CO}_2$ Eurasian shelf waters, a decrease in $p\text{CO}_2$ still can be confirmed when comparing with stable $p\text{CO}_2$ values in the northern ice-covered areas. In this study, to evaluate the responses of surface $p\text{CO}_2$ from ice-covered basin to ice-free basin, we focus on the southern Canada Basin with recent sea ice retreat and treat heavily ice-covered northern Canada Basin as a climatological background.

4. Discussion

4.1. Controlling mechanisms of surface DIC and TALK

The upper ocean of the Pacific Arctic Sector is modulated by Pacific Water, river water and sea ice meltwater (Anderson et al., 2013). Therefore, we use a conservative mixing model of these water sources as a reference framework to elucidate the controlling mechanisms of TALK and DIC. Mixing scenarios are based on the assumption that Pacific water upwells onto the shelf and initially mixes with river water to form a mixture of seawater and river water (hereinafter referred to as modified seawater). This modified seawater then flows northward and is continuously modified by river water. The continuously being modified seawater mixes with sea ice meltwater over the shelf and in the interior basin. Therefore, we use two types of mixing lines in this analysis: (1) Pacific

seawater mixing with river water; and (2) modified seawater mixing with sea ice meltwater. The properties of these three end members are given in the Methods section. The salinity dependence of TAlk and DIC are shown for CHINARE2008 (Fig. 3.5a) and CHINAER2010 (Fig. 3.5b). It should be noted that, depending on location and season, the salinity of this “modified seawater” may be different. Thus instead of one line for the “modified seawater-meltwater mixing”, there may be a group of lines forming an ensemble of mixing properties. Three representative modified seawater sources are used with $S = 26.5$ representing the lowest salinity observed in the ice-free Canada Basin, $S = 30$ representing the lower end of salinity on the Chukchi shelf in summer, and $S = 32.5$ representing the salinity of summer Bering shelf water flowing through the Bering Strait. Another consideration is that Russian Rivers (e.g. Kolyma River) have lower TAlk than North American Rivers (e.g. Yukon River and Mackenzie River) (Cooper et al., 2008). However, except in the very low salinity part (the estuarine and river plume areas), their difference and its effect on the mixing lines is minor. In addition, we also divide our data into four groups, including shelf, slope, basin-ice free (< 15% sea ice cover), and basin-with ice (> 15% sea ice cover), to help identify different controlling mechanisms in specific regions.

4.1.1. Controlling mechanisms of TAlk

A conservative mixing model well explains the distribution of TAlk in shelf, slope, and ice-covered Canada Basin waters. By comparison, most of the TAlk data collected from the ice-free Canada Basin are supported by this mixing model, however, some

deviations of TAlk data away from the conservative mixing lines might be controlled by other mechanisms (Fig. 3.5a, b).

For CHINARE2008, most of the shelf TAlk data had salinities > 30 except one point that has salinity as low as 27.4. For those data with $S > 30$, TAlk data collected on the southern Chukchi shelf follow the mixing line of modified seawater ($S = 32.5$) and meltwater. TAlk data collected on the northern Chukchi shelf follow other mixing lines of modified seawater which has a salinity within a range of 30–32.5 and meltwater. The decreasing salinity of modified seawater is the result of freshwater input from Alaska, which can be demonstrated by low surface salinity along the coast of Alaska (Fig. 3.2c) with the lowest salinity of 27.4 measured near Point Hope, Alaska (Fig. 3.1). Moreover, the TAlk data with the lowest salinity of 27.4 follows the mixing line of Pacific water and river water, which further demonstrates that river water from Alaska is a major contribution of freshwater in this region. Therefore, Bering shelf water is gradually diluted by river water near Alaska to form modified seawater with various salinities after entering the Bering Strait, then these modified seawater sources mix with ice meltwater to control the distribution of surface TAlk.

CHINARE2010 TAlk data show some different and some additional regional distribution patterns when compared to those observed in 2008 due to more intensive sampling in 2010 (Fig. 3.5b). First, TAlk data sampled near the Bering Strait ($< 67^\circ\text{N}$) and over the central northern Chukchi shelf ($> 69.5^\circ\text{N}$ and west of -165.3°W , corresponding to areas north of Herald Shoal and west of Hanna Shoal) followed the mixing line of modified seawater ($S = 32.5$) and meltwater in 2010. Second, TAlk data were densely sampled along the Alaska coast in 2010, which clearly show mixing

between Pacific seawater and river water. These TAlk data are confined to areas near Point Hope, Alaska (67°N-69.5°N) and along the Alaska coast from Point Hope to Barrow Canyon (Fig. 3.1). Third, Only the TAlk data sampled near Barrow Canyon follow the mixing lines of modified seawater ($30 \leq S \leq 32.5$) and meltwater in 2010.

Through a comparison of TAlk distribution in 2008 and 2010, we found spatial and temporal differences which should be associated with river water discharge and sea ice melt. We sampled the Chukchi shelf about 15 days later in 2008 than in 2010. During the sampling period, sea ice was also more extensively melted in 2008. Therefore, surface ice meltwater was largely replaced by inflowing Pacific water, resulting in less significant mixing of modified seawater and meltwater on the Chukchi shelf. Additionally, the influence of river discharge was lower in 2008 because we sampled later in the season, since Yukon River discharge decreases from July on http://nhg.unbc.ca/ipy/m_yukon.html and we sampled in August, 2008. The decreasing river discharge and loss of sea ice meltwater result in relatively higher surface salinity and broad westward extension of the modified seawater on the northern Chukchi shelf as seen in 2008. In addition, we observed two shelf stations which had higher TAlk values and located above the mixing lines in 2010. One sample was collected in Barrow Canyon, while the other was sampled to the northern edge of Herald Shoal. The temperatures of these samples were also lower than adjacent stations. These higher TAlk values may be explained by ventilation of deeper winter remnant water which has higher TAlk due to wintertime brine rejection. Prevailing northerly wind can induce topographically-driven upwelling of water on the northern edge of Herald Shoal, and wind-driven upwelling in

Barrow Canyon or along Beaufort shelf (Mathis et al., 2012; Mountain et al., 1976), which could be the cause of these anomalous TAlk values.

In the slope area, TAlk data in 2008 follow the mixing line of modified seawater and meltwater, while TAlk data in 2010 follow both mixing lines of Pacific seawater-river water and modified seawater-meltwater. Given that sea ice was not completely melted around the slope in 2010, we conclude that ice meltwater should be the dominant freshwater source on the slope after sea ice melted, while rivers greatly influence this area when the basin is still covered by sea ice. In the Canada Basin, some of the TAlk data in the ice-free Canada Basin plot above the mixing line (based on $S = 30$ as the modified seawater), showing higher observed values than predicted via mixing. However, the close association between measured values and those predicted via mixing in the ice-covered Canada Basin still suggests that mixing among different water sources is the major controlling factor. The higher TAlk values away from the mixing line collected from the ice-free basin suggest a potential contribution of river water because river water has high levels of TAlk and contributes significantly to the TAlk in the Arctic Ocean surface waters (Anderson et al., 2004). In addition, higher TAlk values away from the mixing line might also be caused by dissolution of calcium carbonate (CaCO_3) which can increase seawater TAlk.

We further use the relationship of DIC and TAlk to identify the possible explanation of anomalously high TAlk data (Fig. 3.5c for CHINARE2008, Fig. 3.5d for CHINARE2010). TAlk is a quasi-conservative parameter. Thus if TAlk and DIC follow the model mixing line, we can identify mixing as the dominant factor controlling their concentrations. We found that some of the TAlk and DIC data strictly follow the model

mixing line of modified seawater ($S = 30$) and meltwater in 2008 and 2010, indicating that those stations have no anomalous TAlk values. The rest of the 2008 data depart significantly from the model mixing line. In contrast, the rest of the 2010 data just slightly deviate the model mixing line. We also notice that these data deviate to the right of the model mixing line, suggesting the potential influence of river water which has high TAlk but low DIC due to biological production, or the potential dissolution of CaCO_3 which increase TAlk and DIC at a ratio of 2 which increases TAlk more than DIC.

For the assumption of river water contribution to the anomalous high TAlk values in the ice-free Canada Basin, we refer to the low salinity data in the Canada Basin which is a mixture of Pacific water and river water. Then we assume that this low salinity water directly mixes with the surrounding water, which is a mixture of modified seawater and meltwater. In 2008, the lowest salinity station that fell on the Pacific seawater-river mixing line (Fig. 3.5a) has a salinity of 26.4. Moreover, this station was in the ice-free Canada Basin and near the Mackenzie River. In 2010, a similar station was observed in the lightly ice-covered Canada Basin with a salinity of 26.5 (Fig. 3.5b), which was on the East Siberian Sea side. Taylor et al. (2003) suggested that Mackenzie River freshwater is stored in the Canada Basin, while others (Karcher and Oberhuber, 2002; Yamamoto-Kawai et al., 2005) suggest that Mackenzie River water does not constitute the main source of freshwater because it rapidly exits the Arctic through the Canadian Archipelago. Based on our field observations, even though controversy exists, Mackenzie River freshwater could influence the Canada Basin as shown in Fig. 3.5a. The contribution of river runoff from the Siberian continental shelves into the central Arctic Ocean has been reported (Ekwurzel et al., 2001; Yamamoto-Kawai et al., 2005) which

supports the observed low salinity river water in the partially ice-covered Canada Basin in 2010. A direct mixing of such kind of river influenced low salinity seawater with ice meltwater influenced low salinity seawater, could explain some of the anomalous high TAlk data in the ice-free Canada Basin. Here we use 2008 data as an example in which more anomalous high TAlk were observed. As described above, river influenced low salinity seawater has high DIC consumption. However, Lee et al. (2012) reported that this station has small net primary productivity as the other ice-free Canada Basin stations. Thus it might not support larger DIC consumption. We maintain the assumption that the observed DIC consumption occurred during the transit of this water mass toward the basin. Even if this process happened, contribution from mixing with high TAlk river water only explains anomalous TAlk data at three stations (Fig. 3.5c). The same conclusion can be reached in 2010 (river influenced low salinity data is also slightly to the right of the model mixing line but not marked in the figure). This conclusion is reasonable considering that the amount of river flow could not support a deep penetration into the Canada Basin and the river plume is confined to a specific direction. Therefore, the limited river influence raises the possibility of dissolution of CaCO_3 .

Alternatively, dissolution of CaCO_3 can also increase TAlk beyond the mixing model prediction. CaCO_3 is formed in the brine channel of sea ice during winter, and is dissolved when ice melts. This process can increase TAlk while just slightly changing salinity, which could explain these observed higher TAlk values. Previous studies have confirmed the existence and dissolution of CaCO_3 in the Arctic Ocean, e.g. (Rysgaard et al., 2012; Rysgaard et al., 2007). Thus, if this process is a contributing factor, dissolution of CaCO_3 is expected to increase TAlk and DIC at a ratio of 2:1. During the mixing of

modified seawater ($26.5 \leq S \leq 32.5$) and meltwater, the change rates of TAlk/DIC are between 1.01 and 1.02. For comparison, the change rate is 1.26 in 2008 and 1.17 in 2010 in the ice-free Canada Basin. These rates are higher than mixing model, indicating potential dissolution of CaCO_3 in the low net primary productivity ice-free Canada Basin (Lee et al., 2012). A rough estimate of the difference between field-measured TAlk and predicted TAlk from mixing model shows an increase of $81 \mu\text{mol/kg}$ TAlk in 2008 and $40.5 \mu\text{mol/kg}$ TAlk in 2010. These two numbers correspond to a dissolution of 40 and $20 \mu\text{mol/kg}$ CaCO_3 for 2008 and 2010, respectively. About $160\text{--}240 \mu\text{mol/kg}$ of CaCO_3 was estimated from melted sea ice (Rysgaard et al., 2012) and to $640\text{--}960 \mu\text{mol/kg}$ was observed in the summer ice in the Fram Strait (Rysgaard et al., 2013). If we assume a contribution of 20% ice meltwater ($S = 4$) in volume was added into 20 m deep surface mixed layer water ($S = 30$) during sea ice melt to decrease surface salinity to 25, the concentration of CaCO_3 in a range of $32\text{--}190 \mu\text{mol/kg}$ is still comparable to our estimate. Although it is only a rough estimate because the end-member selection should be refined further, we still can suggest that the dissolution of CaCO_3 might cause the anomalously high TAlk values. It should be pointed out that this analysis is based on unfiltered bottle seawater data. Anomalous high TAlk might be caused by the dissolution of CaCO_3 precipitates collected into bottles (unpublished result, see Chapter 2). In the field, CaCO_3 precipitates might sink to deep water without dissolution. If that happens, the contribution of dissolution of CaCO_3 to anomalous high TAlk might be smaller.

4.1.2. Controlling mechanisms of DIC

DIC distribution also follows the mixing model as TAlk but is complicated by the influenced of additional processes, including biological production/remineralization and air-sea CO₂ exchange. On the shelf, all of the DIC data that plot below the mixing lines support high biological production (Fig. 3.5a, b) as reported in previous studies (Bates, 2006; Bates et al., 2011; Bates and Mathis, 2009). This high consumption of DIC is sustained by nutrient-rich Pacific water. In the slope waters, DIC was alternatively controlled by mixing of modified seawater ($S = 30$) and meltwater in 2008 showing insignificant DIC consumption, and by mixing of Pacific seawater and river water in 2010 showing a moderate decrease in DIC.

In contrast, DIC variation is re much smaller in the Canada Basin than in the shelf and slop waters. In the ice-free Canada Basin, most of the 2008 and 2010 DIC data follow the conservative mixing line of modified seawater ($S = 30$) and meltwater, but also show slight increase in DIC (above the mixing line). Atmospheric CO₂ invasion can contribute to a DIC increase in an ice-free Canada Basin on the basis of an undersaturated surface $p\text{CO}_2$. Additionally, DIC-rich subsurface water upwelling to surface also could increase surface DIC. However, this process is less likely to occur because meltwater develops a strong surface stratification in an ice-free basin which inhibits the upward movement of deep water (McLaughlin and Carmack, 2010). As discussed above, dissolution of CaCO₃ and mixing with river water are other processes that could increase DIC. To clarify which processes might contribute to DIC variation, we refer to DIC and TAlk relationship (Fig. 3.5c, d). In the ice-free Canada Basin, some DIC and TAlk strictly follow the model

mixing line of modified seawater ($S = 30$) and meltwater in both 2008 and 2010, showing non-observable signal of CaCO_3 dissolution. For the rest of the data, some of them show slight increase in DIC but some do not. For DIC data falling on the DIC-Salinity mixing line, we conclude that negligible CO_2 invasion or CO_2 invasion is balanced by low primary production. For the DIC data which slightly fall above the mixing line of DIC and salinity but follow the DIC-TAlk conservative mixing line, we suppose that CO_2 invasion compensates the DIC deficit caused by a small amount of CaCO_3 dissolution. This result confirms a slight dissolution of CaCO_3 in the ocean as discussed in section 4.1.1. If the high DIC and TAlk was caused by dissolution of CaCO_3 precipitates in the sampling bottle, the TAlk and DIC data should exhibit a higher TAlk/DIC ratio. For the rest of the data that don't fall on the model mixing line for DIC and TAlk, we hypothesize that the influence of river water; or low primary production; or dissolution of CaCO_3 control DIC variation. In the ice-covered Canada Basin, some DIC data fall on the mixing line between modified seawater ($S = 30$) and meltwater, while the others show a slight decrease in DIC. This moderate DIC consumption supports the observed low $p\text{CO}_2$ values in the lightly ice-covered Canada Basin (78°N - 81°N) in 2008 and 2010.

4.2. Controlling mechanisms of surface $p\text{CO}_2$

4.2.1. Model simulations of factors influencing surface $p\text{CO}_2$

To study which factors might be the most important for surface $p\text{CO}_2$ regulation in the Arctic Ocean, we simulate how these biogeochemical processes, including biology, cooling, mixing, warming and atmospheric CO_2 invasion influence surface $p\text{CO}_2$ (Fig. 3.6). Considering a lack of CaCO_3 concentration data and the relationship of TAlk and

salinity indicates that CaCO_3 particles were spottily distributed in the ice-melted Arctic Basin (see Chapter 2), therefore, we do not include this potential in this model simulation. However, we will discuss and evaluate this issue separately. In this simulation, we use the same mixing scenario as described in section 4.1. The source water is defined as Bering Sea slope water at 200 m, upwelled to the sea surface and with a $p\text{CO}_2$ range of 420–572 μatm . Aided by solar radiation, nutrient-rich Pacific source water results in high biological CO_2 assimilation (B) in the marginal seas (net primary productivity was measured as $114 \pm 132 \text{ mmol m}^{-2} \text{ d}^{-1}$ during summer 2008, Table 3.1). This source $p\text{CO}_2$ value is reduced to 223–306 μatm by a biological CO_2 fixation of 95 $\mu\text{mol kg}^{-1}$. This water is then diluted by river water (R) to $S = 30$, and then by ice meltwater (I) in the Canada Basin. The simulation shows that mixing of river-seawater does not change the $p\text{CO}_2$ level significantly at $S > 15$. However, mixing with sea ice to salinity 25 will greatly reduce $p\text{CO}_2$ by 50–60 μatm due to a very low $p\text{CO}_2$ level in the meltwater. Subsequent increase in temperature (W) of 4 to 6 °C after sea ice retreat would increase $p\text{CO}_2$ by about 50 μatm . Thus, CO_2 increase due to warming would roughly cancel out CO_2 reduction due to mixing with meltwater in the ice-free region.

The warming effect on surface $p\text{CO}_2$ is evaluated through temperature normalized $p\text{CO}_2$ values ($np\text{CO}_2$) (Fig. 3.7), where $p\text{CO}_2$ values are normalized to -1.6 °C (the average temperature of AOS94) using the coefficient proposed by Takahashi et al. (1993). After normalizing surface $p\text{CO}_2$ to the same temperature, there is no significant difference in $np\text{CO}_2$ among these cruises on the shelf. In contrast, the differences are more complex in the southern Canada Basin. First, $p\text{CO}_2$ differences disappear between the western and eastern cruise tracks for 2008 and almost disappear for 2010, suggesting

that temperature increase accounts for the majority of regional surface $p\text{CO}_2$ variation in the ice-free Canada Basin. Second, interannual difference in $np\text{CO}_2$ still exists among these cruises, showing an increasing surface $np\text{CO}_2$ from AOS94 to MR99 and then to CHINARE cruises. In the northern region, low $np\text{CO}_2$ values (78°N – 81°N) in 2008 and 2010 support the report of higher net primary productivity in the newly opened waters sampled in CHINARE2008 cruise (Lee et al., 2012). In the region north of 81°N , AOS94 and CHINARE cruises still show no difference showing no significant warming in this region.

The significant interannual difference in $np\text{CO}_2$ in the southern Canada Basin shows that this region is the most sensitive area to warming with gradually reduced sea ice cover. Based on the simulation (Fig. 3.6), we should observe $p\text{CO}_2$ level of 200–300 μatm for seawater ($S = 25$, $-1.5 < T < 5.5$ °C) in the ice-free Canada Basin. However, we observed higher $p\text{CO}_2$ values of 275 to 367 μatm (Fig. 3.4). We also notice that when all $p\text{CO}_2$ values are normalized to the same temperature, the 2008 and 2010 $np\text{CO}_2$ values are still ~ 70 μatm higher than AOS94 and ~ 50 μatm higher than MR99. If we consider another 50 μatm drop in $p\text{CO}_2$ for AOS94 and MR99 due to mixing with low $p\text{CO}_2$ ice meltwater. The differences in $p\text{CO}_2$ will increase between these cruises. Based on linear TAlk–Salinity, DIC–Salinity, and DIC–TAlk relationship, and very low nutrient availability (Codispoti et al., 2009) and low net primary productivity (Table 3.1) (Lee et al., 2012) in the Canada Basin, we assume near-zero net biological CO_2 fixation in the Canada Basin. Additionally, we suggest that a potential atmospheric CO_2 invasion which

might be the controlling mechanism sustaining the high surface $p\text{CO}_2$ in the ice-free Canada Basin.

4.2.2. Simulation of CO_2 gas invasion into the ice-free Canada Basin

4.2.2.1. Description of CO_2 gas invasion simulation

To calculate the rate of CO_2 gas invasion into the ice-free Canada basin, we first estimate the depth of surface mixed layer in the deep basin. The mixed layer depth evaluation shows that stratification increases with increasing meltwater in the southern Canada Basin. Limited by sample depth resolution, we can only determine that the mixed layer depth was roughly 20 m or slightly shallower. These results are consistent with other observations of very a shallow mixed layer depth in the Canada Basin (Codispoti et al., 2009). Thus this simulation is based on a mixed layer depth of 20 m.

Measured salinity and TAlk data are used for the summer 2008 simulation because this is the only cruise observing the extensive ice-free Canada Basin. The initial conditions used for simulation are listed in Table 3.2. We then assume that before the ice melted in early spring, $p\text{CO}_2$ in the basin was similar to the value under ice-covered conditions measured during AOS94 at 225 μatm and at -1.5°C . An initial DIC value in the early spring condition is calculated from TAlk and $p\text{CO}_2$. Next, the temperature is raised to 0 and 4°C respectively before gas exchange occurs, and a new $p\text{CO}_2$ at that temperature is calculated. For the $p\text{CO}_2$ difference between atmosphere and surface ocean, $\Delta p\text{CO}_2(\text{air-sea})$, a CO_2 invasion flux is also calculated using the equation of Wanninkhof (1992). Wind speed of 7 m/s observed in 1999 is used for the calculation (Murata and Takizawa, 2003). This amount of CO_2 for a daily time step is then added to the DIC inventory in the mixed layer. Using the new DIC and TAlk (TAlk is a constant),

a new $p\text{CO}_2$ is calculated for the next time step, and so on. One could carry out a better simulation by defining or assuming how temperature would change over time, but the above two simulation curves should bracket the CO_2 dynamics in the mixed layer reasonably well. The bottom line is that the $p\text{CO}_2$ curve will approach the atmospheric $p\text{CO}_2$ value after 90-100 days (Fig. 3.8). Similarly, the 1999 conditions are simulated at 0 °C and -1.5 °C. For the summer 1999 conditions, we use the salinity value to calculate an initial TAlk (scaled from 2008 TAlk). The 1999 initial DIC is calculated from this TAlk and an initial $p\text{CO}_2$ of 225 μatm at -1.5 °C (Table 3.2).

The ice-free period for Canada Basin in 2008 was estimated from AMSR-E data (available at: http://www.iup.physik.uni-bremen.de:8084/amsrdata/asi_daygrid_swath/11a/n6250/). It started around July 12 at the 75°N/150°W area. However, early open areas such as leads and polynyas at lower temperature and lower $p\text{CO}_2$ must also permit effective CO_2 gas exchange. Thus we assumed an effective ice-free condition for the summer of 2008 started from early July. By the time of our survey from middle August to early September, an effective ice-free period of 45 to 60 days is thus assumed. The ice-free condition at 75°N lasted until October 20. Thus a total ice-free period of 90–100 days is assumed for the summer of 2008. For the summer of 1999, the ice edge (sea ice cover = 15%) was at the 74°N latitude in the first week of September. Thus we assume a maximum ice-free condition for 60 days at the survey time in the early and middle September of 1999 for the southern Canada Basin.

4.2.2.2. Estimate of CO₂ gas invasion and air-sea CO₂ flux

Based on the ice-free period of 45 days from early July to mid-August during which we surveyed the ice-free Canada Basin, CO₂ replenishment from the atmosphere would raise the surface seawater $p\text{CO}_2$ to about 340 μatm at a temperature of 4°C in this area (Fig. 3.8), which is similar to our observations. This conclusion would be strengthened if $p\text{CO}_2$ in the early spring was higher than the assigned value due to accumulation of carbon from the previous summer. It can also be further supported if the mixed layer depth is shallower or the wind speed is stronger than we used for simulations. Similarly, for a 30 days ice-free period, CO₂ uptake would increase the surface $p\text{CO}_2$ to 280 μatm in the summer of 1999.

In our model approach, the influence of dissolution of CaCO₃ has not been included and is discussed here. CaCO₃ is formed and trapped in sea ice during the formation of sea ice in winter (Dieckmann et al., 2008; Rysgaard et al., 2007). Ikaite, a polymorph of CaCO₃, has been directly observed in sea ice in the Arctic Ocean (Dieckmann et al., 2010) and indirectly through the high TAlk and DIC ratio in sea ice brine (Rysgaard et al., 2007). Trapped CaCO₃ may be dissolved in sea ice or in seawater after being released during sea ice melting in spring and summer. Both of them have the same contribution to carbonate chemistry in surface waters in an ice-free ocean. Dissolution of CaCO₃ increases TAlk and DIC in a 2:1 ratio and decreases $p\text{CO}_2$. Therefore, a decrease in $p\text{CO}_2$ has a potential to take up CO₂ from the surrounding waters or from the atmosphere. It was suggested that dissolution of CaCO₃ could increase a potential of uptake of atmospheric CO₂ in the surface mixed layer by 60 μatm in the Arctic Ocean (Rysgaard et al., 2007) and by 56 μatm in the Antarctic Ocean (Fransson et al., 2011). However, a

decrease in surface $p\text{CO}_2$ cannot support high $p\text{CO}_2$ observed in the ice-free Canada Basin. If we consider the contribution of CaCO_3 dissolution, the magnitude of atmospheric CO_2 invasion should be increased by $\sim 60 \mu\text{atm}$. Some possible explanations could support this scenario: (1) instantaneous wind speeds with an average $>7 \text{ m/s}$ or a higher constant wind speed should be used in the simulation which can increase the amount of air-sea CO_2 exchange; (2) storm events which injects more CO_2 into surface mixed layer or stir CO_2 -rich subsurface water into the surface layer, both of them can rapidly increase surface $p\text{CO}_2$ level. In summary, our conclusion that atmospheric CO_2 invasion is the main mechanism sustaining high surface $p\text{CO}_2$ in the ice-free southern Canada Basin will not change and could be reinforced if we consider CaCO_3 dissolution.

The shallow mixed layer is the key factor determining the fast replenishment of CO_2 in the surface layer. This shallow depth and strong stratification allow a relatively quick re-equilibration with the atmosphere. This rapid increase in surface $p\text{CO}_2$ slows down further CO_2 uptake by decreasing the air-sea $p\text{CO}_2$ gradient ($\Delta p\text{CO}_2$), the driving force for the gas exchange. When this reduction in driving force is included, the CO_2 invasion for a 100-day ice-free period is $6.4 \text{ mmol m}^{-2} \text{ d}^{-1}$ in 2008. This flux is 85% less than the previous estimate of $46 \text{ mmol m}^{-2} \text{ d}^{-1}$ based on an open water condition measured during summer 2002-2004 at the southern margin of the Canada Basin (Bates, 2006). If we apply this asymptotic reduction of driving force to the newly ice-free basin area of $0.6 \times 10^{12} \text{ m}^2$, we estimate an extra CO_2 invasion flux of only $4.6 \times 10^{12} \text{ gC yr}^{-1}$, compared to a much higher previous estimate of $33 \times 10^{12} \text{ gC yr}^{-1}$ under constant $\Delta p\text{CO}_2$.

4.2.3. Potential factors influencing the surface carbon cycle in the ice-free Canada Basin

Light-limited biological primary production (PP) rate will increase when sea ice is thinning and melting and with increased open water area and longer ice-free period (Arrigo et al., 2008; Arrigo and van Dijken, 2011; Codispoti et al., 2009; Pabi et al., 2008). Indeed, we observed increased biological CO₂ removal in the partially ice-covered basin areas. Once the region was ice-free, however, the linear mixing behavior of DIC relative to TAlk indicates a negligible net ecosystem production rate in the central basin areas. Measured NPP rates ($1.9 \pm 1.0 \text{ mmol m}^{-2} \text{ d}^{-1}$, Table 3.1) in the ice-free region in summer 2008 indicate no increase or even possibly a decrease in biological production compared to the ice-covered conditions in summer 1994 ($2.5 \pm 1.1 \text{ mmol m}^{-2} \text{ d}^{-1}$) (Gosselin et al., 1997). Low net biological CO₂ fixation in the Canada Basin is likely due to a poor supply of nutrients to the surface mixed layer as a result of strong stratification from greatly increased meltwater input, at least inside the Beaufort Gyre where freshwater has accumulated in the past decades (McLaughlin and Carmack, 2010). Nutrient availability to surface water would not only limit water column productivity (Codispoti et al., 2009; McLaughlin and Carmack, 2010; Pabi et al., 2008) but also ice-algal productivity (Gradinger, 2009). In addition, warmer temperatures likely would enhance microbial respiration of organic carbon, potentially reducing net community production (Yager and Deming, 1999). Strong stratification and limited nutrient supply to the surface water may have already caused an ecosystem shift towards smaller algae in the Canada Basin, potentially favoring carbon retention and CO₂ release (Li et al., 2009). However, it is difficult to predict the ultimate role of increased stratification versus

sustained wind mixing in these newly ice free regions. Wind-driven upwelling and mixing of nutrient and CO₂ rich subsurface water is expected or already observed to have a major impact on carbon dynamics and ecosystem in the Arctic marginal areas (Carmack and Chapman, 2003; Mathis et al., 2012). Such an impact is likely small in the central Canada basin, and increased stratification is most likely the dominant feature. Moreover, increased warming could promote permafrost thawing and coastal erosion in the Arctic, increasing riverine inputs of organic carbon (Guo and Macdonald, 2006; Hansell et al., 2004) that is subsequently metabolized to CO₂, thus further contributing to the elevated *p*CO₂. Finally, in future years, when sea surface temperature further increases after all ice is melted during summertime, the CO₂ uptake capacity in the Arctic Ocean basin would reduce further because of the warming effect on surface water *p*CO₂.

5. Conclusions

High resolution surveys of sea surface DIC, TAlk, and *p*CO₂ were conducted across the Pacific Sector of the Arctic Ocean from the Bering Strait to the North Pole during the CHINARE2008 and CHINARE2010 cruises. The aims of these studies were to clarify the distribution and controlling mechanisms of the carbonate system, and elucidate how it may respond to the freshening of the Arctic Ocean. Field measurements showed that mixing scenarios of Pacific water and river runoff and of modified seawater and sea ice meltwater control the distribution of carbonate system. Our data also demonstrated that mixing of Pacific water and river runoff was constrained along the Alaska coast over the Chukchi Sea shelf. The inflowing Pacific water through the Bering Strait (*S* = 32.5) was gradually modified by freshwater input from the Alaska to form modified seawater within a salinity range of 30 to 32.5. The modified sea water mixed with surrounding sea ice

meltwater over the broad Chukchi shelf and in the interior Arctic basins. In addition, the properties of shelf modified seawater were associated with the time and location of sampling.

Mixing between different water sources is the dominant factor controlling TAlk distribution, except in the ice-free Canada Basin where it might be influenced by dissolution of CaCO_3 or increased river discharge. Primary production on the shelf is the dominant controlling factor of DIC distribution besides mixing. In contrast, there is no or very limited DIC removal in an ice-free Canada Basin and in the heavily ice-covered Canada Basin. In the ice-free basin, this is due to the limitation of nutrient supply caused by ice meltwater enhanced surface stratification. In the ice-covered basin, this may be due to limitation of biological production by light availability. Moderate DIC consumption can be observed in the lightly ice-covered Canada Basin where light availability supports net primary production. The controlling mechanisms of surface $p\text{CO}_2$ are similar to DIC and additionally influenced by the effect of warming. In regions with extensive sea ice melt, the influence of mixing with low $p\text{CO}_2$ meltwater is probably cancelled out by warming of surface waters. Moreover, the ice-free basin has no appreciable net ecosystem production due to nutrient limitation and dissolution of CaCO_3 decreases surface $p\text{CO}_2$. Therefore, atmospheric CO_2 invasion into the surface waters is the key factor sustaining the high surface $p\text{CO}_2$ in the ice-free basin. However, increasing surface $p\text{CO}_2$ also in turn acts as a barrier to further CO_2 invasion.

Due to the barrier effect of increasing surface $p\text{CO}_2$ and limited primary production, an CO_2 uptake rate of $6.4 \text{ mmol m}^{-2} \text{ d}^{-1}$ is estimated under the conditions in 2008, which is 85% less than the previous estimate of $46 \text{ mmol m}^{-2} \text{ d}^{-1}$ based on an open water

condition at the southern margin of the Canada Basin which was measured during summer 2002-2004. The corresponding CO₂ invasion flux of only 4.6×10^{12} gC yr⁻¹ in the newly ice-free basin area is much smaller than an previous estimate of 33×10^{12} gC yr⁻¹ under constant $\Delta p\text{CO}_2$. Therefore, contrary to the current view, we predict that the CO₂ uptake capacity in the ice-free Arctic Ocean basin will be quickly weaken owing to shallow mixed layer depth and low biological CO₂ fixation.

References

- Aagaard, K. and Carmack, E.C., 1989. The Role of Sea Ice and Other Fresh Water in the Arctic Circulation. *J. Geophys. Res.*, 94(C10): 14485-14498.
- Anderson, L.G. et al., 2013. Source and formation of the upper halocline of the Arctic Ocean. *Journal of Geophysical Research-Oceans*, 118(1): 410-421.
- Anderson, L.G., Dyrssen, D. and Jones, E.P., 1990. An Assessment of the Transport of Atmospheric CO₂ into the Arctic Ocean. *J. Geophys. Res.*, 95(C2): 1703-1711.
- Anderson, L.G., Jutterstrom, S., Kaltin, S., Jones, E.P. and Bjork, G.R., 2004. Variability in river runoff distribution in the Eurasian Basin of the Arctic Ocean. *J. Geophys. Res.*, 109(C1).
- Anderson, L.G., Olsson, K. and Chierici, M., 1998. A carbon budget for the Arctic Ocean. *Global Biogeochem. Cycles*, 12(3): 455-465.
- Arrigo, K.R., van Dijken, G. and Pabi, S., 2008. Impact of a shrinking Arctic ice cover on marine primary production. *Geophys. Res. Lett.*, 35(19).
- Arrigo, K.R. and van Dijken, G.L., 2011. Secular trends in Arctic Ocean net primary production. *J. Geophys. Res.*, 116: C09011.
- Bates, N.R., 2006. Air-sea CO₂ fluxes and the continental shelf pump of carbon in the Chukchi Sea adjacent to the Arctic Ocean. *J. Geophys. Res.*, 111: C10013.
- Bates, N.R., Cai, W.J. and Mathis, J.T., 2011. The Ocean Carbon Cycle in the Western Arctic Ocean: Distributions and Air-Sea Fluxes of Carbon Dioxide. *Oceanography*, 24(3): 186-201.

- Bates, N.R. and Mathis, J.T., 2009. The Arctic Ocean marine carbon cycle: evaluation of air-sea CO₂ exchanges, ocean acidification impacts and potential feedbacks. *Biogeosciences*, 6(11): 2433-2459.
- Brainerd, K.E. and Gregg, M.C., 1995. Surface Mixed and Mixing Layer Depths. *Deep-Sea Research Part I-Oceanographic Research Papers*, 42(9): 1521-1543.
- Cai, W.-J. et al., 2010. Alkalinity distribution in the western North Atlantic Ocean margins. *J. Geophys. Res.*, 115: C08014.
- Carmack, E. and Chapman, D.C., 2003. Wind-driven shelf/basin exchange on an Arctic shelf: The joint roles of ice cover extent and shelf-break bathymetry. *Geophys. Res. Lett.*, 30(14).
- Coachman, L.K. and Aagaard, K., 1988. Transports through Bering Strait - Annual and Interannual Variability. *Journal of Geophysical Research-Oceans*, 93(C12): 15535-15539.
- Coachman, L.K., Aagaard, K. and Tripp, R.B., 1975. *Bering Strait: The Regional Physical Oceanography*. University of Washington Press, Seattle.
- Codispoti, L.A., Flagg, C.N. and Swift, J.H., 2009. Hydrographic conditions during the 2004 SBI process experiments. *Deep-Sea Research Part II*, 56(17): 1144-1163.
- Comiso, J.C., Parkinson, C.L., Gersten, R. and Stock, L., 2008. Accelerated decline in the Arctic Sea ice cover. *Geophys. Res. Lett.*, 35(1).
- Cooper, L.W. et al., 2008. Flow-weighted values of runoff tracers ($\delta^{18}\text{O}$, DOC, Ba, alkalinity) from the six largest Arctic rivers. *Geophys. Res. Lett.*, 35(18).

- Dickson, A.G. and Millero, F.J., 1987. A Comparison of the Equilibrium-Constants for the Dissociation of Carbonic-Acid in Seawater Media. *Deep-Sea Res. I*, 34(10): 1733-1743.
- Dieckmann, G.S. et al., 2008. Calcium carbonate as ikaite crystals in Antarctic sea ice. *Geophys. Res. Lett.*, 35(8).
- Dieckmann, G.S. et al., 2010. Brief Communication: Ikaite ($\text{CaCO}_3 \cdot 6\text{H}_2\text{O}$) discovered in Arctic sea ice. *Cryosphere*, 4(2): 227-230.
- Ekwurzel, B., Schlosser, P., Mortlock, R.A., Fairbanks, R.G. and Swift, J.H., 2001. River runoff, sea ice meltwater, and Pacific water distribution and mean residence times in the Arctic Ocean. *J. Geophys. Res.*, 106(C5): 9075-9092.
- Fransson, A., Chierici, M., Yager, P.L. and Smith, W.O., 2011. Antarctic sea ice carbon dioxide system and controls. *Journal of Geophysical Research: Oceans*, 116(C12): C12035.
- Gosselin, M., Levasseur, M., Wheeler, P.A., Horner, R.A. and Booth, B.C., 1997. New measurements of phytoplankton and ice algal production in the Arctic Ocean. *Deep-Sea Res. II*, 44(8): 1623-1644.
- Gradinger, R., 2009. Sea-ice algae: Major contributors to primary production and algal biomass in the Chukchi and Beaufort Seas during May/June 2002. *Deep Sea Research Part II*, 56(17): 1201-1212.
- Guo, L. and Macdonald, R.W., 2006. Source and transport of terrigenous organic matter in the upper Yukon River: Evidence from isotope (d^{13}C , D^{14}C , and d^{15}N) composition of dissolved, colloidal, and particulate phases. *Global Biogeochem. Cycles*, 20(2): GB2011.

- Guo, X.H. et al., 2008. Seasonal variations in the inorganic carbon system in the Pearl River (Zhujiang) estuary. *Cont. Shelf Res.*, 28(12): 1424-1434.
- Hansell, D.A., Kadko, D. and Bates, N.R., 2004. Degradation of Terrigenous Dissolved Organic Carbon in the Western Arctic Ocean. *Sci*, 304(5672): 858-861.
- Huang, W.J., Wang, Y.C. and Cai, W.J., 2012. Assessment of sample storage techniques for total alkalinity and dissolved inorganic carbon in seawater. *Limnol. Oceanogr. Methods*, 10: 711-717.
- Kaltin, S. and Anderson, L.G., 2005. Uptake of atmospheric carbon dioxide in Arctic shelf seas: evaluation of the relative importance of processes that influence $p\text{CO}_2$ in water transported over the Bering-Chukchi Sea shelf. *Mar. Chem.*, 94(1-4): 67-79.
- Karcher, M.J. and Oberhuber, J.M., 2002. Pathways and modification of the upper and intermediate waters of the Arctic Ocean. *Journal of Geophysical Research: Oceans (1978–2012)*, 107(C6).
- Lee, S.H., Joo, H.M., Liu, Z.L., Chen, J.F. and He, J.F., 2012. Phytoplankton productivity in newly opened waters of the Western Arctic Ocean. *Deep-Sea Research Part II*, 81-84: 18-27.
- Li, W.K.W., McLaughlin, F.A., Lovejoy, C. and Carmack, E.C., 2009. Smallest Algae Thrive As the Arctic Ocean Freshens. *Sci*, 326(5952): 539.
- Lundberg, L. and Haugan, P.M., 1996. A Nordic Seas–Arctic Ocean carbon budget from volume flows and inorganic carbon data. *Global Biogeochem. Cycles*, 10(3): 493-510.

- Maslanik, J.A. et al., 2007. A younger, thinner Arctic ice cover: Increased potential for rapid, extensive sea-ice loss. *Geophys. Res. Lett.*, 34(24).
- Mathis, J.T. et al., 2012. Storm-induced upwelling of high $p\text{CO}_2$ waters onto the continental shelf of the western Arctic Ocean and implications for carbonate mineral saturation states. *Geophys. Res. Lett.*, 39.
- McLaughlin, F.A. and Carmack, E.C., 2010. Deepening of the nutricline and chlorophyll maximum in the Canada Basin interior, 2003-2009. *Geophys. Res. Lett.*, 37(24): L24602.
- McPhee, M.G., Proshutinsky, A., Morison, J.H., Steele, M. and Alkire, M.B., 2009. Rapid change in freshwater content of the Arctic Ocean. *Geophys. Res. Lett.*, 36.
- Mehrbach, C., Culberso, Ch, Hawley, J.E. and Pytkowic, Rm, 1973. Measurement of the Apparent Dissociation-Constants of Carbonic-Acid in Seawater at Atmospheric-Pressure. *Limnol. Oceanogr.*, 18(6): 897-907.
- Millero, F.J., Graham, T.B., Huang, F., Bustos-Serrano, H. and Pierrot, D., 2006. Dissociation constants of carbonic acid in seawater as a function of salinity and temperature. *Mar. Chem.*, 100(1-2): 80-94.
- Mountain, D.G., Coachman, L.K. and Aagaard, K., 1976. Flow through Barrow Canyon. *J. Phys. Oceanogr.*, 6(4): 461-470.
- Murata, A. and Takizawa, T., 2003. Summertime CO_2 sinks in shelf and slope waters of the western Arctic Ocean. *Cont. Shelf Res.*, 23(8): 753-776.
- Pabi, S., van Dijken, G.L. and Arrigo, K.R., 2008. Primary production in the Arctic Ocean, 1998–2006. *J. Geophys. Res.*, 113(C8).

- Perovich, D.K., 2011. The Changing Arctic Sea Ice Cover. *Oceanography*, 24(3): 162-173.
- Peterson, B.J. et al., 2002. Increasing river discharge to the Arctic Ocean. *Sci*, 298(5601): 2171-2173.
- Pickart, R.S. et al., 2010. Evolution and dynamics of the flow through Herald Canyon in the western Chukchi Sea. *Deep-Sea Research Part II-Topical Studies in Oceanography*, 57(1-2): 5-26.
- Pierrot, D., Lewis, E. and Wallace, D.W.R., 2006. MS Excel Program Developed for CO₂ System Calculations. ORNL/CDIAC-105a. Carbon Dioxide Information Analysis Center, Oak Ridge National Laboratory, U.S. Department of Energy, Oak Ridge, Tennessee. doi: 10.3334/CDIAC/otg.CO2SYS_XLS_CDIAC105a (Available at http://cdiac.ornl.gov/ftp/co2sys/CO2SYS_calc_XLS_v2.1/).
- Pierrot, D. et al., 2009. Recommendations for autonomous underway *p*CO₂ measuring systems and data-reduction routines. *Deep-Sea Res. II*, 56(8–10): 512-522.
- Rabe, B. et al., 2011. An assessment of Arctic Ocean freshwater content changes from the 1990s to the 2006-2008 period. *Deep-Sea Research Part I-Oceanographic Research Papers*, 58(2): 173-185.
- Rysgaard, S. et al., 2012. Ikaite crystals in melting sea ice - implications for *p*CO₂ and pH levels in Arctic surface waters. *Cryosphere*, 6(4): 901-908.
- Rysgaard, S., Glud, R.N., Sejr, M.K., Bendtsen, J. and Christensen, P.B., 2007. Inorganic carbon transport during sea ice growth and decay: A carbon pump in polar seas. *J. Geophys. Res.*, 112: C03016.

- Rysgaard, S. et al., 2013. Ikaite crystal distribution in winter sea ice and implications for CO₂ system dynamics. *Cryosphere*, 7(2): 707-718.
- Schlitzer, R., 2014. Ocean data view, <http://odv.awi.de>, 2014.
- Serreze, M.C. et al., 2006. The large-scale freshwater cycle of the Arctic. *J. Geophys. Res.*, 111(C11): C11010.
- Steinacher, M., Joos, F., Frolicher, T.L., Plattner, G.K. and Doney, S.C., 2009. Imminent ocean acidification in the Arctic projected with the NCAR global coupled carbon cycle-climate model. *Biogeosciences*, 6(4): 515-533.
- Stroeve, J.C. et al., 2012. The Arctic's rapidly shrinking sea ice cover: a research synthesis. *Clim. Change*, 110(3-4): 1005-1027.
- Takahashi, T., Olafsson, J., Goddard, J.G., Chipman, D.W. and Sutherland, S.C., 1993. Seasonal variation of CO₂ and nutrients in the high-latitude surface oceans: A comparative study. *Global Biogeochem. Cycles*, 7(4): 843-878.
- Taylor, J.R., Falkner, K.K., Schauer, U. and Meredith, M., 2003. Quantitative considerations of dissolved barium as a tracer in the Arctic Ocean. *Journal of Geophysical Research-Oceans*, 108(C12).
- Wang, M.Y. and Overland, J.E., 2009. A sea ice free summer Arctic within 30 years? *Geophys. Res. Lett.*, 36.
- Wanninkhof, R., 1992. Relationship between Wind-Speed and Gas-Exchange over the Ocean. *Journal of Geophysical Research-Oceans*, 97(C5): 7373-7382.
- Wassmann, P. and Reigstad, M., 2011. Future Arctic Ocean Seasonal Ice Zones and Implications for Pelagic-Benthic Coupling. *Oceanography*, 24(3): 220-231.

- Weingartner, T. et al., 2005. Circulation on the north central Chukchi Sea shelf. *Deep-Sea Research Part II*, 52(24-26): 3150-3174.
- Weiss, R.F., 1974. Carbon dioxide in water and seawater: the solubility of a non-ideal gas. *Mar. Chem.*, 2(3): 203-215.
- Woodgate, R.A., Aagaard, K. and Weingartner, T.J., 2005a. Monthly temperature, salinity, and transport variability of the Bering Strait through flow. *Geophys. Res. Lett.*, 32(4): L04601.
- Woodgate, R.A., Aagaard, K. and Weingartner, T.J., 2005b. A year in the physical oceanography of the Chukchi Sea: Moored measurements from autumn 1990-1991. *Deep-Sea Research Part II*, 52(24-26): 3116-3149.
- Yager, P.L. and Deming, J.W., 1999. Pelagic microbial activity in an arctic polynya: Testing for temperature and substrate interactions using a kinetic approach. *Limnol. Oceanogr.*, 44(8): 1882-1893.
- Yamamoto-Kawai, M., McLaughlin, F.A., Carmack, E.C., Nishino, S. and Shimada, K., 2009. Aragonite Undersaturation in the Arctic Ocean: Effects of Ocean Acidification and Sea Ice Melt. *Sci*, 326(5956): 1098-1100.
- Yamamoto-Kawai, M., Tanaka, N. and Pivovarov, S., 2005. Freshwater and brine behaviors in the Arctic Ocean deduced from historical data of delta d¹⁸O and alkalinity (1929-2002 AD). *J. Geophys. Res.*, 110(C10).

Table 3.1. Water column primary productivity measured in CHINARE2008 (unit: mg/m²/day, s.d. stands for standard deviation)^a

Region	Date	Longitude	Latitude	Bottom Depth [m]	Primary Productivity [mg/m ² /day]	Summary		
						<i>n</i>	mean	s.d.
Marginal Sea	2008-08-01	-169.03	68.00	51	393.24			
Marginal Sea	2008-08-02	-168.99	70.00	31	143.16			
Marginal Sea	2008-08-03	-164.03	70.50	37	21.94			
Marginal Sea	2008-08-03	-168.97	70.99	37	12.92	7	114.2	132.4
Marginal Sea	2008-08-04	-161.98	71.49	41	115.84			
Marginal Sea	2008-08-04	-163.98	71.54	37	76.86			
Marginal Sea	2008-08-06	-169.00	73.00	71	35.20			
Canada Basin ice-free areas	2008-08-12	-157.99	75.83	568	0.86			
Canada Basin ice-free areas	2008-08-07	-158.99	74.51	1134	2.38			
Canada Basin ice-free areas	2008-09-05	-171.99	75.67	1637	2.02			
Canada Basin ice-free areas	2008-08-10	-154.42	72.20	1785	1.72	7	1.9	1.0
Canada Basin ice-free areas	2008-08-08	-155.97	73.99	2517	3.70			
Canada Basin ice-free areas	2008-08-14	-147.99	75.99	3863	0.96			
Canada Basin ice-free areas	2008-08-11	-152.00	75.00	3889	1.50			

a. Primary productivity data is courtesy of Dr. S. H., Lee, these data have been published in Lee et al. (2012).

Table 3.2. Initial conditions used for simulations of atmospheric CO₂ invasion

	CHINARE2008	CHINARE2008	CHINARE2008	MR99 ^a	MR99 ^a
mixing depth [m]	20	20	20	20	20
salinity	24.78	24.78	24.78	26.5	26.5
water temperature [°C]	-1.5	0	4	-1.5	0
TAlk [μmol/kg]	1853.7	1853.7	1853.7	1982	1982
DIC [μmol/kg]	1750.3	1750.3	1750.3	1860.3	1860.3
<i>p</i> CO ₂ (water) [μatm]	223	239	288	223	240
<i>p</i> CO ₂ (air) [μatm]	375	375	375	360.1	360.1
wind speed [m/s]	7	7	7	7	7

a MR99 data is courtesy of A. Murata which has been published in Murata and Takizawa (2003).

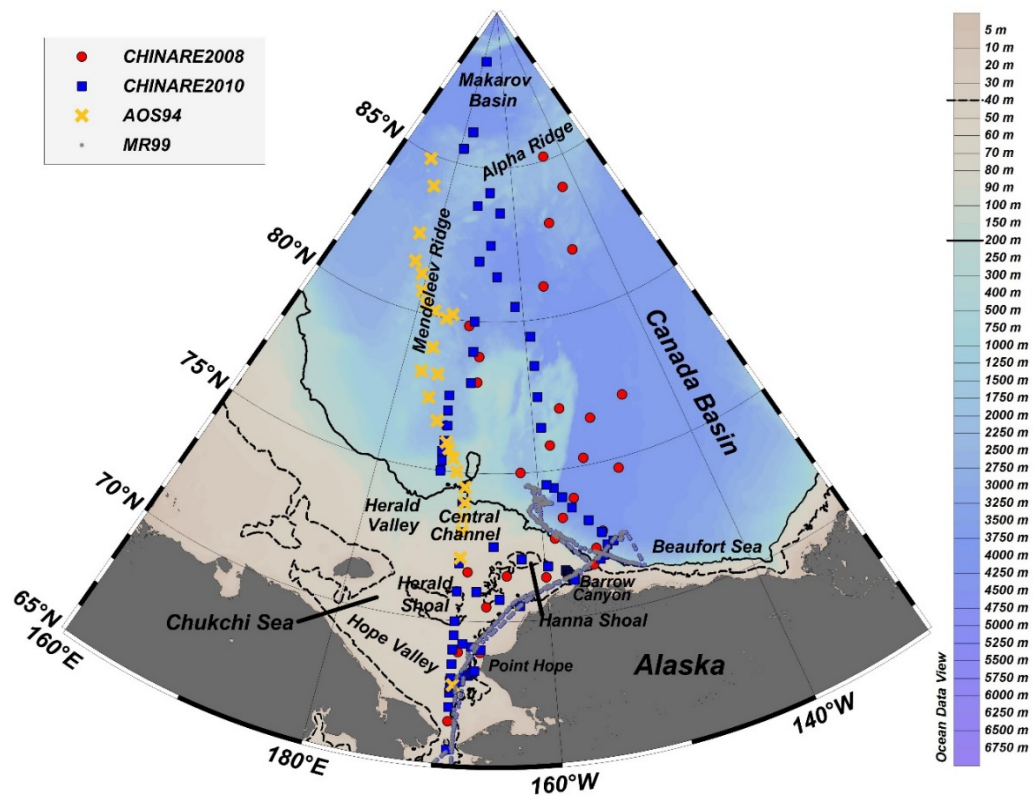


Figure 3.1. Discrete sampling stations of CHINARE2008, CHINARE2010, AOS94 cruises and underway cruise track of MR99 cruise. The black dashed lines indicate the 40 m isobath. The black solid lines indicate the 200 m isobath. This figure is plotted using Ocean Data View (Schlitzer, 2014).

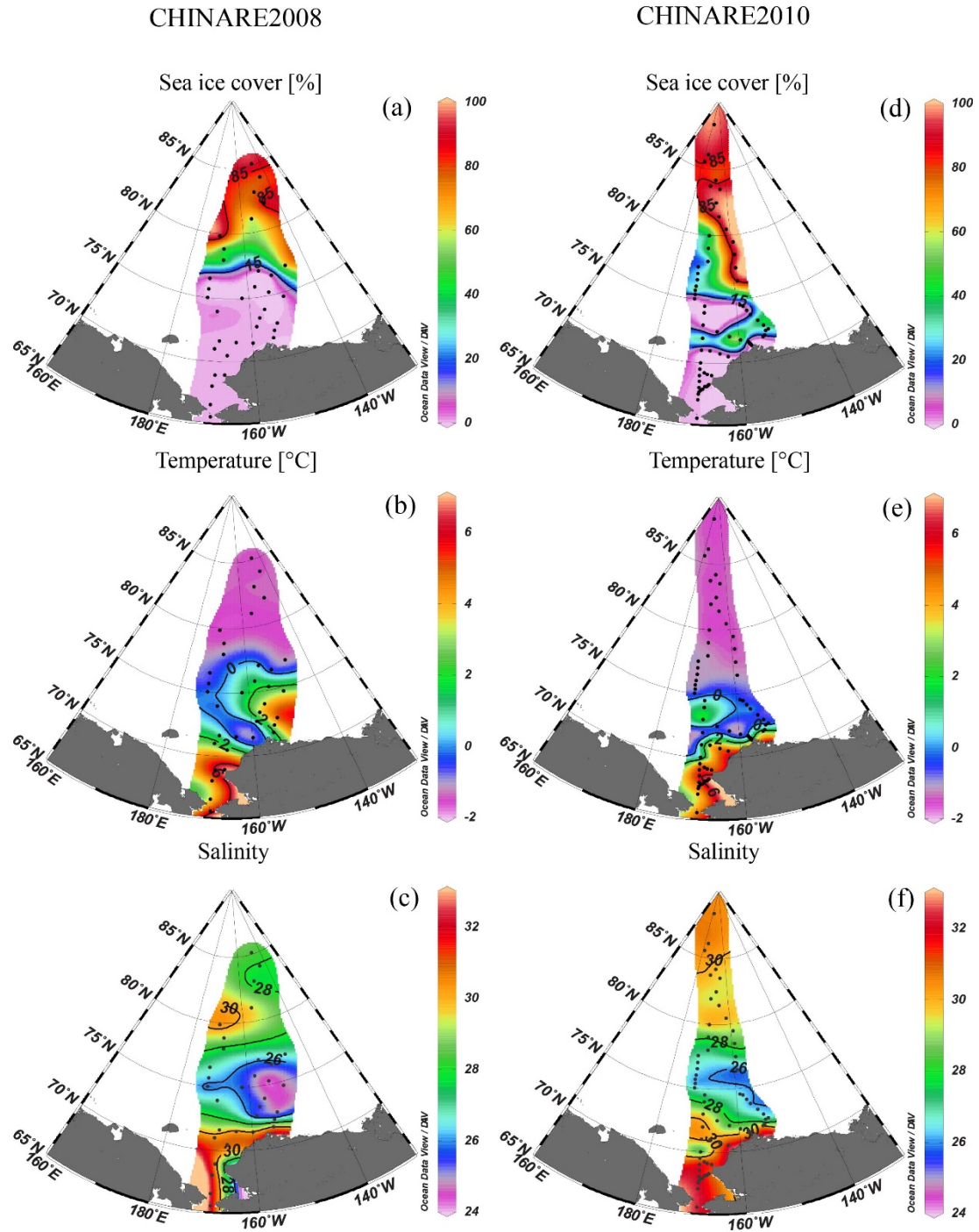


Figure 3.2. Distributions of surface sea ice cover, temperature, and salinity for CHINARE2008 (left panel) and CHINARE2010 (right panel). The contours are plotted using DIVA gridding method.

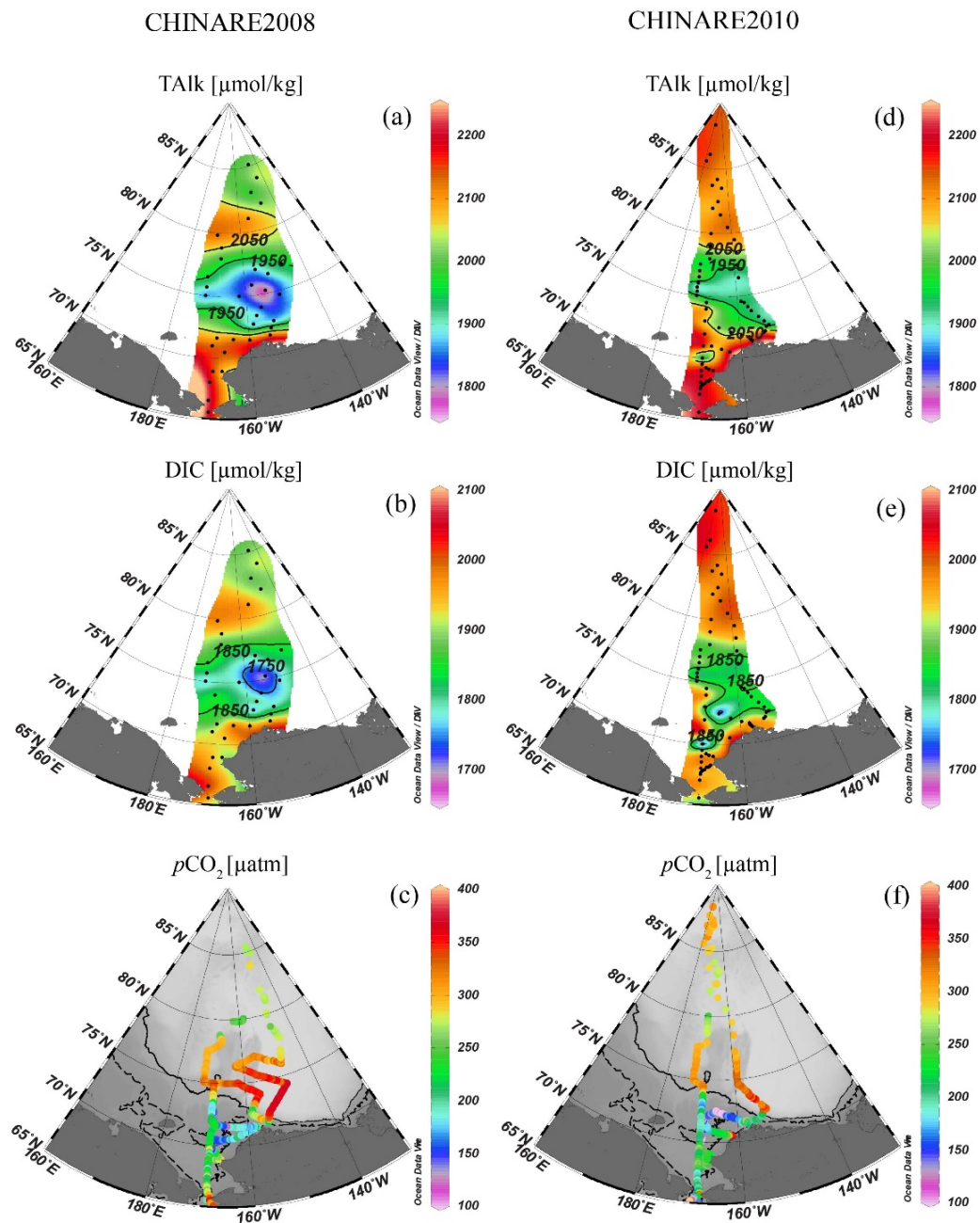


Figure 3.3. Distributions of sea surface TALK, DIC, and $p\text{CO}_2$ for CHINARE2008 (left panel) and CHINARE2010 (right panel). The contours are plotted using DIVA gridding method.

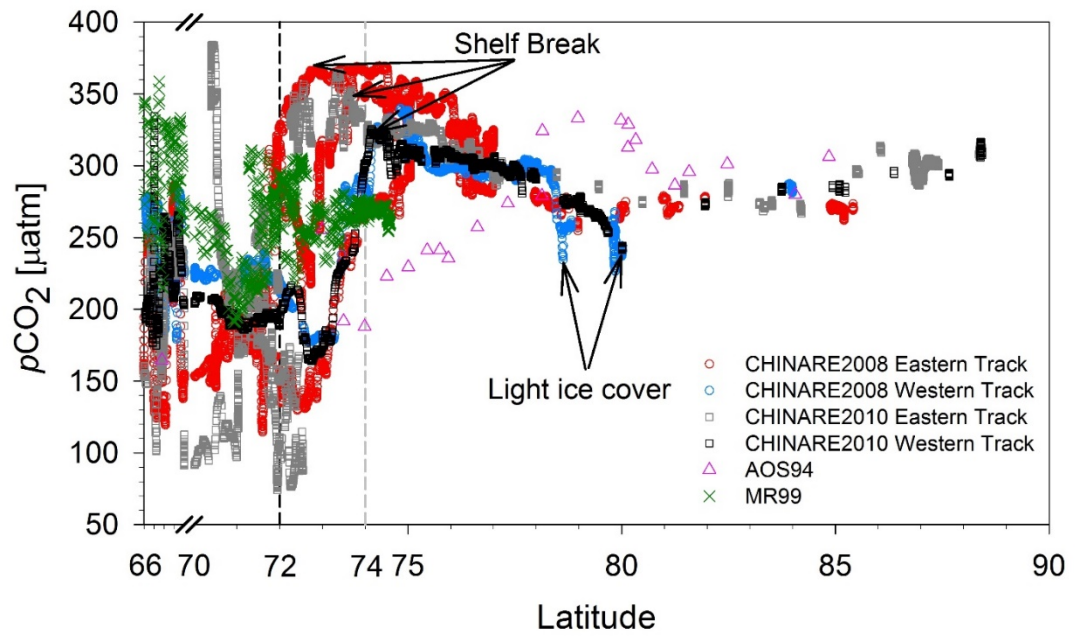


Figure 3.4. Latitudinal distribution of sea surface $p\text{CO}_2$ for CHINARE2008, CHINARE2010, AOS94 and MR99 cruises. Black dashed line marks latitude of 72°N. Gray dashed line marks latitude of 74°N.

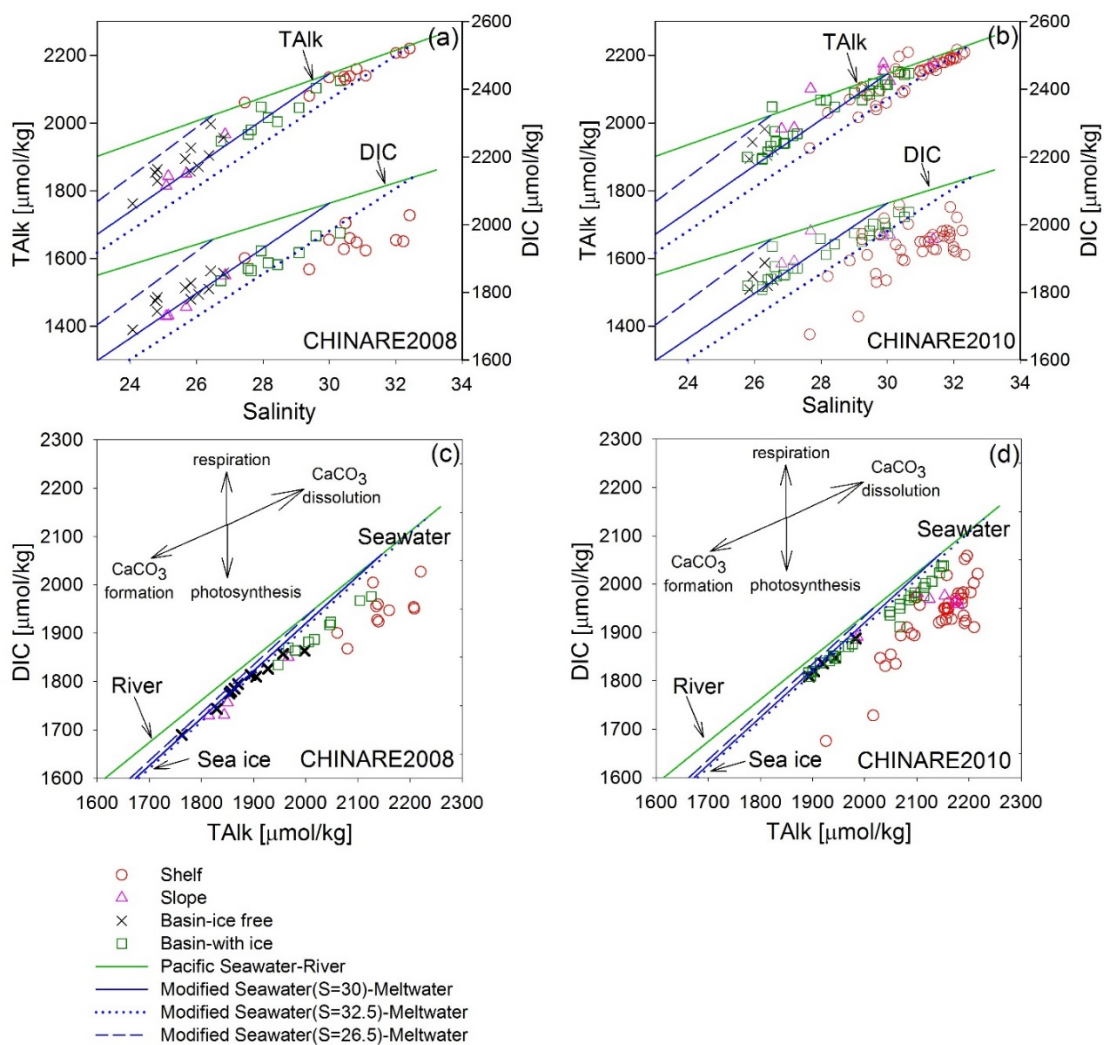


Figure 3.5. Relationship between TALK, DIC, and Salinity during CHINARE2008 (a, c) and CHINARE2010 (b, d). Data are from surface and are separated into shelf, slope, basin-ice free (ice cover < 15%), and basin-with ice (ice cover > 15%) regions. The green solid line is the theoretical mixing line of Pacific seawater and river water. The blue dashed, solid, and dotted lines are the mixing lines of modified seawater (Pacific seawater diluted by the river water to $S = 26.5$, $S = 30$, and $S = 32.5$) with ice meltwater, respectively.

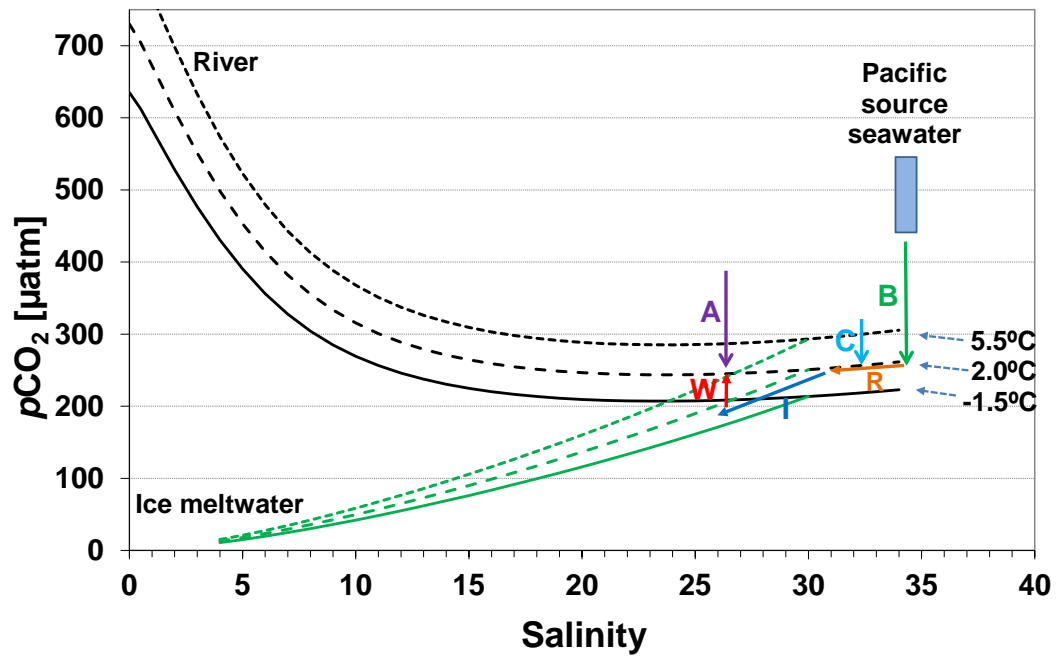


Figure 3.6. Model simulations of factors influencing surface water $p\text{CO}_2$ in the Arctic Ocean. The letters and arrows represent processes with B standing for biology (green), C—cooling (light blue), R—river input (orange), I—ice melt (dark blue), W—warming (red), and A—atmospheric CO_2 invasion (purple). The three black curves represent $p\text{CO}_2$ variation during the mixing between seawater and river water at three temperatures while the three green curves represent mixing between seawater and meltwater at these temperatures.

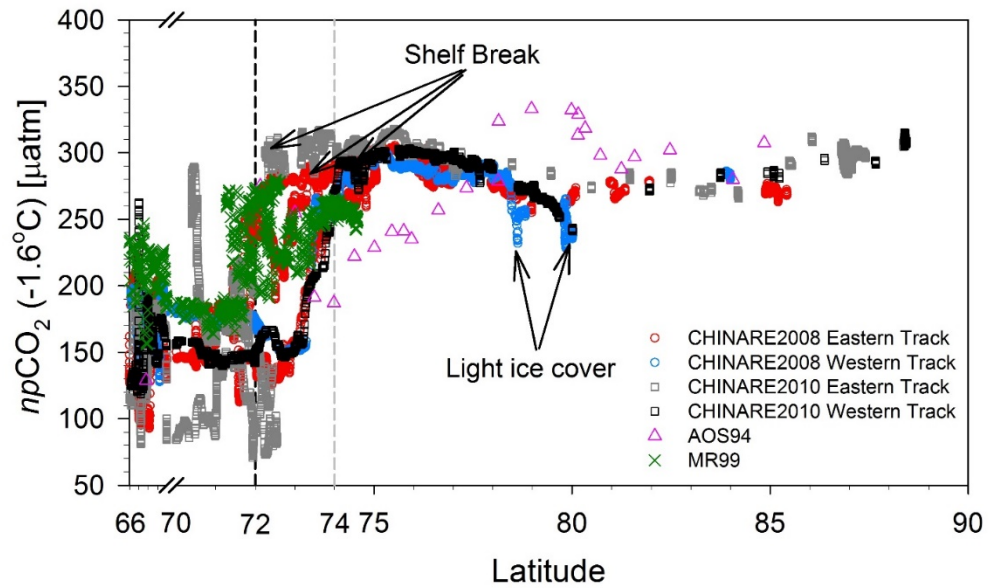


Figure 3.7. Latitudinal distribution of normalized sea surface $p\text{CO}_2$ to -1.6°C for CHINARE2008, CHINARE2010, AOS94 and MR99 cruises. All of the measured surface $p\text{CO}_2$ values are normalized to the AOS94 average surface temperature (-1.6°C) using the equation of Takahashi et al. (1993). Black dashed line marks latitude of 72°N . Gray dashed line marks latitude of 74°N .

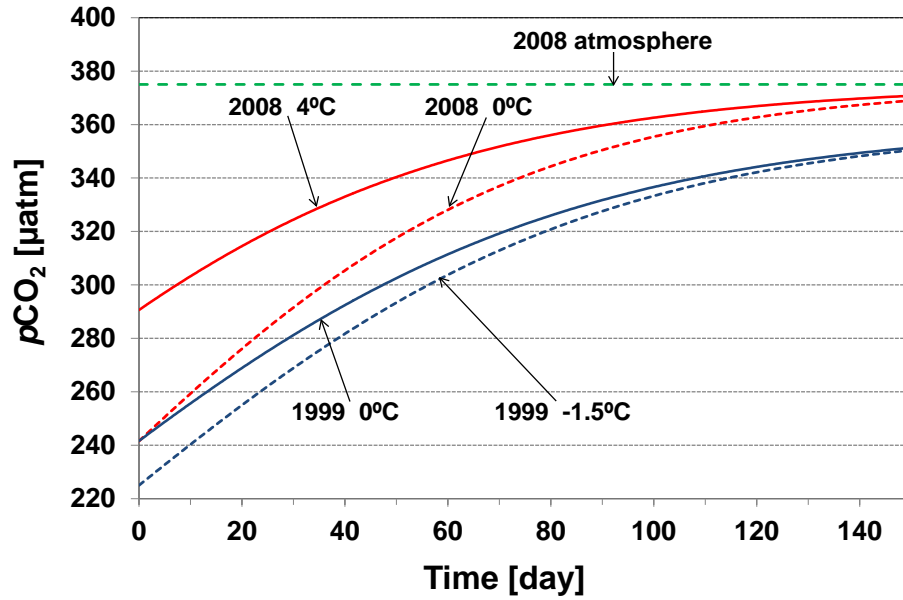


Figure 3.8. Model simulations of sea surface $p\text{CO}_2$ variation responding to atmospheric CO_2 invasion for CHINARE2008 and MR99 cruises. Red lines simulate atmospheric CO_2 invasion for CHINARE2008 at 4 °C (solid) and at 0 °C (dashed). Blue lines simulate atmospheric CO_2 invasion for MR99 at 0 °C (solid) and at -1.5 °C (dashed). The green dashed line indicates the average atmospheric $p\text{CO}_2$ in summer 2008.

CHAPTER 4

THE INFLUENCE OF RECENT SEA ICE RETREAT ON ACCELERATED CO₂ UPTAKE AND CARBON CYCLING IN THE INTERIOR BASIN OF THE WESTERN ARCTIC OCEAN³

³ To be submitted to *Journal of Geophysical Research*

Abstract

To study how carbon cycling responds to sea ice melt in the deep Arctic Basin, we measured the marine inorganic carbonate system and other biogeochemical parameters in the water column over the Chukchi Abyssal Plain, Canada Basin, and Makarov Basin during the Chinese Arctic Research Expedition (CHINARE) in summer 2010. These data were compared with those collected during the Arctic Ocean Section 1994 cruise (AOS94) to conclude that carbon cycling is strongly modulated by sea ice retreat in the western Arctic Ocean. The influence of sea ice melt on carbon cycling has latitudinal features. Sea ice melt creates more open water on the shelves in summer. Thus more brine water was produced during the formation of sea ice and then this winter shelf water was advected into the interior Arctic basin along the upper halocline layer (UHL). We observed broadened and deepened UHL in the Chukchi Abyssal Plain and northern Canada Basin with increased nutrient and dissolved inorganic carbon inventories. On the other hand, freshwater accumulated in the surface of the Chukchi Abyssal Plain might also inhibit upward supply of deep nutrient-rich water which would limit the CO₂ uptake capacity from the atmosphere into the Arctic Ocean due to a decrease in biological production. In the high latitude northern Canada basin with newly opened water, we found that an increase in primary production is associated with early stage of sea ice melt, and confirmed this conclusion through a subsurface increase in DIC within and above the UHL. In the heavily ice-covered Makarov Basin, we observed an increase in subsurface DIC in 2010 which was not observed in 1994. However, a similar DIC profile was observed at lower latitude Arlis Plateau in 1994. The shift in location can be related to the influence of Pacific water and a shift in surface circulation regime. To describe how

carbon cycling responds to sea ice melt, we built a conceptual model: CO₂ is fixed at the beginning of sea ice melt, then the carbon cycling is modified due to accumulation of freshwater in the surface with limited air-sea gas exchange, and finally, carbon uptake capacity will be decreased due to limited nutrient supply and enhanced stratification and atmospheric CO₂ invasion.

1. Introduction

Low biological production was observed in the ice-covered central Arctic Ocean in early times (Gosselin et al., 1997)(English, 1961; Kinney et al., 1971). Recent global caused nonlinear responses in sea surface temperature increase (Steele et al., 2008) and dramatic sea-ice retreat (Perovich and Richter-Menge, 2009), leading to a prediction that the Arctic Ocean basins will be ice-free in summer within 25 years (Wang and Overland, 2009). An increase in biological production has been suggested due to greater open water area and a longer duration of growing season for the summer Arctic Ocean (Arrigo et al., 2008; Arrigo and van Dijken, 2011). It was also suggested that the loss of sea ice could increase underwater irradiance and photosynthesis and therefore increase biological produion after the loss of sea ice (Lalande et al., 2009; Nishino et al., 2009).

Correspondingly, high biological production rates and low surface water $p\text{CO}_2$ values were observed on the continental shelf with ice totally or partially melted (Bates, 2006; Hill and Cota, 2005; Kirchman et al., 2009), indicating a potential for enhanced uptake of CO_2 from the atmosphere after sea ice melt.

Circulation in the Arctic Ocean also plays an important role on primary production by supplying or suppressing nutrient-rich subsurface water to the surface ocean.

Proshutinsky and Johnson (1997) showed that wind-driven anticyclonic circulation regime and cyclonic circulation regime could alternate at intervals of 5–7 years in the central Arctic. The central Arctic Ocean accumulates freshwater, particularly within the Beaufort Gyre (McPhee et al., 2009) due to the Ekman convergence (Proshutinsky et al., 2009) during the anticyclonic circulation regime. In contrast, the Canada Basin receives

water contribution from the Eurasian side during the cyclonic circulation regime and the Beaufort Gyre releases accumulated freshwater and exports them to the north Atlantic Ocean (Proshutinsky et al., 2002). In the past decade, freshwater was accumulated within the Beaufort Gyre due to the dominant anticyclonic circulation (Giles et al., 2012; Proshutinsky et al., 2009). Therefore, surface waters of the southern Canada Basin have significantly freshened (Yamamoto-Kawai et al., 2009b), and experienced a decrease in nutrient availability (McLaughlin and Carmack, 2010), a shift in the phytoplankton community towards smaller cell size (Li et al., 2009), a rise in surface seawater $p\text{CO}_2$ (Cai et al., 2010b; Else et al., 2013), and a decrease in calcium carbonate mineral saturation state (Robbins et al., 2013; Yamamoto-Kawai et al., 2009a). The interactions could potentially inhibit an increase in primary production and an uptake of CO_2 from the atmosphere.

On the contrary, recent direct field observation also reported increased biological production in the newly opened waters in the deep Canada Basin with a 10–90% sea ice cover (Lee et al., 2012). In addition, Nishino et al. (2011) postulated that the biological production will be enhanced outside the Beaufort Gyre due to the nutrient supply from shelves and greater light penetration. Whether biological production and CO_2 uptake are promoted or suppressed as a result of sea ice melt in the Arctic Ocean basin is controversy and is an important unknown resolved issue that hinds our understanding of how the Arctic Ocean CO_2 uptake capacity will change in responding to future warming and sea ice loss. It is also unclear if previous studies just respond to specific stages of sea ice melt.

In this study, we attempt to resolve this controversy through a comparison of geochemical conditions between a state with perennial sea ice cover in 1994 and a state with varying ice cover in 2010 in the western Arctic Ocean basin. In particular, we examine the spatial and temporal variation of inorganic carbon parameters and nutrients in water column to see whether biological production has been enhanced or suppressed as a result of sea ice melt. To do this, we first use dissolved inorganic carbon (DIC) concentration to represent the changes in primary production in response to sea ice melt. Second, we remove the contributions of mixing, denitrification, formation/dissolution of calcium carbonate (CaCO_3) to observed DIC values to generate aerobically-produced DIC. Regional changes in aerobically-produced DIC reflect how biological production (surface) and subsurface recycle respond to sea ice melt. The differences in depth integrated aerobically-produced DIC between 2010 and 1994 are then used to represent the temporal changes.

2. Method

Sampling stations of the Arctic Ocean Section cruise in summer 1994 (AOS94) and the Chinese Arctic Research Expedition in summer 2010 (CHINARE2010) are shown in Fig. 4.1. AOS94 was conducted in the Arctic Ocean between 24 July and 12 September in 1994 aboard CCGS *Louis S. St-Laurent*. This cruise began on the shallow Chukchi Sea shelf/slope (e.g. station 7), advanced into the Chukchi Abyssal Plain (e.g. station 10), Arlis Plateau (station 14), the vicinity of Canada Basin (station 18), and then surveyed across the Mendeleev Ridge into the Makarov Basin (e.g. station 20, 23, and 29). CHINARE2010 investigated similar regions from the Makarov Basin to the Chukchi Sea

shelf during August 20–29, 2010 aboard the R/V *Xuelong*. During CHINARE2010, water sample collection started in the Makarov Basin (station BN13), continued across the Mendeleev Ridge and into the Canada Basin (station SR18), then across the Chukchi Abyssal Plain (e.g. stations SR16, M03, and M05) onto the Chukchi Sea shelf and slope (e.g. station M07). It should be noted that most of the sampling stations were located in the Canada Basin in 2010, while only stations sampled in the Chukchi Abyssal Plain and station 18 were in the Canada Basin in 1994.

2.1. Sampling and analyses for CHINARE2010 cruise

Discrete samples were sampled in the water column for analyses of dissolved inorganic carbon (DIC), total alkalinity (TAlk), inorganic nutrients, dissolved oxygen (DO), and stable oxygen isotopic compositions ($\delta^{18}\text{O}$). DIC and TAlk were analyzed by us at the University of Georgia. Inorganic nutrients data were provide by Jiangfan Chen of the second institute of oceanography, China. DO data were from Weidong Ji of the third institute of oceanography, China. $\delta^{18}\text{O}$ data were provided by Ming Chen of Xiamen University, China.

A SeaBird CTD 911 system and a 24-bottle rosette equipped with 12 L Niskin bottles were used. DIC and TAlk samples were collected into clean 250 mL borosilicate glass bottles. 1 mL of seawater was removed from the bottle to allow for thermal expansion during storage, and then 100 μL of saturated mercuric chloride solution was added to halt biological activity. The bottles were then sealed using Apiezon[®] L greased ground-glass stoppers and stored at 4°C in the dark before analysis. DIC was determined by non-dispersive infrared method and TAlk was determined by open-cell potentiometric GRAN

titration. DIC and TAlk were measured using automated analyzers (Apollo SciTech, USA). The analytical techniques and procedures were documented in Cai et al. (2010a) and Huang et al. (2012). Both TAlk and DIC measurements have a precision of better than 0.1% ($\pm 2 \mu\text{mol/kg}$), with the accuracy set by calibration against certified reference materials for oceanic carbon dioxide studies provided by A. G. Dickson, Scripps Institution of Oceanography.

Water samples for dissolved inorganic nitrate, phosphate, and silicate were measured aboard using a San⁺⁺ automated continuous flow analyzer (SKALAR Inc.). The analytical methods for nutrients were documented in Grasshoff et al. (1983). The precision of these nutrient measurements was $\pm 0.1 \mu\text{M}$ for nitrate and silicate, and $\pm 0.03 \mu\text{M}$ for phosphate. DO was determined using the spectrophotometry based Winkler titration method (Carpenter, 1965; Pai et al., 1993; Strickland and Parsons, 1968; Winkler, 1888). The precision of DO measurements is $1 \mu\text{mol kg}^{-1}$.

$\delta^{18}\text{O}$ was analyzed using mass spectrometer. $\delta^{18}\text{O}$ is a measure of the ratio of stable isotopes $^{18}\text{O}/^{16}\text{O}$, referenced to Vienna-Standard Mean Ocean Water (V-SMOW). It is reported in the units of per mil and defined in Eq. (1):

$$\delta^{18}\text{O}(\text{‰}) = \left(\frac{\left(\frac{^{18}\text{O}}{^{16}\text{O}} \right)_{\text{sample}}}{\left(\frac{^{18}\text{O}}{^{16}\text{O}} \right)_{\text{standard}}} - 1 \right) \times 1000 \quad (1)$$

The precision of $\delta^{18}\text{O}$ measurements is estimated to be $\pm 0.1\text{‰}$.

2.2. Arctic Ocean Section 1994 (AOS94) data

The 1994 Arctic Ocean Section cruise (AOS94) data, including DIC, TAlk, nutrients, and DO, were downloaded (data is accessible via:

<http://cdiac.ornl.gov/ftp/oceans/CARINA/L.S.St.Laurent/18SN199407/>) and were used

for a comparison with CHINARE2010 data. $\delta^{18}\text{O}$ data of AOS94 were retrieved from

“Global Seawater Oxygen-18 Database-v1.2.1” (Schmidt et al., 1999) accessible via

<http://data.giss.nasa.gov/o18data/>. $\delta^{18}\text{O}$ data of AOS94 were referenced to V-SMOW.

2.3. Separating changes in DIC due to physical mixing and various biogeochemical processes

To study how surface biological production responds to sea ice melt, we need to estimate aerobically-produced DIC in subsurface. Thus we need to remove the contributions of other processes which also contribute to DIC variation. These processes include physical mixing among water masses, denitrification at the bottom of Bering Sea and Chukchi Sea shelves, formation/dissolution of calcium carbonate (CaCO_3). Here we present the basis and how we use both DIC and TAlk to correct their contributions.

2.3.1. Calculation of source water fractions and uncertainty

We consider four water masses, including Atlantic water (AW), Pacific water (PW), sea ice meltwater (SIM), and meteoric water (MW, runoff and precipitation) in the Pacific sector of the Arctic Ocean. River runoff and precipitation are combined because they have similar $\delta^{18}\text{O}$ values and river runoff dominates the meteoric water (Schlosser et al., 2002). The fractional contribution of these water masses to a specific water sample can be computed from a four-component mass balance model. In this model approach,

three conservative tracers are required to calculate fractions of the four water sources. Here we follow past choices of conservative tracers of $\delta^{18}\text{O}$, salinity (S), and “phosphate star” (PO_4^*) (Ekwurzel et al., 2001). PO_4^* was defined in Eq. (2) by Broecker et al. (1998),

$$\text{PO}_4^* = \text{PO}_4 + \text{O}_2 / 175 - 1.95 \quad (2)$$

where PO_4 and O_2 are the field observed concentrations of phosphate and dissolved oxygen, respectively, in the global ocean (in $\mu\text{mol/kg}$). This equation assumes that the generation of 1 mole PO_4 will lead to a consumption of 175 moles of O_2 . Thus the total quantity of PO_4^* is conservative. The fractions are calculated using the following four-component mass balance Eqs. (3–6)

$$f_{SIM} + f_{MW} + f_{PW} + f_{AW} = 1 \quad (3)$$

$$S_{SIM} f_{SIM} + S_{MW} f_{MW} + S_{PW} f_{PW} + S_{AW} f_{AW} = S_m \quad (4)$$

$$\delta^{18}\text{O}_{SIM} f_{SIM} + \delta^{18}\text{O}_{MW} f_{MW} + \delta^{18}\text{O}_{PW} f_{PW} + \delta^{18}\text{O}_{AW} f_{AW} = \delta^{18}\text{O}_m \quad (5)$$

$$\text{PO}_{4SIM}^* f_{SIM} + \text{PO}_{4MW}^* f_{MW} + \text{PO}_{4PW}^* f_{PW} + \text{PO}_{4AW}^* f_{AW} = \text{PO}_{4m}^* \quad (6)$$

where subscripts SIM , MW , PW , and AW represent the four end members of sea ice meltwater, meteoric water, Pacific water, and Atlantic water, respectively. Subscript m indicates field measurements. f denotes fraction. Note that sea ice formation, which rejects brine into the underlying waters, will result in a negative fraction of sea ice meltwater. The properties of end members are listed in Table 4.1.

Once the fractional contributions of various source waters in a specific water parcel are estimated, we can predict DIC and TALK in this water parcel by the sum of the product of fraction and corresponding DIC or TALK value assigned to each end-member,

$$X_{predicted} = X_{SIM}f_{SIM} + X_{MW}f_{MW} + X_{PW}f_{PW} + X_{AW}f_{AW} \quad (7)$$

where X denotes DIC or TAlk. X_{SIM} , X_{MW} , X_{PW} , and X_{AW} are the assigned DIC or TAlk values for sea ice meltwater, meteoric water, Pacific water, and Atlantic water end members.

The uncertainties of f and predicted DIC and TAlk are estimated by a statistical method. Assuming a normal distribution of assigned end-member properties, we randomly generate end-member properties based on their mean and standard deviation and use them to calculate f and predicted DIC and TAlk in each model run. This calculation is repeated 1000 times for each discrete sample and we can get a range of f , predicted DIC and TAlk. The uncertainty of our calculation is reported as the standard deviation of these 1000 runs.

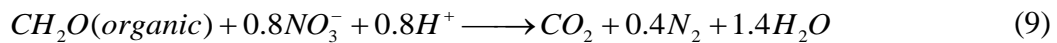
2.3.2. Removing the influences of denitrification and formation/dissolution of CaCO_3

DIC and TAlk in seawater are modified by denitrification when flowing from the Pacific side over the broad Bering Sea and Chukchi Sea shelves. DIC and TAlk are also decreased/increased by formation/dissolution of CaCO_3 during sea ice formation/melting over the shelf and in the basin.

DIC and TAlk changes caused by denitrification can be estimated from the anaerobic respiration of organic matter over the shelves. The anaerobic respiration of organic matter consists of nitrate and phosphate released at a ratio < 16 , indicating the process of denitrification caused by bacterial conversion of fixed nitrogen to nitrogen gas as in Eq. (8). Denitrification has been confirmed over the broad Bering Sea and Chukchi Sea

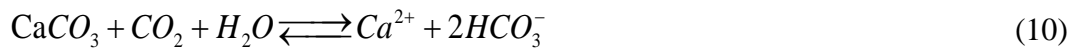
shelves (Devol et al., 1997) and this process increases DIC. Thus its contribution to DIC should be removed when we need to estimate aerobically-produced DIC changes, because winter Pacific water flushing over the bottom of the shelves contributes to the halocline water in the interior Arctic Basin. The amount of changes in DIC and TAlk through denitrification can be evaluated from the definition of the tracer N^* (Eq. 8) which was discussed in detail by Gruber and Sarmiento (1997). As shown in Eq. (9), 1 mole of nitrate denitrified through denitrification will increase 1 mol TAlk and 1.25 mol DIC. In contrast to anaerobic respiration, DIC and TAlk values can also be influenced by aerobic respiration and production. The aerobic respiration, which changes nitrate and phosphate at a ratio of $N/P=16$, contributes to an increase in DIC but only slightly decreases TAlk at a ratio of $TAlk/DIC=-17/106$ if Redfield ratio applies. N^* would not be changed by the aerobic respiration, allowing us to remove the contribution of denitrification from observed DIC and TAlk values. Given that the winter Pacific water has already carried a signal of denitrification ($\sim 4 \mu\text{mol/kg}$, negative N^*), which is averaged from the 200 m layer in the northern Bering Sea (P14N cruise, part of the World Ocean Circulation Experiment section–WOCE), We deduct this initial N^* value from field observations and use the net changes in N^* to calculate the contribution of denitrification on DIC and TAlk.

$$N^* = (N - 16P + 2.90) * 0.87 \quad (8)$$



where N and P are the concentrations of nitrate and phosphate.

DIC and TAlk values are also affected by formation/dissolution of CaCO₃ over the shelves and in the interior Arctic. CaCO₃ mineral (ikaite) is formed in the sea ice in late fall and winter, which is trapped in the sea ice matrix during sea ice formation and released during sea ice melt (Rysgaard et al., 2012; Rysgaard et al., 2014). Dissolution of released CaCO₃ increases DIC and TAlk values at a ratio of 1:2. The chemical reaction of this process is shown in Eq. (10).



In short, TAlk changes consist of contributions from mixing, denitrification, aerobic production/respiration of organic matter, and formation/dissolution of CaCO₃. We can quantitatively estimate the first two terms. However, we do not have Ca²⁺ data and cannot directly estimate how much organic matter was aerobically produced/respired on the shelf and in the basin. As showed above, DIC changes are contributed by the same processes as TAlk and by an additional air-sea exchange. Considering we cannot separate the contribution of air-sea exchange to DIC, and considering that air-sea exchange can be neglected below the surface mixed layer, we attribute the mixing and denitrification corrected DIC and TAlk values (DIC(TAlk)_(measured)–DIC(TAlk)_(mixing)–DIC(TAlk)_(denitrification)) to the contributions of aerobic production/respiration of organic matter and formation/dissolution of CaCO₃. In the surface mixed layer, we run the same calculation because air-sea exchange was limited in the totally ice-covered condition in 1994 and partially/totally ice-covered condition in 2010. This calculation in surface water could underestimate the contribution of biological production and overestimate that of CaCO₃. Thus our approach will handle DIC removal/addition well below the surface

mixed layer but will only minimally reflect biological removal in the surface mixed layer.

The properties of DIC and TAlk for end members are listed in Table 4.1. DIC and TAlk values of sea ice meltwater are scaled to salinity 4 from 5 used in Cai et al. (2010b). Kolyma (Russian) and Mackenzie (American) Rivers are the two main rivers in the respective region and thus their flow-weighted average is used as the TAlk value of meteoric river (Cooper et al., 2008). The DIC value is not available but can be calculated from a TAlk/DIC ratio of 0.856 for meteoric river waters (Guo et al., 2008). DIC and TAlk values of winter Pacific water are calculated from the mixing line of sea ice meltwater (Cai et al., 2010b) and Pacific water ($S = 33.3$) measured at 200 m layer near the Bering Sea shelf break during the P14N cruise because river discharge decreases in winter. DIC and TAlk values of Atlantic water are averages at the temperature maximum layer of 1994 and 2010 cruises.

3. Results

3.1. Vertical distributions of temperature, salinity, nutrients, DIC and TAlk in AOS94 and CHINARE2010

The section profiles of temperature, salinity and nutrients in the top 300 m layer for AOS94 and CHINARE2010 are shown in Fig. 4.2 and Fig. 4.3, respectively. The section profiles of TAlk and DIC for both cruises is shown in Fig. 4.4. Striking differences in temperature and salinity were observed in the Chukchi Abyssal Plain (74–78°N, Fig. 4.1) between AOS94 and CHINARE2010, while only slight differences were observed north of 84°N between two years. As the upper halocline layer (UHL) has been well

characterized with a salinity range of 32.8–33.5 and has a core salinity of 33.1 (Jones and Anderson, 1986), it is used as the reference layer for the following description. Low temperature water (~ 1.5 °C) dominated the top 100 m layer and had a salinity gradient of 30.5–33.1 in the Chukchi Abyssal Plain in AOS94, but it extended to ~ 200 m and had a larger salinity gradient of 26.5–33.1 in CHINARE2010. This low temperature surface layer was shallower over the Arlis Plateau ($\sim 78^\circ\text{N}$) and was stably located at ~ 50 m over the Mendeleev Ridge and in the Makarov Basin ($> 80^\circ\text{N}$) in 1994. In contrast, this low temperature surface layer was located at shallower layer and was gradually shoaling in the Canada Basin ($< 84^\circ\text{N}$) and was stably located at a ~ 65 m layer over the Mendeleev Ridge at about 84°N in 2010, which was ~ 15 m deeper than in AOS94.

Nutrient concentrations ranging from 0–20 $\mu\text{mol/kg}$ for nitrate, 0–3.5 $\mu\text{mol/kg}$ for phosphate and 0–60 $\mu\text{mol/kg}$ for silicate were observed in both cruises (Fig. 4.2 and 4.3). We observed high concentrations of nutrients on the bottom of the Chukchi shelf and in the subsurface waters of the interior basin in 1994 and 2010. The subsurface nutrient maximum in the interior basin is associated with the UHL ($S \sim 33.1$), which has a nutrient-rich source of winter Pacific water exported from the shelf and is characteristic in the Canada Basin as reported in many previous observations (Jones and Anderson, 1986; Kinney et al., 1970; Moore et al., 1983). High nutrient concentrations showed discontinuity from the shelf to the Chukchi Abyssal Plain and were not observed from the Arlis Plateau to the Makarov Basin in 1994 and was small in the Makarov Basin in 2010, which indicates a boundary of higher nutrient Pacific origin halocline water and lower nutrient Atlantic origin halocline water over the sampling areas. On the broad shelf, the highest concentration of nitrate in 1994 (~ 17 $\mu\text{mol/kg}$) was ~ 3 $\mu\text{mol/kg}$ higher than in

2010 (~14 $\mu\text{mol/kg}$). Correspondingly, phosphate was ~1.1 $\mu\text{mol/kg}$ higher and silicate was ~8 $\mu\text{mol/kg}$ higher in 1994 than in 2010. In the interior Arctic basin, subsurface nutrient maximum (e.g., up to 18 $\mu\text{mol/kg}$ for nitrate) was observed in the halocline waters in the Chukchi Abyssal Plain (75–76°N) in 1994 (Fig. 4.2). By comparison, the subsurface nutrient maximum in the Arctic Basin was observed broadly (74–84°N) and has the highest concentrations located farther north (78–80°N) in 2010 (Fig. 4.3). The UHL related subsurface nutrient maximum is a characteristic of Canada Basin. More stations were sampled in 2010 (up to 84°N) in the Canada Basin than in 1994 (up to 76°N) lead to our observation of broader area of subsurface nutrient maximum in 2010. It also suggests that the boundary of Pacific origin halocline water and Atlantic origin halocline water located over Arlis Plateau and Mendeleev Ridge. Thus no upper halocline water was observed over them. The situation in AOS94 was supported by field Barium observations (Guay and Falkner, 1997) and high contribution of East Siberian Sea source river runoff over the Mendeleev Ridge (78–80°N) resulting from the cyclonic circulation regime (Proshutinsky et al., 2002). In contrast, the small signal of subsurface nutrient maximum in the Makarov Basin in 2010 might indicate less influence of Pacific upper halocline water (Fig. 4.3, >84°N).

The UHL is also characteristic for high DIC and TAlk (Fig. 4.4), which is supplied by advection of winter Pacific water from the shelf (Jones and Anderson, 1986). Winter Pacific water increases in DIC and TAlk by receiving brine which is rejected from surface waters during the formation of sea ice. In addition, winter Pacific water also increases in DIC through remineralization of organic matter in the water column and by flushing over the shelf bottom where organic matter is remineralized (Cooper et al., 1997;

Jones and Anderson, 1986). The UHL ($32.8 < S < 33.5$) corresponds to a TALK range of 2250–2270 $\mu\text{mol/kg}$ and a DIC range of 2190–2200 $\mu\text{mol/kg}$ in the Arctic Basin which were summarized from field observations in 1994 and 2010 (Fig. 4.4).

3.2. Regional differences in the depth of DIC, apparent oxygen utilization and phosphate maxima

Considering the latitudinal variation in sea ice cover and the regional variation in the contribution of Pacific origin upper halocline water, we divide the sampling stations of 1994 and 2010 into five groups for a historical comparison, including the slope ($< 75^\circ\text{N}$), Chukchi Abyssal Plain ($75\text{--}78^\circ\text{N}$), northern Canada Basin ($78\text{--}80^\circ\text{N}$, to the eastern flank of Mendeleev Ridge), Arlis Plateau ($\sim 78^\circ\text{N}$, close to Mendeleev Ridge), and Makarov Basin ($80\text{--}88^\circ\text{N}$, to the western flank of Mendeleev Ridge). All of the study areas were ice-covered in 1994, while it was ice free over the slope, partially ice-covered (15–85%) in the northern Canada Basin and heavily ice-covered ($>85\%$) in the Makarov Basin in 2010. The depth profiles of DIC, apparent oxygen utilization (AOU) and phosphate (PO_4) are plotted for CHINARE2010 (Fig. 4.5a–4.5d) and for AOS94 (Fig. 4.5e–4.5i). AOU is calculated from an equation ($\text{AOU} = \text{O}_{2(\text{saturated})} - \text{O}_{2(\text{measured})}$), where a positive AOU indicates that organic matter is respired and oxygen is utilized. PO_4 is used because it is in excess in the Arctic Ocean.

DIC, AOU, and PO_4 are mutually coupled in the biogeochemical processes. Generally DIC, AOU and PO_4 maxima are at the same depth if only biologically-related processes occurred in a single water mass. However, their maxima depths could be decoupled if other processes, such as various water masses mixing and formation/dissolution of

CaCO₃, are included. Our field observations (Fig. 4) showed that DIC, AOU, and PO₄ maxima were variable but appeared at the same depth over the slope, Arlis Plateau and Makarov Basin. In the Chuckchi Abyssal Plain and the northern Canada Basin, DIC and AOU maxima occurred at the same depth while PO₄ maximum occurred at a shallower depth. The depths of maxima and their corresponding salinities are summarized in Table 4.2. There was no water sample collected from the Arlis Plateau in 2010 and there was no significant subsurface increase in DIC, AOU, and PO₄ in the Makarov Basin in 1994.

Five characteristics are summarized from the variation in the depth of DIC and AOU maxima, and agreement/disagreement of the layer of PO₄ maximum and the layer of DIC and AOU maxima. First, DIC and AOU maxima layers, which had a salinity range of 33.2–33.6 and a depth range of 150–200 m for 2010 (Fig. 4.4a-c) and a salinity range of 33.1–33.4 and a depth range of 80–100 m for 1994 (Fig. 4.4e-g) in the slope region, Chukchi Abyssal Plain, and northern Canada Basin, corresponded to the winter Pacific water characterized upper halocline layer (UHL). AOU and DIC maxima layer ($S > 33.1$) corresponds to the lower part of UHL suggests that Pacific origin upper halocline water was a major supplier of subsurface DIC maximum in these regions in both 1994 and 2010. By comparison, lower salinity Pacific origin upper halocline water, which has less salt production on the upper stream western Chukchi Shelf ($32.0 < S < 32.4$) (Shimada et al., 2005), influenced the Arlis Plateau in 1994 and Makarov Basin in both 2010 where the DIC and AOU maxima has a smaller salinity of 32.7. However, Pacific origin upper halocline water has not influenced the Makarov Basin in 1994. Instead, Atlantic water, which had no significant increase in subsurface nutrient, was the dominant water mass in the Makarov Basin. Moreover, no subsurface DIC increase was observed too. Second,

PO₄ maximum layer was at the same depth as DIC and AOU over the slope, while it was located above the UHL in the Chukchi Abyssal Plain and northern Canada Basin. The difference might be related to that shelf exported organic matter rapidly sank to the sediments and was remineralized, and then exported into the UHL by winter advection. Codispoti et al. (2009) reported that the respiration rate in the Canada Basin were exceptionally low, indicating that the shelf produced/exported organic matter is recycled within the shelf system. It also indicates that in situ production/cycling in the interior basins is an additional source contributing to DIC inventory in the water column in the Pacific origin UHL influenced regions. Third, in areas where PO₄ maximum layer disagreed with that of DIC and AOU, PO₄ maximum layer was ~50 m above that of DIC and AOU maxima in 2010 while that was 10–20 m in 1994 due to broadening of UHL in 2010 which could trap organic matter to the top of the halocline layer and let it to be remineralized. Fourth, PO₄ maximum layers were deeper in 2010 (100–150 m) than 1994 (75–77 m) due to freshwater accumulation in surface waters which was caused by the melt of sea ice and change in the surface circulation regimes. This difference indicates that surface fixed carbon can be stored in the deeper waters in 2010. Fifth, a large increase in subsurface PO₄, DIC and AOU was observed in the Arlis Plateau while not observed in the Makarov Basin in 1994. By comparison, a same situation was observed in the higher latitude Makarov Basin in 2010. In short, all these differences between 1994 and 2010 might contribute and complicate carbon cycling studies in an association with sea ice cover and surface circulation regime.

4. Discussion

4.1. Choices and uncertainties of conservative end members

To estimate organic carbon cycling in the response to sea ice retreat, we need to precisely define the fractional contributions of various source waters. As shown in section 2.3, a four-component conservative mixing model is used in this study. The selection of $\delta^{18}\text{O}$, salinity, and PO_4^* as conservative tracers is on the basis of the following considerations. $\delta^{18}\text{O}$ and salinity have been widely used to separate freshwater from seawater in the Eurasian Arctic e.g. (Bauch et al., 1995; Ostlund and Hut, 1984; Schlosser et al., 1994) and in the Canadian Arctic e.g. (Macdonald et al., 2002; Melling and Moore, 1995; Yamamoto-Kawai et al., 2005) due to their conservative behavior and distinct characteristics in various end members. To further separate Pacific water from Atlantic water, one more independent tracer is required to determine their fractional contributions. There have been efforts using various tracers, including nutrient relationship of nitrate and phosphate (Jones et al., 2008; Jones et al., 1998; Jones et al., 2003; Yamamoto-Kawai et al., 2008), silicate (Bauch et al., 1995), TAlk (Anderson et al., 2004), and phosphate (Ekwurzel et al., 2001). In these approaches, using nitrate and phosphate relationships assumes that changes in nutrient concentrations are a result of mixing between Pacific water and Atlantic water. However, this approach cannot account for denitrification which results in a loss of nitrate while does not change phosphate over the Bering Sea and Chukchi Sea shelves (Devol et al., 1997; Tanaka et al., 2004). Silicate is a useful tool to study the influence of Pacific water in the Arctic Ocean due to its higher concentration than Atlantic water and sea ice meltwater. However, Arctic rivers

also have high silicate concentrations in a wide range of ~25–160 $\mu\text{mol/kg}$ (Gordeev et al., 1996; Letolle et al., 1993; Macdonald et al., 1989; Makkaveev and Stunzhas, 1995). Great uncertainty in the silicate concentration for meteoric water limits its application to trace Pacific water in the upper 30 m (Jones et al., 1998). TAlk is also affected by production/mineralization of organic matter over the broad shelves and by denitrification at the bottom of shelves, making it less favorable to compute the fractions of source waters.

Phosphate concentrations of these end members are distinguishable in the Arctic Ocean. Arctic rivers have low phosphate concentrations of close to zero (Gordeev et al., 1996; Macdonald et al., 1989; Macdonald and Wong, 1987; Makkaveev and Stunzhas, 1995). By comparison, Pacific water has highest phosphate concentration (2.3 μM), Atlantic water has a moderate value (0.9 μM), and the phosphate concentration in sea ice meltwater (0.5 μM) is slightly higher than that in river runoff (Macdonald et al., 1989). The gradient of phosphate concentration among various source waters facilitates the separation among various source waters.

During microbial respiration of organic matter, phosphate increases while O_2 is consumed following the Redfield ratio. Therefore, PO_4^* (Eq. 2) has been defined and extensively used a conservative parameter to trace deep water in the ocean (Broecker et al., 1998). However, air-sea oxygen exchange renders PO_4^* no longer a conservative tracer in surface waters with high biological production. Given that (1) interior Arctic basin is less influenced by nutrient-rich Bering Strait inflow, which might result in low primary production (Codispoti et al., 2005); (2) the study area is heavily/partially covered by sea ice which inhibits air-sea gas exchange; (3) PO_4^* of winter Pacific water, which

contributes to the upper halocline water, could not be significantly altered during the transit from the Bering Sea to the Arctic Ocean due to low biological production and sea ice cover in winter, therefore, we choose PO_4^* to study the contributions of different source waters although uncertainties still exist.

The properties of sea ice meltwater are carefully evaluated and chosen. S_{SIM} has a mean value of 4 (Ekwurzel et al., 2001) representing the salinity of multiyear sea ice which dominates the interior basin; $\delta^{18}O_{SIM}$ is -2‰ which was from the direct measurements made in ice cores during the Surface Heat Budget of the Arctic Ocean (SHEBA) study (Eicken et al., 2002; Macdonald et al., 2002). The calculated fraction of SIM (f_{SIM}) is not sensitive to the selected $\delta^{18}O_{SIM}$ values. A sensitivity test shows that f_{SIM} differences are only within -1 to 2% if we use a $\delta^{18}O_{SIM}$ value of 0.3‰ which was used for the entire Arctic surface waters (Yamamoto-Kawai et al., 2005). $PO_4^*_{SIM}$ is 0.4 $\mu\text{mol/kg}$ (Ekwurzel et al., 2001). The properties of meteoric water are: S_{MW} is set to 0; $\delta^{18}O_{MW}$ of -20.7‰ is a flow-weighted value of Kolyma River and Mackenzie River (Cooper et al., 2008) because both of them flow into our study area. Although the flow-weighted $\delta^{18}O$ value of Kolyma River (-22.2‰) is close to that of Mackenzie River (-19.2‰), Kolyma River has a smaller TAlk value (449 $\mu\text{mol/kg}$) than that of Mackenzie River (1540 $\mu\text{mol/kg}$). The intercept of a relationship of surface TAlk and salinity at $S = 0$ (about 900 $\mu\text{mol/kg}$) indicates that the surface waters in our study area received contribution from both rivers. $PO_4^*_{MW}$ is 0.1 $\mu\text{mol/kg}$ (Ekwurzel et al., 2001). The properties of Pacific water are: S_{PW} is set to 32.7 to represent the salinity of winter Pacific water based on Roach et al. (1995), Ekwurzel et al. (2001) and Woodgate et al. (2005); $\delta^{18}O_{PW}$ is -1.1‰ indicating the characteristic of winter Pacific water (Cooper et al.,

1997); PO_4^{*PW} is 2.4 $\mu\text{mol/kg}$ (Ekwurzel et al., 2001). The properties of Atlantic water are: S_{AW} (34.83) and $\delta^{18}O_{AW}$ (0.27‰) are averages of salinity and $\delta^{18}O$ values at the temperature maximum layer which were collected during the AOS94 and CHINARE2010 cruises. These values are close to 34.87 and 0.24‰ which were averaged from the temperature maximum layer in the Eurasian Basin (Yamamoto-Kawai et al., 2005); Given that PO_4^{*AW} could be modified during the transit from the Eurasian Basin to the Canada Basin due to the influences of sea ice formation/melt and air-sea O_2 exchange, we average the PO_4^* values at the temperature maximum layer in 1994 and 2010 and get a mean value of 0.62 $\mu\text{mol/kg}$. The result of a sensitivity test shows that the fractions of Atlantic water would be up to 106% in the Atlantic water dominated layers when using a mean value of 0.7 $\mu\text{mol/kg}$ for PO_4^* which was suggested in Ekwurzel et al. (2001), while the uncertainties can be constrained within 2% when using the PO_4^* value assigned in this work.

It should be noted that the Pacific inflow through the Bering Strait has a larger variability than the other source waters because of the influence of seasonal processes on the Bering and Chukchi Sea shelves. Large variation in the chemical properties of the inflowing Pacific water results in higher uncertainties in the calculated fraction of Pacific water. We use average salinity from January to April to representative winter Pacific water properties and thus to minimize such influence in the calculation (Woodgate et al., 2005). The properties of end members are summarized in Table 4.1.

The fractional contributions of water estimated from Eqs (3–6) are sensitive to the choice of end-member composition and to the analytical errors. The choice of end-member has potentially a greater impact on calculated results than analytical errors which

only produce random errors. If we assign the analytical errors of $S = 0.01$, $\delta^{18}O = 0.1\%$, and $PO_4^{*} = 0.03$, the uncertainties for fractions of SIM ($0.5\% \pm 0.1\%$), MW ($0.5\% \pm 0.1\%$), PW ($1.4\% \pm 0.3\%$), and AW ($1.3\% \pm 0.3\%$) and the corresponding uncertainties of predicted DIC ($4 \pm 1 \mu\text{mol/kg}$) and TAlk ($5 \pm 1 \mu\text{mol/kg}$) are small and can be neglected. Larger uncertainties are from the large variability in end-member composition. Using the ranges of end-member uncertainties given in Table 4.1, the uncertainties are listed: for fractions of SIM ($0.5\% \pm 0.1\%$), MW ($0.5\% \pm 0.2\%$), PW ($3.7\% \pm 0.3\%$), and AW ($3.5\% \pm 0.3\%$), and the corresponding uncertainties of predicted DIC ($5 \pm 2 \mu\text{mol/kg}$) and TAlk ($6 \pm 3 \mu\text{mol/kg}$). Larger uncertainties of fractions of PW ($3.7\% \pm 0.3\%$) and AW ($3.5\% \pm 0.3\%$) indicates that the system is most sensitive to the uncertainties in the composition of PW and AW due to their larger contributions. We further compare predicted TAlk which are calculated from the mixing model with field measurements of TAlk (data not presented). The result also shows that our predicted TAlk and measured TAlk are in good agreement in a range of -4 – $4 \mu\text{mol/kg}$ for most of the data below the upper halocline layer because dissolution of $CaCO_3$ could occur within in the UHL, consolidating our data quality and reliability of conservative mixing model.

4.2. Aerobically-related carbon cycling in the water column in an association with sea ice retreat

We remove the contributions of mixing, denitrification and dissolution/formation of $CaCO_3$ from field measurements of DIC to get aerobically-produced DIC values.

Hereinafter we refer to it as ΔDIC . Depth profiles of ΔDIC and fractions of various source waters are plotted in Fig. 4.6. A positive ΔDIC below the surface mixed layer means that field measurement of DIC is larger than estimated DIC, indicating organic

matter remineralization. However, air-sea CO₂ gas exchange could also result in positive DIC values in the surface mixed layer (~20–30 m). Air-sea exchange is limited when the surface water is heavily covered by sea ice, such as all study areas in 1994 and the Makarov Basin in 2010. In the sea ice covered regions, cracks of sea ice, lead, and polynya are the major pathways for gas exchange. Although it is also demonstrated that sea ice becomes permeable to CO₂ during summer in both Arctic and Antarctic (Delille et al., 2007; Nomura et al., 2010; Papakyriakou and Miller, 2011; Rysgaard et al., 2007; Semiletov et al., 2004), air-sea gas exchange in ice-covered region was generally small and can be neglected (Bates and Mathis, 2009). This is supported by our observation that the most negative Δ DIC observed in surface water and deep surface mixed layer in the ice-covered region in both 1994 and 2010. Air-sea exchange will be enhanced after the start of sea ice melting. We got positive surface Δ DIC in the Chukchi Abyssal Plain with $f(\text{SIM})$ up to 0.1 and slightly negative Δ DIC in the northern Canada Basin with $f(\text{SIM})$ up to 0.05 in 2010. Lower sea ice cover and longer duration of open water result in positive surface Δ DIC in the Chukchi Abyssal Plain in 2010, indicating air-sea exchange exceeds the surface biological fixation of carbon. Atmospheric CO₂ invasion is supported by the undersaturated surface $p\text{CO}_2$ (calculated from surface DIC and TAlk) with respect to the atmosphere in 2010. By comparison, less amount of CO₂ invasion into the surface water or higher surface biological production result in a slightly negative surface Δ DIC in the northern Canada Basin. In addition, we observed negative Δ DIC just below the surface mixed layer in the partially ice-melted regions in 2010 and in the ice-covered surface waters in 1994, indicating surface carbon fixation no matter if the ocean is covered by sea

ice during summer. It is related to thinning of sea ice and increased radiation penetrate through sea ice and increased temperature in summer.

Subsurface Δ DIC maximum is another feature of water column carbon cycling in the Pacific UHL influenced Chukchi Abyssal Plain and northern Canada Basin. Negative $f(\text{SIM})$, which corresponds to brine water rejection during sea ice formation in water, is observed in the subsurface waters in the Chukchi Abyssal Plain ($\sim -4\%$, ~ 200 m) and in the northern Canada Basin ($\sim -2\%$, $\sim 100\text{--}150$ m) in 2010. The depths of brine water corresponded to the UHL and a large fraction of Pacific water (up to 60%), indicating the influence from the shelf. This layer also corresponds to the highest subsurface Δ DIC, showing the largest contribution of winter Pacific water to the DIC inventory in the interior Arctic Basin. As discussed above, Pacific upper halocline water influenced Chukchi Abyssal Plain in both 1994 and 2010. We observed that the $f(\text{SIM})$ is about 0.02 more negative in 2010 than 1994. The more negative $f(\text{SIM})$ demonstrates larger amount of winter Pacific water was exported into the interior basin which result in a broadened UHL in 2010. Increased export of shelf origin upper halocline water might be related to more open water over the shelves during winter due to increased air temperature and thus more brine could be produced and into interior basin. To the northern Canada Basin, given that the subsurface water was less influenced by winter Pacific water contribution (negative $f(\text{SIM})$) than in the Chukchi Abyssal Plain. Therefore, a higher subsurface Δ DIC maximum ($78 \mu\text{mol/kg}$, 150 m) than ($55 \mu\text{mol/kg}$, 200 m) in the Chukchi Abyssal Plain confirms higher surface primary production and remineralization of organic matter in the subsurface layer of the northern Canada Basin. High primary productivity was also observed in newly opened surface water in deep Arctic basins in summer 2008 by direct

rate measurements by Lee et al. (2012). The reoccurrence of high carbon fixation in the partially ice-covered basin might indicate a connection between enhanced primary production and an early stage of sea ice melt. By comparison, the surface fixation of carbon should be smaller in the southern Chukchi Abyssal Plain due to more freshwater accumulated in the surface which might limit upward of nutrient supply.

Subsurface Δ DIC maximum is also important in water column carbon cycling in the Atlantic halocline water dominated Arlis Plateau and Makarov Basin. An increase in subsurface Δ DIC was observed in the Makarov Basin in 2010 with high fractional contribution of Pacific water of ~ 0.5 . In contrast, similar pattern was not observed in 1994. By comparison, a similar subsurface Δ DIC increase was observed in the Arlis Plateau in 1994 with a large contribution of ~ 0.5 from Pacific water. It seems this pattern has been shifted to the high latitude which might be related to warming or a shift in surface circulation regime. Although the Makarov Basin was still covered by sea ice in summer 2010, increased amount of melt pond which allow light to penetrate through sea ice might be a possible mechanism to support surface carbon fixation. Similar phytoplankton blooms was observed beneath the sea ice in the Chukchi Sea which is controlled by this mechanism (Arrigo et al., 2012; Arrigo et al., 2014). Under the circumstance of continued transformation to a younger ice pack and the loss of oldest and thickest sea ice (Maslanik et al., 2007), we speculate enhanced primary production can be observed even the basin is still heavily covered by sea ice, which might be earlier than current condition of enhanced primary production around the ice margin.

The regional differences in carbon fixation can be estimated from depth integrated Δ DIC values (Fig. 4.7). As stated earlier, Δ DIC reported here (Fig. 4.6a-d) combines the

contributions of shelf-origin and in situ-origin aerobic production/respiration of organic matter. We cannot further separate in situ contribution from shelf contribution. To evaluate whether sea ice melt increases or decreases primary production and if regional differences exist, we compare the DIC inventory from surface down to the layer of AOU and DIC maxima. However, a comparison of regional differences may reflect better in situ recycling as the winter advective water progressively moves northward. Subsurface Δ DIC minimum (~ 30 m) is used to represent the surface condition in basins where air-sea exchange contributes to an increase in DIC, although it still might underestimate surface carbon fixation. In the winter Pacific water influenced Chukchi Abyssal Plain, DIC inventory is higher ($42\text{--}44$ g C/m²) in sea ice extensively melted 2010 when comparing with ice-covered condition (10 g C/m²) in 1994. More winter Pacific origin halocline water formed on the shelf and exported into the interior basin results in an increased DIC inventory due to more open water on the shelves in summer. However, the depth of UHL is depressed due to the accumulation of fresh water in the surface, which might limit the availability of upward supply of nutrients. On the other hand, broadened UHL traps sinking organic matter to its top and allows the organic matter decomposed according to the disagreement of PO₄ maximum layer and AOU and DIC maxima layer. It also means that broadened UHL could prevent organic matter from sinking to the deep basin. These combined effects might result in an accumulation of inorganic carbon in the halocline layer. The DIC inventory does not vary in the Chukchi Abyssal Plain ($75.5\text{--}77.5^\circ\text{N}$) in 2010, however, it increases rapidly ($77.5\text{--}78.0^\circ\text{N}$) to 55 g C/m² at station SR16 which is about 10 g C/m² higher than those in the Chukchi Abyssal Plain. We further consolidate the conclusion of enhanced primary production around sea ice margin from the highest

subsurface Δ DIC value and we confirm that sinking organic carbon can be remineralized rapidly from the surface to the UHL. In addition, the remineralized organic matter might be collected during the transit of water moving northward. However, rapid increase in DIC inventory confirms an enhanced primary production around ice margin.

Additionally, we do not see any difference in carbon inventory in the Makarov Basin over the past decade (-8 gC/m² in 2010 vs. -11 to -1 gC/m² in 1994). In summary, we suppose that carbon cycling responds to different stages of sea ice melt, including ice-covered stage, partially ice-melted stage, and ice-free stage. We will show a conceptual model in the following section.

4.3. A Conceptual model of carbon cycling responding to stages of sea ice melt

Through a combination of DIC, T , S , and nutrient profiles from the Chukchi Abyssal Plain to Canada Basin and to the Makarov Basin, we present a conceptual model based on the stages of ice melt and associated changes in water density structure and light and nutrient availability to explain the contrasting responses of the Arctic Ocean basin CO₂ dynamics to sea ice melt over time and space (Fig. 4.8). During the initial ice melt stage (stage I) (Fig. 4.8a), sea ice thinning and melting promotes biological production, but mixed layer net community production (NCP) rates are limited by the availability of light. In this scenario, surface ocean CO₂ uptake from the atmosphere is limited by the nearly complete sea ice cover, leading to relatively low seawater p CO₂. This stage represents basin conditions of summer in 1990s as well as present-day early spring. During stage II, sea ice becomes thinner and melt pond and open water areas become significant, resulting in improved light condition and higher biological production

(Arrigo et al., 2012; Lee et al., 2012). The depth of a rapid increase in nutrients, the nutricline, also shoals due to a relatively weak subsurface stratification (Fig. 4.8b). In this stage, CO₂ uptake from the atmosphere is higher but is still limited by heavy ice coverage and outweighed by increases in biological CO₂ removal, leading to very low seawater *p*CO₂, and to the summer conditions in the northern Canada Basin at present and the partially melt slope water in 1990s and early 2000s. Then in stage III (Fig. 4.8c), excessive melt water creates a highly stratified subsurface layer that nearly completely blocks nutrient supplies from below the nutricline to the very shallow surface mixed layer (Cai et al., 2010b; McLaughlin and Carmack, 2010; Nishino et al., 2011; Tremblay et al., 2011). At this stage, rapid CO₂ uptake from the atmosphere outweighs biological removal, leading to high sea surface *p*CO₂. In addition, while biological production likely will extend below the mixed layer and thus contribute to carbon cycling at the deep depths, this production has no control on the surface water *p*CO₂. We emphasize that any particular area in the Arctic Ocean basin may have experienced a transition from stage I to II and then even to III from spring to later summer as a seasonal phenomenon nowadays but with stages II and III occurs either first time ever or more often after 2007 than before as a long term trend. We suggest that the Arctic Ocean basin ecosystem and carbon dynamics, at various extent depending on the location and season, are in the process of switching from a system with ice-limited low light, low production and low air-sea CO₂ gas exchange to a highly productive and relatively low gas exchange intermediate state, and then to a moderately productive but with rapid air-sea exchange system (now manifests only in the Chukchi Abyssal Plain or anywhere within the Beaufort Gyre).

What will be the future CO₂ uptake rate if the Arctic Ocean basin eventually becomes ice-free during summer in two to a few decades? The current nearly ice-free southern basin provided a good example for the future summertime ice-free Arctic Ocean. A 43 $\mu\text{mol/kg}$ increase of DIC as a result of CO₂ uptake from the atmosphere in the southern basin surface water would translate into an average of 13 $\text{mmol/m}^2/\text{d}$ of CO₂ uptake flux if an average mixed layer depth of 20 m and an open ice period of 60 days at the time of survey are applied. This flux is 5 to 10 times of an earlier estimate of the current central Arctic Ocean basin that was extrapolated from the Beaufort Slope to the basin by assuming zero CO₂ flux in ice-covered areas (Bates and Mathis 2009). Note also that our CO₂ uptake flux is estimated based on an integrated flux over an ice open season, which is more realistic, while the earlier estimate was based on observed instantaneous $p\text{CO}_2$ at the time of observation made in the slope area, the $p\text{CO}_2$ of which can be much higher than the earlier season $p\text{CO}_2$ and thus lead to lower air-sea flux. Using an area of 4,489,000 km^2 , for the central Arctic Ocean basins and an effective ice-open period of 90 days (Bates and Mathis 2009), we thus estimate that an ice-free central Arctic Ocean basin can take up a total of 65 TgC per year (during summer). The current central basin CO₂ uptake flux is only 5 to 20 TgC yr^{-1} , in addition to an uptake flux of 60-150 TgC yr^{-1} in the margin areas (Bates and Mathis 2009). Thus, assuming a similar flux in the marginal seas, a summertime ice-free Arctic Ocean basin could effectively increase the Arctic Ocean CO₂ uptake capacity by 50-100%.

5. Conclusion

Through a comparison of data collected during the CHINARE2010 cruise with that collected from AOS94 cruise, we aimed to elucidate how carbon cycling responds to sea ice melt and how a shift in ocean circulation regime affects carbon cycling. Through a comparison of field observed data, we observed deepened and broadened Pacific origin upper halocline layer in the interior Arctic in 2010. These changes might be associated with increased summer open water area over the shelves through which more brine water could be produced during late fall and winter and be exported to interior of the Arctic Ocean.

In addition, we further evaluated aerobically-related carbon cycling in the interior Arctic basins by removing the contributions of denitrification, formation/dissolution of CaCO_3 to observed DIC and TAlk values. Though a combined analysis with the regional differences in the disagreement of the layer of PO_4 maximum and the layer of AOU and DIC maxima, we found that the influence of sea ice melt on carbon cycling has latitudinal features which corresponded to various stages of sea ice melt. The analysis showed that shelf exported organic matter should sink fast to the slope and be remineralized. Then the remineralized inorganic product is exported into the interior Arctic along with the upper halocline water in winter. In the nearly ice-free Chukchi Abyssal Plain and northern Canada Basin, deepened and broadened upper halocline layer might prevent sinking of organic carbon to deep sediments. Moreover, an accumulation of freshwater in the surface might inhibit the upward movement of high carbon and nutrient water and might limit surface primary production. In the partially ice-covered northern Canada Basin where freshwater accumulation is less and sea ice is just melted, we observed enhanced

primary production which can be reflected by an increase in surface ΔDIC which is larger than the subsurface maximum in the lower latitude Chukchi Abyssal Plain. In the heavily ice-covered Makarov Basin, an increase in subsurface ΔDIC was observed in the Makarov Basin in 2010 with high fractional contribution of Pacific water of ~ 0.5 . In contrast, similar pattern was not observed in 1994. By comparison, a similar subsurface ΔDIC increase was observed in the Arlis Plateau in 1994 with a large contribution of ~ 0.5 from Pacific water. It seems this pattern has been shifted to the high latitude which might be related to warming or a shift in surface circulation regime.

Finally, we presented a conceptual model based on the stages of ice melt and associated changes in water density structure and light and nutrient availability to explain the contrasting responses of the Arctic Ocean basin CO_2 dynamics to sea ice melt over time and space.

References

- Anderson, L.G., Jutterstrom, S., Kaltin, S., Jones, E.P. and Bjork, G.R., 2004. Variability in river runoff distribution in the Eurasian Basin of the Arctic Ocean. *J. Geophys. Res.*, 109(C1).
- Arrigo, K.R. et al., 2012. Massive Phytoplankton Blooms Under Arctic Sea Ice. *Science*, 336(6087): 1408-1408.
- Arrigo, K.R. et al., 2014. Phytoplankton blooms beneath the sea ice in the Chukchi sea. *Deep-Sea Research Part Ii-Topical Studies in Oceanography*, 105: 1-16.
- Arrigo, K.R., van Dijken, G. and Pabi, S., 2008. Impact of a shrinking Arctic ice cover on marine primary production. *Geophys. Res. Lett.*, 35(19).
- Arrigo, K.R. and van Dijken, G.L., 2011. Secular trends in Arctic Ocean net primary production. *J. Geophys. Res.*, 116: C09011.
- Bates, N.R., 2006. Air-sea CO₂ fluxes and the continental shelf pump of carbon in the Chukchi Sea adjacent to the Arctic Ocean. *J. Geophys. Res.*, 111: C10013.
- Bates, N.R. and Mathis, J.T., 2009. The Arctic Ocean marine carbon cycle: evaluation of air-sea CO₂ exchanges, ocean acidification impacts and potential feedbacks. *Biogeosciences*, 6(11): 2433-2459.
- Bauch, D., Schlosser, P. and Fairbanks, R.G., 1995. Freshwater balance and the sources of deep and bottom waters in the Arctic Ocean inferred from the distribution of H₂¹⁸O. *Prog. Oceanogr.*, 35(1): 53-80.
- Broecker, W.S. et al., 1998. How much deep water is formed in the Southern Ocean? *J. Geophys. Res.*, 103(C8): 15833-15843.

- Cai, W.-J. et al., 2010a. Alkalinity distribution in the western North Atlantic Ocean margins. *J. Geophys. Res.*, 115: C08014.
- Cai, W.J. et al., 2010b. Decrease in the CO₂ Uptake Capacity in an Ice-Free Arctic Ocean Basin. *Science*, 329(5991): 556-559.
- Carpenter, J.H., 1965. The Chesapeake Bay Institute technique for the Winkler dissolved oxygen method. *Limnol. Oceanogr.*, 10(1): 141-143.
- Codispoti, L.A., Flagg, C., Kelly, V. and Swift, J.H., 2005. Hydrographic conditions during the 2002 SBI process experiments. *Deep-Sea Research Part II*, 52(24-26): 3199-3226.
- Codispoti, L.A., Flagg, C.N. and Swift, J.H., 2009. Hydrographic conditions during the 2004 SBI process experiments. *Deep-Sea Research Part II*, 56(17): 1144-1163.
- Cooper, L.W. et al., 2008. Flow-weighted values of runoff tracers ($\delta^{18}\text{O}$, DOC, Ba, alkalinity) from the six largest Arctic rivers. *Geophys. Res. Lett.*, 35(18).
- Cooper, L.W., Whitley, T.E., Grebmeier, J.M. and Weingartner, T., 1997. The nutrient, salinity, and stable oxygen isotope composition of Bering and Chukchi Seas waters in and near the Bering Strait. *J. Geophys. Res.*, 102(C6): 12563-12573.
- Delille, B., Jourdain, B., Borges, A.V., Tison, J.L. and Delille, D., 2007. Biogas (CO₂, O₂, dimethylsulfide) dynamics in spring Antarctic fast ice. *Limnol. Oceanogr.*, 52(4): 1367-1379.
- Devol, A.H., Codispoti, L.A. and Christensen, J.P., 1997. Summer and winter denitrification rates in western Arctic shelf sediments. *Cont. Shelf Res.*, 17(9): 1029-1050.

- Eicken, H., Krouse, H.R., Kadko, D. and Perovich, D.K., 2002. Tracer studies of pathways and rates of meltwater transport through Arctic summer sea ice. *J. Geophys. Res.*, 107(C10).
- Ekwurzel, B., Schlosser, P., Mortlock, R.A., Fairbanks, R.G. and Swift, J.H., 2001. River runoff, sea ice meltwater, and Pacific water distribution and mean residence times in the Arctic Ocean. *J. Geophys. Res.*, 106(C5): 9075-9092.
- Else, B.G.T. et al., 2013. Further observations of a decreasing atmospheric CO₂ uptake capacity in the Canada Basin (Arctic Ocean) due to sea ice loss. *Geophys. Res. Lett.*, 40(6): 1132-1137.
- English, T.S., 1961. Some biological oceanographic observations in the central North Polar Sea drift station Alpha, 1957-1958. Arctic Institute of North America.
- Giles, K.A., Laxon, S.W., Ridout, A.L., Wingham, D.J. and Bacon, S., 2012. Western Arctic Ocean freshwater storage increased by wind-driven spin-up of the Beaufort Gyre. *Nature Geoscience*, 5(3): 194-197.
- Gordeev, V.V., Martin, J.M., Sidorov, I.S. and Sidorova, M.V., 1996. A reassessment of the Eurasian river input of water, sediment, major elements, and nutrients to the Arctic Ocean. *Am. J. Sci.*, 296(6): 664-691.
- Grasshoff, K., Ehrhardt, M. and Kremling, K., 1983. *Methods of seawater analysis*. Verlag Chemie, Weinheim, Germany.
- Gruber, N. and Sarmiento, J.L., 1997. Global patterns of marine nitrogen fixation and denitrification. *Global Biogeochem. Cycles*, 11(2): 235-266.
- Guay, C.K. and Falkner, K.K., 1997. Barium as a tracer of Arctic halocline and river waters. *Deep-Sea Research Part II*, 44(8): 1543-1569.

- Guo, X.H. et al., 2008. Seasonal variations in the inorganic carbon system in the Pearl River (Zhujiang) estuary. *Cont. Shelf Res.*, 28(12): 1424-1434.
- Hill, V. and Cota, G., 2005. Spatial patterns of primary production on the shelf, slope and basin of the Western Arctic in 2002. *Deep-Sea Research Part II*, 52(24-26): 3344-3354.
- Huang, W.J., Wang, Y.C. and Cai, W.J., 2012. Assessment of sample storage techniques for total alkalinity and dissolved inorganic carbon in seawater. *Limnol. Oceanogr. Methods*, 10: 711-717.
- Jones, E.P. and Anderson, L.G., 1986. On the Origin of the Chemical Properties of the Arctic Ocean Halocline. *J. Geophys. Res.*, 91(C9): 10759-10767.
- Jones, E.P., Anderson, L.G., Jutterstrom, S. and Swift, J.H., 2008. Sources and distribution of fresh water in the East Greenland Current. *Prog. Oceanogr.*, 78(1): 37-44.
- Jones, E.P., Anderson, L.G. and Swift, J.H., 1998. Distribution of Atlantic and Pacific waters in the upper Arctic Ocean: Implications for circulation. *Geophys. Res. Lett.*, 25(6): 765-768.
- Jones, E.P. et al., 2003. Tracing Pacific water in the North Atlantic Ocean. *Journal of Geophysical Research-Oceans*, 108(C4).
- Kinney, P., Arhelger, M.E. and Burrell, D.C., 1970. Chemical characteristics of water masses in the Amerasian Basin of the Arctic Ocean. *J. Geophys. Res.*, 75(21): 4097-4104.
- Kinney, P.J., Loder, T.C. and Groves, J., 1971. Particulate and dissolved organic matter in the Amerasian Basin of the Arctic Ocean. *Limnol. Oceanogr.*, 16(1): 132-137.

- Kirchman, D.L. et al., 2009. Standing stocks, production, and respiration of phytoplankton and heterotrophic bacteria in the western Arctic Ocean. *Deep Sea Research Part II: Topical Studies in Oceanography*, 56(17): 1237-1248.
- Lalande, C., Belanger, S. and Fortier, L., 2009. Impact of a decreasing sea ice cover on the vertical export of particulate organic carbon in the northern Laptev Sea, Siberian Arctic Ocean. *Geophys. Res. Lett.*, 36.
- Lee, S.H., Joo, H.M., Liu, Z.L., Chen, J.F. and He, J.F., 2012. Phytoplankton productivity in newly opened waters of the Western Arctic Ocean. *Deep-Sea Research Part II*, 81-84: 18-27.
- Letolle, R. et al., 1993. ^{18}O Abundance and Dissolved Silicate in the Lena Delta and Laptev Sea (Russia). *Mar. Chem.*, 43(1-4): 47-64.
- Li, W.K.W., McLaughlin, F.A., Lovejoy, C. and Carmack, E.C., 2009. Smallest Algae Thrive As the Arctic Ocean Freshens. *Science*, 326(5952): 539.
- Macdonald, R.W. et al., 1989. Composition and Modification of Water Masses in the Mackenzie Shelf Estuary. *J. Geophys. Res.*, 94(C12): 18057-18070.
- Macdonald, R.W., McLaughlin, F.A. and Carmack, E.C., 2002. Fresh water and its sources during the SHEBA drift in the Canada Basin of the Arctic Ocean. *Deep-Sea Research Part I*, 49(10): 1769-1785.
- Macdonald, R.W. and Wong, C.S., 1987. The Distribution of Nutrients in the Southeastern Beaufort Sea - Implications for Water Circulation and Primary Production. *J. Geophys. Res.*, 92(C3): 2939-2952.
- Makkaveev, P.N. and Stunzhas, P.A., 1995. Hydrochemical characteristics of the Kara Sea. *Oceanology of the Russian Academy of Sciences*, 34(5): 600-605.

- Maslanik, J.A. et al., 2007. A younger, thinner Arctic ice cover: Increased potential for rapid, extensive sea-ice loss. *Geophys. Res. Lett.*, 34(24).
- McLaughlin, F.A. and Carmack, E.C., 2010. Deepening of the nutricline and chlorophyll maximum in the Canada Basin interior, 2003-2009. *Geophys. Res. Lett.*, 37(24): L24602.
- McPhee, M.G., Proshutinsky, A., Morison, J.H., Steele, M. and Alkire, M.B., 2009. Rapid change in freshwater content of the Arctic Ocean. *Geophys. Res. Lett.*, 36.
- Melling, H. and Moore, R.M., 1995. Modification of Halocline Source Waters during Freezing on the Beaufort Sea Shelf: Evidence from Oxygen Isotopes and Dissolved Nutrients. *Cont. Shelf Res.*, 15(1): 89-113.
- Moore, R.M., Lowings, M.G. and Tan, F.C., 1983. Geochemical Profiles in the Central Arctic Ocean - Their Relation to Freezing and Shallow Circulation. *Journal of Geophysical Research-Oceans and Atmospheres*, 88(C4): 2667-2674.
- Nishino, S. et al., 2011. Enhancement/reduction of biological pump depends on ocean circulation in the sea-ice reduction regions of the Arctic Ocean. *J. Oceanogr.*, 67(3): 305-314.
- Nishino, S., Shimada, K., Itoh, M. and Chiba, S., 2009. Vertical double silicate maxima in the sea-ice reduction region of the western Arctic Ocean: Implications for an enhanced biological pump due to sea-ice reduction. *J. Oceanogr.*, 65(6): 871-883.
- Nomura, D., Eicken, H., Gradinger, R. and Shirasawa, K., 2010. Rapid physically driven inversion of the air-sea ice CO₂ flux in the seasonal landfast ice off Barrow, Alaska after onset of surface melt. *Cont. Shelf Res.*, 30(19): 1998-2004.

- Ostlund, H.G. and Hut, G., 1984. Arctic Ocean Water Mass Balance from Isotope Data. *Journal of Geophysical Research-Oceans*, 89(C4): 6373-6381.
- Pai, S.C., Gong, G.C. and Liu, K.K., 1993. Determination of Dissolved-Oxygen in Seawater by Direct Spectrophotometry of Total Iodine. *Mar. Chem.*, 41(4): 343-351.
- Papakyriakou, T. and Miller, L., 2011. Springtime CO₂ exchange over seasonal sea ice in the Canadian Arctic Archipelago. *Annals of Glaciology*, 52(57): 215-224.
- Perovich, D.K. and Richter-Menge, J.A., 2009. Loss of Sea Ice in the Arctic. *Annual Review of Marine Science*, 1: 417-441.
- Proshutinsky, A., Bourke, R.H. and McLaughlin, F.A., 2002. The role of the Beaufort Gyre in Arctic climate variability: Seasonal to decadal climate scales. *Geophys. Res. Lett.*, 29(23).
- Proshutinsky, A. et al., 2009. Beaufort Gyre freshwater reservoir: State and variability from observations. *J. Geophys. Res.*, 114.
- Proshutinsky, A.Y. and Johnson, M.A., 1997. Two circulation regimes of the wind driven Arctic Ocean. *Journal of Geophysical Research-Oceans*, 102(C6): 12493-12514.
- Roach, A.T. et al., 1995. Direct Measurements of Transport and Water Properties through the Bering Strait. *J. Geophys. Res.*, 100(C9): 18443-18457.
- Robbins, L.L. et al., 2013. Baseline Monitoring of the Western Arctic Ocean Estimates 20% of Canadian Basin Surface Waters Are Undersaturated with Respect to Aragonite. *PLOS ONE*, 8(9): e73796.
- Rysgaard, S. et al., 2012. Ikaite crystals in melting sea ice - implications for *p*CO₂ and pH levels in Arctic surface waters. *Cryosphere*, 6(4): 901-908.

- Rysgaard, S., Glud, R.N., Sejr, M.K., Bendtsen, J. and Christensen, P.B., 2007. Inorganic carbon transport during sea ice growth and decay: A carbon pump in polar seas. *J. Geophys. Res.*, 112: C03016.
- Rysgaard, S. et al., 2014. Temporal dynamics of ikaite in experimental sea ice. *Cryosphere*, 8(4): 1469-1478.
- Schlitzer, R., 2014. Ocean data view, <http://odv.awi.de>, 2014.
- Schlösser, P., Bauch, D., Fairbanks, R. and Böning, G., 1994. Arctic river-runoff: mean residence time on the shelves and in the halocline. *Deep Sea Research Part I*, 41(7): 1053-1068.
- Schlösser, P. et al., 2002. Decrease of river runoff in the upper waters of the Eurasian Basin, Arctic Ocean, between 1991 and 1996: Evidence from delta $d^{18}O$ data. *Geophys. Res. Lett.*, 29(9).
- Schmidt, G., Bigg, G. and Rohling, E., 1999. "Global seawater oxygen-18 database - v1.21", <http://data.giss.nasa.gov/o18data/>.
- Semiletov, I., Makshtas, A., Akasofu, S.I. and Andreas, E.L., 2004. Atmospheric CO₂ balance: The role of Arctic sea ice. *Geophys. Res. Lett.*, 31(5).
- Shimada, K. et al., 2005. Halocline structure in the Canada basin of the arctic ocean. *Geophys. Res. Lett.*, 32(3).
- Steele, M., Ermold, W. and Zhang, J.L., 2008. Arctic Ocean surface warming trends over the past 100 years. *Geophys. Res. Lett.*, 35(2).
- Strickland, J. and Parsons, T., 1968. Determination of dissolved oxygen. *A Practical Handbook of Seawater Analysis*. Fisheries Research Board of Canada, Bulletin, 167: 71-75.

- Tanaka, T. et al., 2004. N deficiency in a well-oxygenated cold bottom water over the Bering Sea shelf: influence of sedimentary denitrification. *Cont. Shelf Res.*, 24(12): 1271-1283.
- Tremblay, J.E. et al., 2011. Climate forcing multiplies biological productivity in the coastal Arctic Ocean. *Geophys. Res. Lett.*, 38.
- Wang, M.Y. and Overland, J.E., 2009. A sea ice free summer Arctic within 30 years? *Geophys. Res. Lett.*, 36.
- Winkler, L.W., 1888. Die Bestimmung des im Wasser gelösten Sauerstoffes. *Berichte der deutschen chemischen Gesellschaft*, 21(2): 2843-2854.
- Woodgate, R.A., Aagaard, K. and Weingartner, T.J., 2005. Monthly temperature, salinity, and transport variability of the Bering Strait through flow. *Geophys. Res. Lett.*, 32(4): L04601.
- Yamamoto-Kawai, M., McLaughlin, F.A., Carmack, E.C., Nishino, S. and Shimada, K., 2008. Freshwater budget of the Canada Basin, Arctic Ocean, from salinity, $d^{18}O$, and nutrients. *J. Geophys. Res.*, 113(C1).
- Yamamoto-Kawai, M., McLaughlin, F.A., Carmack, E.C., Nishino, S. and Shimada, K., 2009a. Aragonite Undersaturation in the Arctic Ocean: Effects of Ocean Acidification and Sea Ice Melt. *Science*, 326(5956): 1098-1100.
- Yamamoto-Kawai, M. et al., 2009b. Surface freshening of the Canada Basin, 2003-2007: River runoff versus sea ice meltwater. *J. Geophys. Res.*, 114.
- Yamamoto-Kawai, M., Tanaka, N. and Pivovarov, S., 2005. Freshwater and brine behaviors in the Arctic Ocean deduced from historical data of $\delta d^{18}O$ and alkalinity (1929-2002 AD). *J. Geophys. Res.*, 110(C10).

Table 4.1. End-member properties of sea ice meltwater, meteoric water, Pacific water, and Atlantic water

End-member	Salinity	$\delta^{18}\text{O}$ [‰]	PO_4^* [$\mu\text{mol}/\text{kg}$]	TAlk [$\mu\text{mol}/\text{kg}$]	DIC [$\mu\text{mol}/\text{kg}$]
Sea ice meltwater (SIM)	4±1	-2.0±0.1	0.4±0.2	360	320
Meteoric water (MW)	0±0	-20.7±0.2	0.1±0.1	995	1040
Pacific water (PW)	32.7±0.2	-1.1±0.2	2.4±0.3	2211	2148
Atlantic water (AW)	34.83±0.0 2	0.27±0.07	0.62±0.01	2297	2153

Table 4.2. A summary of the depths of PO₄, DIC, and AOU maxima in 1994 and 2010

			Slope	Chukchi Abyssal Plain	northern Canada Basin	Arlis Plateau	Makarov Basin
1994	PO ₄	Salinity	33.1	32.8	33	32.7	N/A
		Depth [m]	100	77	75	51	N/A
	DIC & AOU	Salinity	33.1	33.3	33.4	32.7	N/A
		Depth [m]	100	97	82	51	N/A
2010	PO ₄	Salinity	33.2	32.9	32.9	N/A	32.7
		Depth [m]	150	150	100	N/A	50
	DIC & AOU	Salinity	33.2	33.6	33.6	N/A	32.7
		Depth [m]	150	200	150	N/A	50

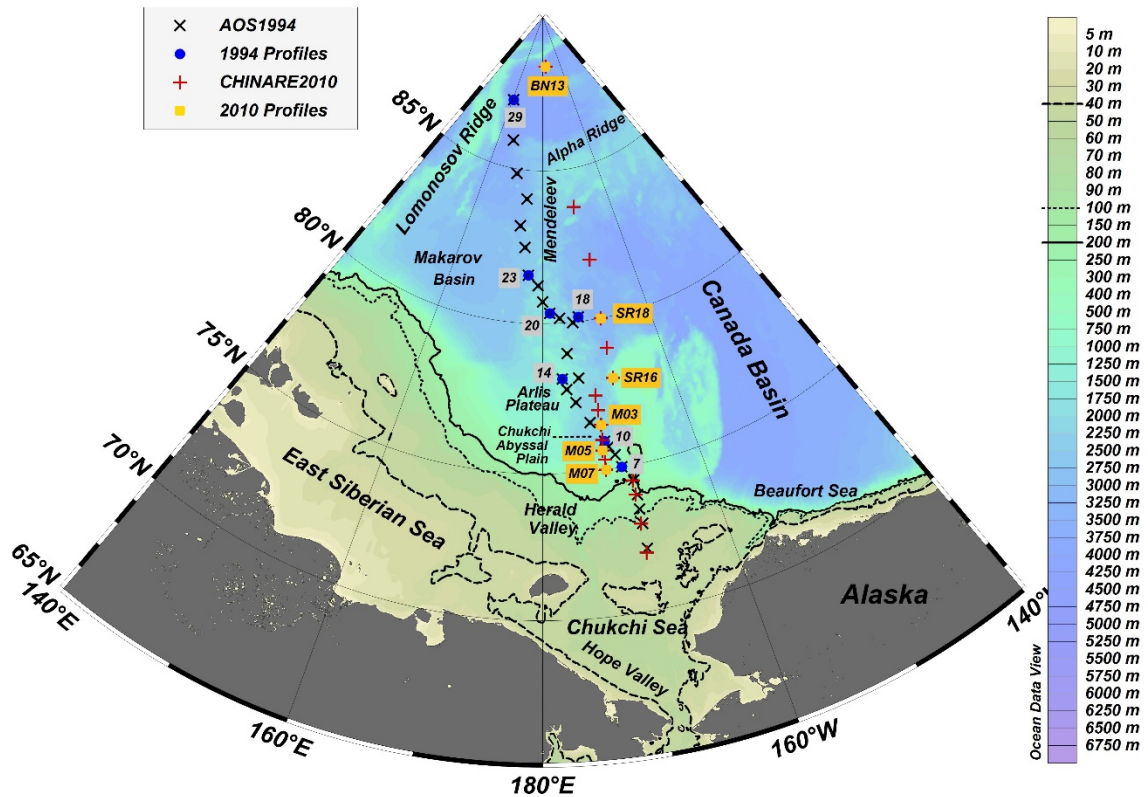


Figure 4.1. Discrete sampling stations of CHINARE2010 and AOS94. The black crosses indicate stations of AOS94. The dark red pluses indicate stations of CHNARE2010. Some stations are used for a comparison between AOS94 (solid blue circle) and CHINARE2010 (solid yellow square). The station numbers of these stations are labeled beside for AOS94 (gray background) and CHINARE2010 (yellow background). The black dashed, dotted, and solid lines indicate the 40 m, 100 m, and 200 m isobath, respectively. This figure is plotted using Ocean Data View (Schlitzer, 2014).

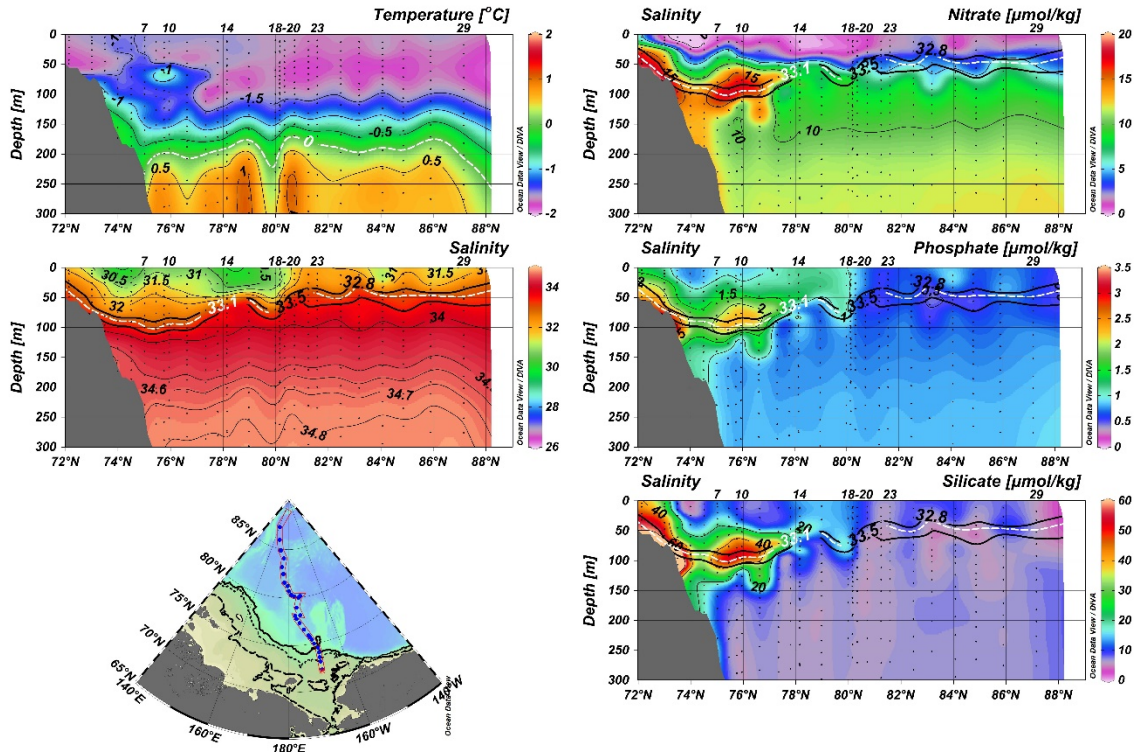


Figure 4.2. Sections of temperature, salinity, nitrate, phosphate, and silicate along a section from the Chukchi Sea shelf to the North Pole in AOS94. In the section of temperature, an isosurface for 0 °C is marked with a bold white dashed line. In the sections of salinity, nitrate, phosphate, and silicate, isosurface of $S = 33.1$ (bold white dashed line) and of 32.8 and 33.5 (bold black solid lines) are plotted over the contour (color) maps. The salinity range of 32.8 and 33.5 characterizes the upper halocline water which has a core salinity of 33.1.

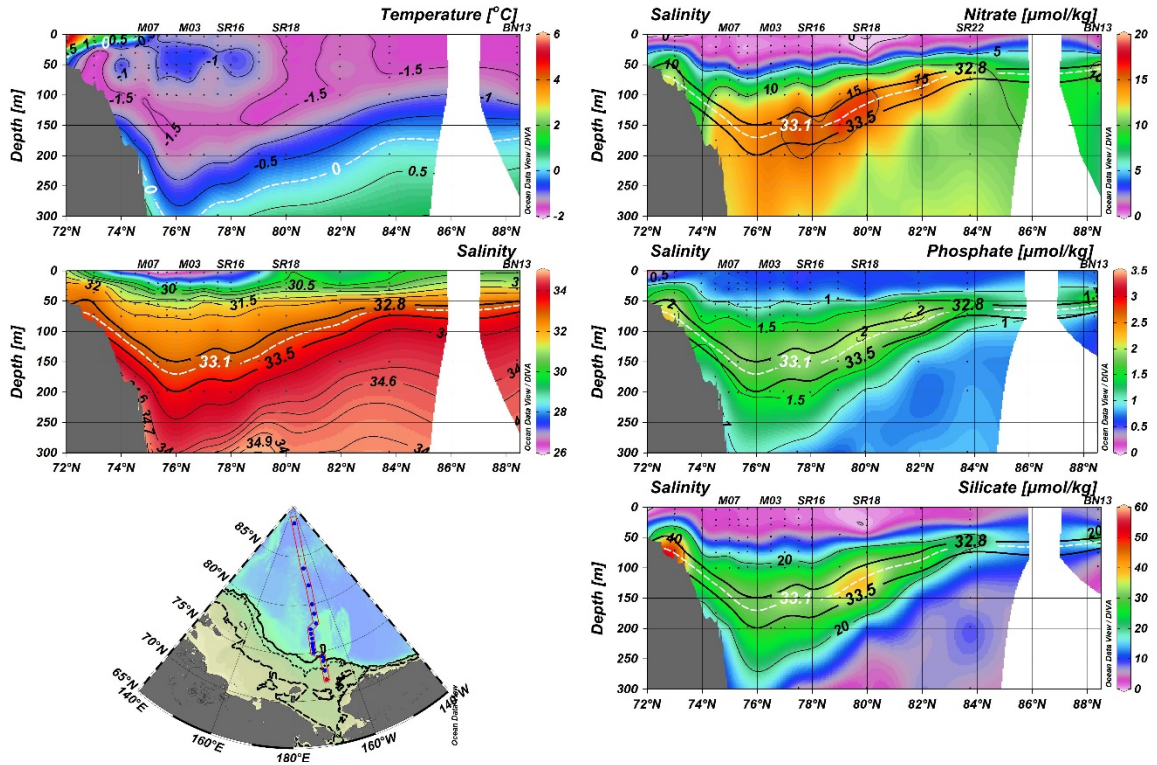


Figure 4.3. Sections of temperature, salinity, nitrate, phosphate, and silicate along a section from the Chukchi Sea shelf to the North Pole in CHINARE2010. In the section of temperature, an isosurface for 0 °C is marked with a bold white dashed line. In the sections of salinity, nitrate, phosphate, and silicate, isosurface of $S = 33.1$ (bold white dashed line) and of 32.8 and 33.5 (bold black solid lines) are plotted over the contour (color) maps. The salinity range of 32.8 and 33.5 characterizes the upper halocline water which has a core salinity of 33.1.

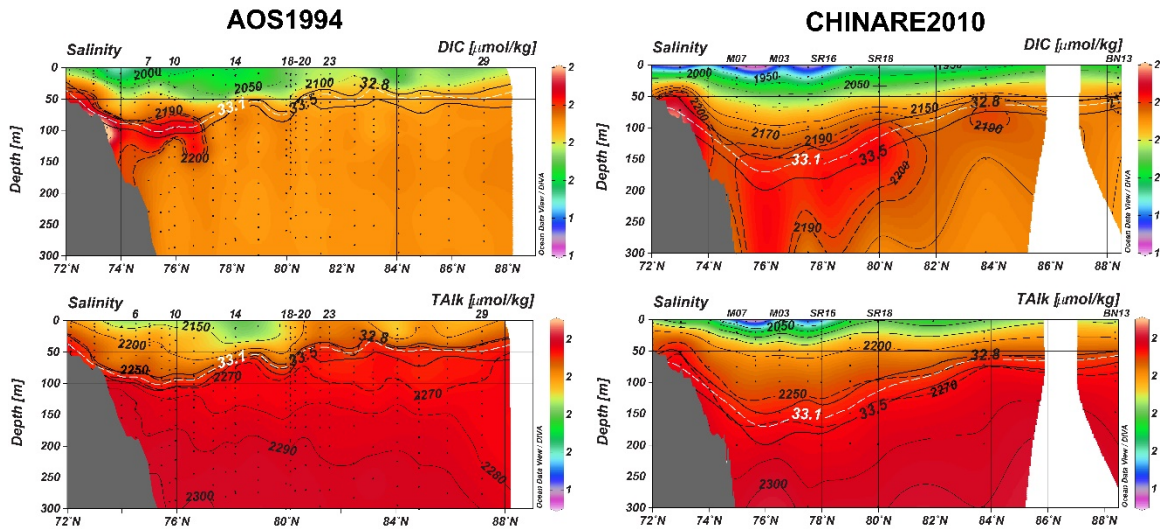


Figure 4.4. Sections of DIC and TAlk in AOS94 and CHINARE2010. Isosurface of $S = 33.1$ (bold white dashed line) and of 32.8 and 33.5 (bold black solid lines) are plotted over the contour (color) maps. The salinity range of 32.8 and 33.5 characterizes the upper halocline water which has a core salinity of 33.1. The contour lines of DIC = 2190 and 2200 and of TAlk = 2250 and 2700 $\mu\text{mol/kg}$ are marked with black dashed lines.

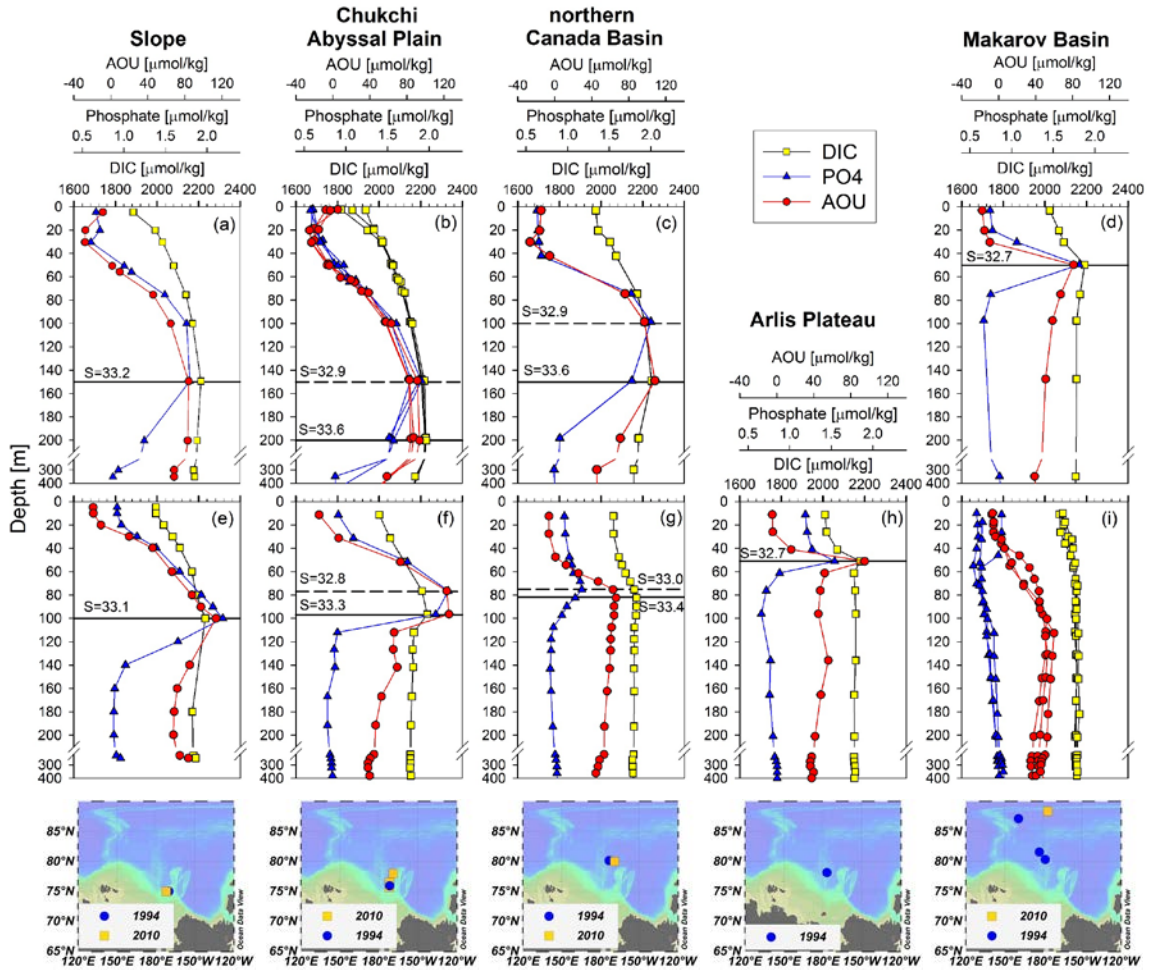


Figure 4.5. Depth profiles of DIC, phosphate (PO₄), and AOU in CHINARE2010 (a–d) and AOS94 (e–i) and sampling stations (bottom panel). Solid yellow squares, solid blue triangles, and solid red dots indicate DIC, phosphate, and AOU, respectively. The black solid horizontal reference line indicates the layer of DIC, AOU and PO₄ maximum in (a, d, e, and h), and indicates indicate the layer of DIC, AOU and PO₄ maximum in (b, c, f, and g). The black dashed horizontal reference line indicates the layer of PO₄ maximum in (b, c, f, and g).

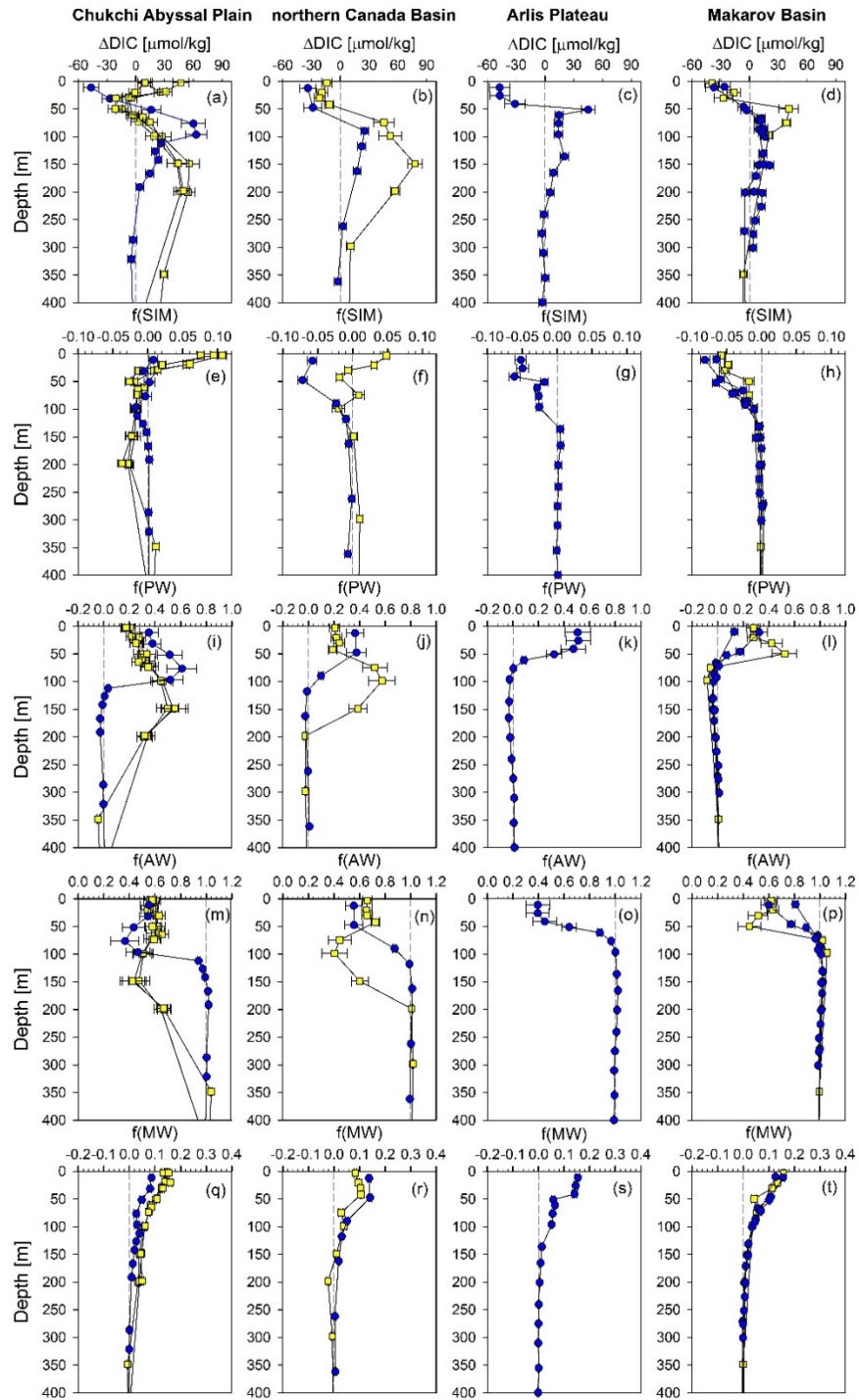


Figure 4.6. Depth profiles of aerobically-related Δ DIC (measured – predicted) and fractions of sea ice meltwater (SIM), Pacific water (PW), Atlantic water (AW), and meteoric water (MW) in AOS94 and CHINARE2010. Solid yellow squares indicate 2010 data. Solid blue dots indicate 1994 data.

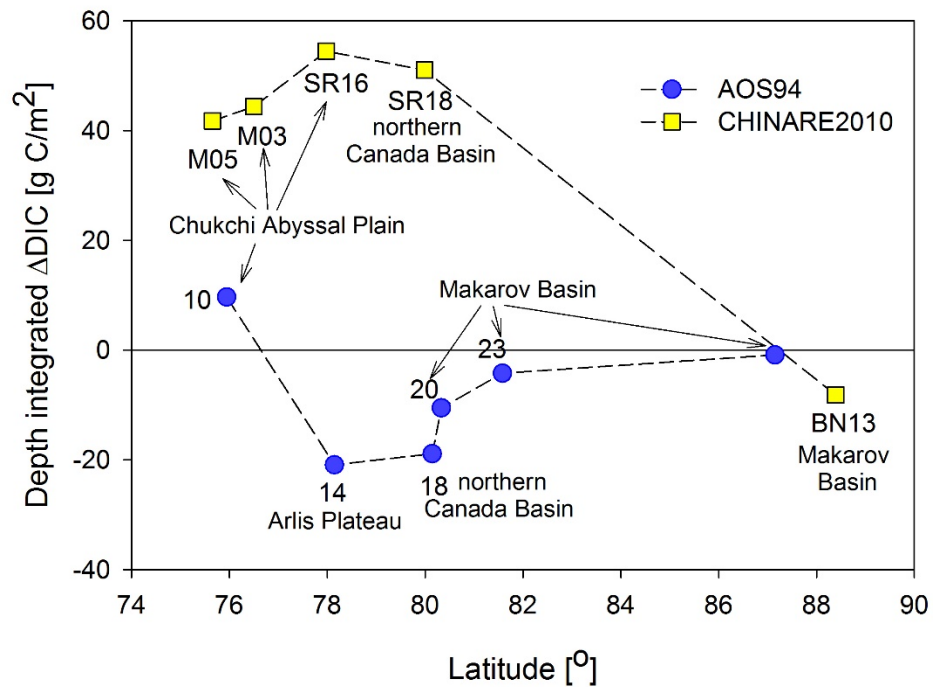


Figure 4.7. Depth integrated aerobically-related Δ DIC (measured – predicted) in AOS94 and CHINARE2010. Δ DIC is integrated from surface to the layer of DIC and AOU maxima. Sampling stations (M05–SR18) were partially ice-covered (<85% sea ice cover) and BN13 was heavily ice-covered (>85% sea ice cover) in 2010. All sampling stations were heavily ice-covered in 1994.

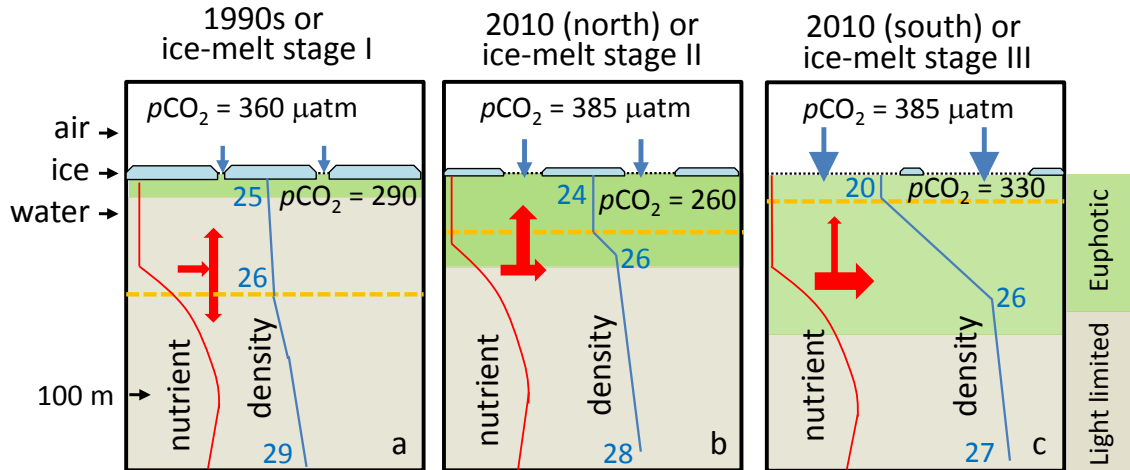


Figure 4.8. A conceptual model illustrating the rapid sea ice retreat and the associated physical, biogeochemical and biological changes during summer through three stages of sea ice melt. Light blue blocks at sea surface represent sea ice. Blue arrows indicate the direction and size of CO_2 gas flux. Blue lines represent water density with the numbers, for example 26, meaning 1.026 kg m^{-3} . Red lines represent NO_3^- concentrations. The brown-dashed lines represent the bottom of the surface mixed layer, which decreases as ice-melt progresses. The density and nutrient structures presented here are based on observations along the CHINARE2010 cruise track. The red arrows indicate the intensity of vertical mixing and lateral advection.

CHAPTER 5

SUMMARY

Major research questions in the Arctic Ocean are how the rate of biological production in sea surface and carbon cycle and fluxes in surface and water column respond to warming and sea ice melt. The Arctic Ocean has featured characteristics of ubiquitously low surface temperatures and seasonal sea ice cover. These characteristics make the Arctic Ocean different from the temperate oceans. Low surface temperature allows the Arctic Ocean to sequester more CO₂ from the atmosphere. However, perennial sea ice cover hampers air-sea gas exchange. Moreover, perennial sea ice cover also inhibits the exploration in the interior Arctic Ocean, resulting in a paucity of measurements of carbonate parameters. Accompanying with rapid retreat of sea ice in recent summers, field studies of the inorganic CO₂ system in the Arctic Ocean are feasible and increasing. However, there is still a lack of knowledge about sampling artifacts and controlling mechanisms which determine the carbon cycle in the Arctic Ocean. Any work contributing to these unknowns will constrain the uncertainties in the estimate of global oceanic carbon fluxes.

This dissertation addresses these scientific and technical questions through studying the Arctic carbon cycle during the Chinese National Arctic Research Expedition (CHINARE) in summer 2008 and 2010. These goals were achieved through (1) an assessment of internal consistency of carbonate system between field measurements of $p\text{CO}_2$ and $p\text{CO}_2$ values calculated from bottle measurements of DIC and TALK using the

data collected during CHINARE2010 cruise in chapter 2; (2) the concentrations of carbonate system parameters, including dissolved inorganic carbon (DIC), total alkalinity (TAlk), and partial pressure of carbon dioxide ($p\text{CO}_2$) in surface waters to delineate their distributions and controlling mechanisms in chapter 3; and (3) the distribution of carbonate system parameters and changes in carbon cycling in the water column over an area from the Chukchi Sea shelf to the North Pole in both AOS94 and CHINARE2010 cruises to study how inorganic CO_2 system responds to sea ice melt in chapter 4.

In Chapter 2, we used recent high precision and accuracy Arctic Ocean field measurements of DIC, TAlk, and $p\text{CO}_2$, along with seven sets of carbonic acid dissociation constants, to evaluate the internal consistency of the inorganic CO_2 system and to identify best-fit sets of dissociation constants. We focused on the calculation of $p\text{CO}_2$ from DIC and TAlk, because DIC and TAlk were usually the only two carbonate parameters measured in the early studies in the Arctic Ocean. Moreover, we can use similar assessments in the temperate ocean to compare with our studies. Our observations showed that the constants of *Mehrbach* and *Lueker* yielded the best internal consistency over the temperature range of -1.5 to 10.5 °C and the salinity range of 25.8 to 33.1. Incorporating our findings with the recommendations of prior work in lower-latitude oceans, we recommended the use of these two sets of constants for studies of the global oceanic carbonate system. We observed that $\Delta p\text{CO}_2$ (calculated–measured) decreased with increasing latitude and concluded that this pattern is associated with the temperature and salinity dependencies of K_1 and K_2 . The $\Delta p\text{CO}_2$ values in our study areas, excluding the partially ice-covered Canada Basin, were 1.5 ± 5.7 μatm for *Mehrbach* and 2.3 ± 5.4 μatm for *Lueker*. This good agreement indicates highly accurate $p\text{CO}_2$ calculations, even

though K_1 and K_2 for these calculations were extrapolated to use in the low temperature Arctic Ocean. We also observed that mean $\Delta p\text{CO}_2$ value for *Mehrbach* and *Lueker* were $\sim 5 \mu\text{atm}$ lower in the colder and ice-covered Canada Basin than that in the warmer Bering Sea. Although this difference is equivalent to the standard deviation of field measurements, we did observe a slight trend of decrease in $\Delta p\text{CO}_2$ with decreasing temperature. It might indicate that the calculated $p\text{CO}_2$ might be underestimated in the practice of extrapolation to lower temperatures, with the uncertainty to be $\sim 5 \mu\text{atm}$ in accuracy.

Sampling artifacts were also evaluated in Chapter 2. We observed large differences in $\Delta p\text{CO}_2$ only in the southern Canada Basin, a region has partial sea ice cover ($<35\%$ ice cover; $\Delta p\text{CO}_2 = -22 \mu\text{atm}$). Thus we assessed the potential influences of several processes on the variation of $\Delta p\text{CO}_2$ values. The influence of river water on shelf surface waters, in situ sea ice meltwater on Canada Basin waters, atmospheric CO_2 invasion into the surface layer of sea ice meltwater, and insufficient flushing of Niskin bottle were all judged to be negligible. Dissolution of CaCO_3 (ikaite) in our sample bottles might, however, be sufficient to explain the large $\Delta p\text{CO}_2$ values characteristic of the partially ice-covered southern Canada Basin. More solid evidence is needed to verify the potential importance of this process.

In Chapter 3, we used high resolution data of surface DIC, TAlk, and $p\text{CO}_2$ collected during the CHINARE2008 and CHINARE2010 cruises to study their distributions and controlling mechanisms. These two cruises covered a large area crossing the Bering Strait to the North Pole, facilitating the study of CO_2 system in ice-free, partially ice-covered,

and heavily ice-covered Arctic regions. Field measurements showed that mixing of Pacific water and river runoff was constrained along the Alaska coast over the Chukchi Sea shelf. The inflowing Pacific water through the Bering Strait ($S = 32.5$) was gradually modified by freshwater input from the Alaska to form modified seawater within a salinity range of 30 to 32.5. The modified sea water mixed with surrounding sea ice meltwater over the broad Chukchi shelf and in the interior Arctic basins. In addition, the properties of shelf modified seawater were associated with the time and location of sampling.

Mixing between various water sources was the dominant factor in controlling TALK distribution, except in the ice-free southern Canada Basin where it might be influenced by dissolution of CaCO_3 or increased river discharge. In addition to mixing, high primary production on the shelf dominantly controlled DIC distribution. In contrast, there was no or very limited DIC removal in an ice-free Arctic basin and in the heavily ice-covered Canada Basin. However, there was a moderate DIC removal in the partially ice-covered Canada Basin.

An air-sea gas exchange simulation approach was adopted in Chapter 3 to study the mechanism which was sustaining the high surface $p\text{CO}_2$ in the ice-free Canada Basin. Atmospheric CO_2 invasion into the surface waters was identified as the key factor contributing to the field observations. Furthermore, the simulation also indicated that increasing surface $p\text{CO}_2$ would in turn acts as a barrier to further CO_2 invasion. Due to the barrier effect of increasing surface $p\text{CO}_2$ and limited primary production, an CO_2 uptake rate of $6.4 \text{ mmol m}^{-2} \text{ d}^{-1}$ was estimated under the conditions in 2008, which was 85% less than the previous estimate of $46 \text{ mmol m}^{-2} \text{ d}^{-1}$ based on an open water condition at the southern margin of the Canada Basin which was measured during summer 2002-

2004. The corresponding CO₂ invasion flux of only 4.6×10^{12} gC yr⁻¹ in the newly ice-free basin area was much smaller than an estimate of 33×10^{12} gC yr⁻¹ under constant $\Delta p\text{CO}_2$. Therefore, contrary to the current view, we predicted that the CO₂ uptake capacity in the ice-free Arctic Ocean basin will be quickly weakened owing to shallower mixed layer depth and low biological CO₂ fixation and increased surface $p\text{CO}_2$ values due to atmospheric CO₂ invasion.

In Chapter 4, we evaluated the carbon cycling in the water column in AOS94 and CHINARE2010 and compared the differences in carbon cycling between these two cruises. Our aims were to elucidate how carbon cycling responds to sea ice melt and how a shift in ocean circulation regime affects carbon cycling. Through a comparison of field observed data, we observed deepened and broadened Pacific origin upper halocline layer in the interior Arctic in 2010. These changes might be associated with increased summer open water area over the shelves through which more brine water could be produced during late fall and winter and be exported to interior of the Arctic Ocean.

We further evaluated aerobically-related carbon cycling in the interior Arctic basins by removing the contributions of denitrification, formation/dissolution of CaCO₃ to observed DIC and TALK values. Then we found that the influence of sea ice melt on carbon cycling has latitudinal features which corresponded to various stages of sea ice melt. In the nearly ice-free southern Canada Basin, broadened upper halocline layer allowed organic matter to be remineralized in the upper ocean and prevented the sinking of organic particles into sediments. Moreover, freshwater accumulated in surface waters might inhibit upward supply of deep nutrient-rich water, which would limit the CO₂ uptake capacity from the atmosphere due to a decrease in biological production. In the

interior Arctic featured with newly opened water, we confirmed that an increase in primary production was associated with the early stage of sea ice melt, and confirmed this conclusion through a subsurface increase in DIC and increased DIC inventory above the upper halocline layer. In the heavily ice-covered Makarov Basin, an increase in subsurface Δ DIC was observed in the Makarov Basin in 2010 with high fractional contribution of Pacific water of ~ 0.5 . In contrast, similar pattern was not observed in 1994. By comparison, a similar subsurface Δ DIC increase was observed in the Arlis Plateau in 1994 with a large contribution of ~ 0.5 from Pacific water. It seems this pattern has been shifted to the high latitude which might be related to warming or a shift in surface circulation regime.

In a combination of carbon cycling corresponding to sea ice melt, we built a conceptual model to describe carbon cycling at different stages of sea ice melt: CO_2 is fixed at the beginning of sea ice melt, then the carbon cycling is modified due to accumulation of freshwater in the surface with limited air-sea gas exchange, and finally, carbon uptake capacity will be decreased due to limited nutrient supply and enhanced stratification and atmospheric CO_2 invasion.

This dissertation improves our understanding of carbon cycle and fluxes in the Arctic Ocean basins and margins. Our underway sea-surface $p\text{CO}_2$ distribution study in the newly opened ocean basin is a complete new contribution to the literature. Our 2008 and 2010 carbonate chemistry depth profile study illustrates for the first time a major change in the carbonate geochemistry between 1994 and recent years, and suggests major changes likely have been occurred in the associated physical and biological drivers for carbonate geochemistry in the deep Arctic Ocean basins.